

UNIVERSITY OF OKLAHOMA

GRADUATE COLLEGE

STUDY OF METAL-ENHANCED FLUORESCENCE OF
DYE DOPED SILICA NANOPARTICLES

A DISSERTATION

SUBMITTED TO THE GRADUATE FACULTY

in partial fulfillment of the requirements for the

Degree of

DOCTOR OF PHILOSOPHY

By

KALANI BUDDIKA GUNAWARDANA

Norman, Oklahoma

2012

STUDY OF METAL-ENHANCED FLUORESCENCE OF DYE DOPED SILICA
NANOPARTICLES

A DISSERTATION APPROVED FOR THE
DEPARTMENT OF CHEMISTRY AND BIOCHEMISTRY

BY

Dr. Ronald L. Halterman, Chair

Dr. Richard W. Taylor

Dr. Wai Tak Yip

Dr. Shaorong Liu

Dr. Lloyd A. Bumm

© Copyright by KALANI BUDDIKA GUNAWARDANA 2012
All Rights Reserved.

I dedicate this dissertation to my parents and my husband for their endless love and support.

Acknowledgements

This work would not have been possible without the help and support of many people. First and foremost I would like to express my deepest gratitude to my advisor Dr. Ronald Halterman for his excellent guidance, encouragement, and patience and for providing me an excellent atmosphere for doing research. This work would not be possible without his vision.

I also want to thank the my graduate committee members, Dr. Richard Taylor for his guidance and support rendered to me from my first year, and the other committee members Dr. Lloyd Bumm, Dr. Wai Tak Yip and Dr. Shaorong Liu for their advice and guidance and constructive feedback throughout my graduate study.

My special thanks to Anuradha Singh, for being a wonderful friend and all my lab mates Shawna Ellis, Mekala Shekar, NathanGreen, Saravanan Ramaswamy and Justin Garret for their help and friendship. I am also grateful to Daminda Dahanayake, Loius Jackson and Qiong Lei for the support given to me in my research. There are still many other friends I want to thank without listing their names.

My heartfelt gratitude to my parents, Thilak Wijewardana and Marian Senanakaye and two sisters for their endless love, support and encouragement given to me through all those hard times. I must thank my loving husband Samantha Gunawardana for being by me at all times and guiding me in times of darkness. Finally, I want to thank my son Kavith and my daughter Sathmi for being so good, making me happy and letting me forget all the hard times and giving each new day for a fresh start.

Table of Contents

Acknowledgements	iv
Table of Contents	v
List of Tables	ix
List of Figures.....	x
Abstract.....	xix
Chapter 1: Introduction.....	1
1.1 Origination of Surface Plasmon Resonance	3
1.2 Metal-Fluorophore Interactions.....	6
1.3 Metal-Enhanced Fluorescence.....	8
1.3.1 Effect of Concentrated Localized Fields on MEF.....	11
1.3.2 Effect of Modification of Radiative Decay rate on MEF	13
1.3.3 Distance Dependency between Metal and Fluorophore on MEF.....	15
1.3.4 Radiative Plasmon and Plasmon Scattering	16
1.3.5 Effects of Coupled Plasmons on MEF	19
1.4 Research Focus.....	19
1.5 Chapter 1 References.....	21
Chapter 2: Study of Place Exchange of Alkanethiol Tethered Fluorescent Dyes and Ligands on Gold Nanoparticle Surface	24
2.1 Chapter Overview.....	24
2.2 Introduction	26
2.3 Results and Discussion.....	31
2.3.1 Synthesis of Gold Nanoparticles	31

2.3.2 Capping Gold Nanoparticles with Fluorescent Dyes	35
2.3.3 Stability of Sol/Dye Mixtures.....	37
2.3.4 Controlling the Density of Dye Loaded on the Nanoparticle Surface.....	39
2.3.5 Estimation of Amount of Alkanethiols Required For Saturation	49
2.3.6 Molar Fluorescence of Adsorbed Dye.....	51
2.3.6 Study of Place Exchange of Alkanethiols on AuNP Surface	54
2.4 Chapter Summary	62
2.5 Experimental.....	63
2.5.1 Preparation of 13 nm Diameter AuNPs by Standard Citrate Reduction ...	63
2.5.2 Experimental Procedure for Preparation of sol/dye/MUC Series, for Controlling the Density of Dye Loaded on AuNP Surface.	64
2.5.3 Place Exchange of Citrate Capping of AuNPs with 11- Mercaptoundecanoate (MUA).....	65
2.5.4 Place Exchange of Citrate Capping of AuNPs with.....	66
CH ₃ O(CH ₂ CH ₂ O) ₂ C ₁₀ H ₂₀ SH)	66
2.5.6 Correction for Inner-filtering Effects	67
2.6 Chapter 2 References.....	71
Chapter 3: Metal-Enhanced Fluorescence of Dye Doped Silica Nanoparticles by Metal- Fluorophore Aggregation	73
3.1 Chapter Overview.....	73
3.2 Introduction	74
3.3 Results and Discussion.....	78
3.3.1. Metal-Fluorophore Aggregation by Electrostatic Interactions.....	78

4.3.1 Study of Spectral Overlap of BODIPY Doped Layered SiNPs with 13 nm AuNPs.....	133
4.3.2 Conclusions on Wavelength Dependence on MEF	136
4.4 Enhancement of Layered Dye Doped SiNPs.....	137
4.5 Chapter Summary	138
4.6 Experimental.....	139
4.6.1 Metal-Fluorophore Aggregation of Layered RhB Doped SiNPs using DTC Chemistry (Layered-1)	139
4.6.2 Metal-Fluorophore Aggregation of Layered RhB Doped SiNPs using DTC Chemistry (Layered-2)	140
4.6.3 Metal-Fluorophore Aggregation of Layered RhB Doped SiNPs using DTC Chemistry (Layered-3)	141
4.6.4 Metal-Fluorophore Aggregation of Layered Rubpy Doped SiNPs using DTC Chemistry	141
4.6.5 Metal-Fluorophore Aggregation of Layered BODIPY Doped SiNPs using DTC Chemistry	142
3.5.6 Fluorescence and Absorbance Measurements.....	143
4.7 Chapter 4 References.....	144

List of Tables

Table 1 Estimation of amount of Alkanethiols required for surface saturation of AuNPs.	50
Table 2 Estimated amount of disulfide molecules per AuNP.	61
Table 3 Absorbance and transmittance of sol/dye mixtures at 250 nm.....	70
Table 4 Corrected values of sol/dye fluorescence for inner filter effects.....	70
Table 5 List of facts about the amounts of dye molecules incorporated in silica.	108

List of Figures

Figure 1.1 Origination of surface plasmon oscillation under the effect of an electromagnetic field. [6].....	3
Figure 1.2 Deactivation pathways of an excited fluorophore near a gold nano particle. [13]	6
Figure 1.3 Schematic representation of the near-field interactions modifying the free space condition of the fluorophore causing metal-enhanced fluorescence (MEF).	8
Figure 1.4 Jabloski diagrams of fluorophore at free space condition (top), additional excitation and emission pathways produced by the near-field interactions due to the presence of the metal nanoparticles (bottom).....	10
Figure 1.5 Representation of interaction of resonant metal colloid with the electric field of incident light. The lines represent the direction of electric fields. Fluorophore is shown in the near -field of the colloid. [1d]	12
Figure 2.1 Place-exchange of tethered fluorescent dyes and ligands on AuNP surface.	25
Figure 2.2 Self assembled monolayer of alkanethiols on gold surface. (Diagram produced by Lloyd Bumm)	27
Figure 2.3 Well-ordered SAM on a flat surface (left), and non-ordered SAM on curved surface (right).	29
Figure 2.4 Absorbance spectra of citrate capped 13 nm diameter AuNPs in water.	33
Figure 2.5 Structure of BODIPY decylthioacetate.....	36
Figure 2.6 Normalized absorbance and emission of BODIPY decylthioacetate.....	36
Figure 2.7 11-Mercaptoundecanoic acid.	38
Figure 2.8 Competing ligand- (11-mercaptoundecanoate)-(MUA)	40

Figure 2.9 Absorbance of 1.2 nM AuNPs after ligand exchange with varying concentrations (0-50 μ M) of MUA.	40
Figure 2.10 Fluorescence emission of 1 μ M BODIPY decylthioacetate with varying MUA (mercaptoundecanoate) concentrations (0-50 μ M) in 85 % ethanol. Samples excited at 521 nm.	41
Figure 2.11 Average fluorescence emission of sol/dye mixtures containing 0.4 μ M BODIPY, 1.5mL AuNPs with varying concentrations of MUA 0-10 μ M (a-h) and the fluorescence emission 0.4 μ M dye without AuNPs (free-dye). Samples were excited at 521 nm.	43
Figure 2.12 Fluorescence emission of supernatants of sol/dye mixtures containing 0.4 μ M BODIPY, 1.5 mL AuNPs and varying concentrations of MUA (0-10 μ M) and fluorescence emission of 0.4 μ M dye without AuNPs (free-dye). Samples were excited at 521 nm.	44
Figure 2.13 Fluorescence isotherms of sol/dye mixtures and supernatants, generated by plotting the average fluorescence emission maxima of sol/dye mixtures and supernatants against the MUA concentration (Fluorescence maxima was measured at 530 nm).	45
Figure 2.14 Fluorescence isotherms of sol/dye mixtures and supernatants, and sol/dye mixtures corrected for the inner-filter effects, generated by plotting the average fluorescence emission maxima of sol/dye mixtures and supernatants against the MUA concentration.	47
Figure 2.15 Concentration of absorbed dye on AuNP surface against the MUA concentration.	48

Figure 2.16 Variation of relative molar fluorescence of the absorbed dye against the concentration of the dye absorbed dye on AuNP surface.....	52
Figure 2.17 Variation of relative molar fluorescence of the absorbed dye against the concentration of the dye absorbed dye on AuNP surface (0.1-0.3 μ M).....	53
Figure 2.18 Orientation of tethered dye on AuNP surface without the competing ligand (left) and with the competing ligand (right).	54
Figure 2.19 Fluorescence isotherms of BODIPY pre-capped sol/dye mixtures against varying MUA concentrations. Fluorescence of the samples were measured at immediately after mixing MUA (0h), after 4 h and after 24 h.	55
Figure 2.20 Structure of $\text{CH}_3\text{O}(\text{CH}_2\text{CH}_2\text{O})_2\text{C}_{10}\text{SCOCH}_3$	57
Figure 2.21 Structure of the thioacetate cleaved ligand-"ether capping"	57
Figure 2.22 Fluorescence isotherms of BODIPY pre-capped sol/dye mixtures against varying $\text{CH}_3\text{O}(\text{CH}_2\text{CH}_2\text{O})_2\text{C}_{10}\text{SH}$ concentrations. Fluorescence of the samples was measured at 4 h and 48 h after addition of the ligand.	58
Figure 2.23 Structure of the disulfide.....	60
Figure 2.24 Absorbance spectra of ether capped AuNPs (0.6nM) with varying amounts of disulfide.....	61
Figure 2.25 Typical cell configuration for right angle fluorometry. Window parameters (X,Y and U,V). [14]	68
Figure 2.26 Absorbance of AuNPs capped with varying amounts of MUA.....	69
Figure 3.1 Enhanced emissions near silver nanoparticle monomer and dimer.[8]	76
Figure 3.2 Formation of variety of metal-fluorophore aggregates through electrostatic binding between MUA coated AuNPs and APTES coated dye doped SiNPs.	78

Figure 3.3 Enhanced dye molecules located beyond the quenching region of the metal.	79
Figure 3.4 Normalized absorbance and fluorescence emission of Rhodamine B.	80
Figure 3.5 Amide coupling of APTES with RhB.....	80
Figure 3.6 Synthesis of dye doped silica. [15]	81
Figure 3.7 Absorbance spectra of 3.2 nM AuNPs before and after place exchange with MUA in milipore water.	83
Figure 3.8 Absorbance of 1.5 mL of MUA capped AuNPs upon varying additions of RhB doped SiNPs as described in text.	85
Figure 3.9 Fluorescence emission of control samples of RhB doped SiNPs (without AuNPs) in water. Samples were prepared by adding varying amounts of SiNPs to milipore water (1.5 mL). Fluorescence emission was measured by exciting the samples at 550 nm at 5 nm slit width.	86
Figure 3.10 Fluorescence emission of varying additions of RhB doped SiNPs to MUA capped AuNPs (1.5 mL) in milipore water (as described in the text). Fluorescence emission was measured by exciting the samples at 550 nm at 5nm slit width.....	86
Figure 3.11 Fluorescence isotherms of fluorescence maxima of control samples (without AuNPs) and AuNP-SiNP aggregates against amount of SiNPs added. Fluorescence emission was measured by exciting the samples at 550 nm at 5 nm slit width. Emission maxima were measured at 575 nm.	87
Figure 3.12 Fluorescence isotherms of fluorescence maxima of control samples and AuNP-SiNP aggregates before and after correction for inner-filter effects. Fluorescence	

emission was measured by exciting the samples at 550 nm at 5 nm slit width. Emission maxima was measured at 575 nm.....	88
Figure 3.13 Dithiocarbamate bond formation on gold.....	90
Figure 3.14 Formation of metal-fluorophore aggregates using DTC chemistry.....	92
Figure 3.15 Fluorescence emission of DTC coupled 1:1 AuNP:SiNP mixtures and controls; without CS ₂ and without AuNPs (free SiNP). Samples were prepared as described in text, in 70% ethanol, samples were excited 550 nm at 5 nm slit width.	95
Figure 3.16 Fluorescence emission of DTC coupled 10:1 AuNP:SiNP mixtures and controls; AuNP and SiNPs without CS ₂ and SiNPs without AuNPs (free SiNP). Samples were prepared as described in text, in 70% ethanol and excited at 550 nm at 5 nm slit width.	95
Figure 3.17 Fluorescence emission of DTC coupled 20:1 AuNP:SiNP mixtures and controls; AuNP and SiNP without CS ₂ and SiNPs without AuNPs (free SiNP).....	96
Figure 3.18 Fluorescence emission of DTC coupled RhB doped SiNPs (20 uL) from preparation-2, with varying amount of AuNPs after day 1. Samples were prepared as in text in 85% ethanol. Samples were excited at 545 nm at 5nm slit width.	98
Figure 3.19 Absorbance spectra of DTC coupled metal-fluorophore aggregates and control samples (1mL AuNPs and SiNPs without CS ₂ from preparation -2) after day 1.	99
Figure 3.20 Absorbance spectra of DTC coupled metal-fluorophore aggregates from preparation -2, after day 1 and day 5.....	99

Figure 3.21 Fluorescence emission of the sample with the highest enhancement (from preparation -2) over time (inset-emission of control samples). Samples were excited at 545 nm at 5nm slit width.....	100
Figure 3.22 Absorbance spectra of the sample with the largest enhancement (from preparation -2) after day 1, day 5 and day 7.....	101
Figure 3.23 TEM images of an enhanced metal-fluorophore aggregates (SiNPs from preparation -2) over time (after 2 days -left and after 14 days-right).....	102
Figure 3.24 Variation of the enhancement factor with increasing amounts of AuNPs over time (preparation-2).....	103
Figure 3.25 Variation of the enhancement factor with increasing amounts of AuNPs, over time (SiNPs from preparation -2).....	104
Figure 3.26 Variation of enhancement factor with increasing amount of AuNPs (preparation-3).....	105
Figure 3.27 TEM image of gold silica aggregates at higher magnification (SiNPs from preparation -2).	106
Figure 3.28 Fluorescence emission of Rhodamine B dilution series at monomolar concentrations (replicates 1,2,&3).....	107
Figure 4.1 Chemical structure of (a) Rhodamine B, (b) Rubpy [tris(bipyridine) ruthenium (II) dichloride] and (c) carboxy-BODIPY.	119
Figure 4.2 Structure of dye doped layered silica nanoparticle.	122
Figure 4.3 Spectral overlap of normalized fluorescence emission and absorbance of RhB with normalized absorbance of 13 nm AuNP plasmon.....	123

Figure 4.4 Fluorescence emission of metal-fluorophore aggregates of DTC coupled layered RhB doped SiNPs (layered-1) after 2 days and after 8 days, and the fluorescence of the control sample. Samples were excited at 545 nm at 5nm slit width. 124

Figure 4.5 Fluorescence emission of varying amounts of layered RHB doped SiNPs, DTC COupled with 0.5 mL of AuNPs (Layered-2, samples excited at 545 nm)..... 125

Figure 4.6 Fluorescence emission of varying amounts of layered RhB doped SiNPs . Samples excited at 545 nm at 5nm slit width. 126

Figure 4.7 Enhancement factor of DTC coupled metal-fluorophore aggregates formed by mixing varying amounts of layered-2 RhB doped SiNPs with 0.5 mL of AuNPs. Enhancement plotted against the amount of SiNPs added. 126

Figure 4.8 Absorbance of metal fluorophore aggregates formed by DTC coupling of varying amounts (10-100 μ L) of layered-2 RhB doped SiNPs with 0.5 mL of AuNPs and the absorbance of control sample with 0.5 mL AuNPs without SiNPs. 127

Figure 4.9 Fluorescence emission of metal fluorophore aggregates formed by mixing 20 μ L of DTC activated layered-3 RhB doped SiNPs with varying amounts of AuNPs(left). Control samples were prepared by mixing the same ratios of SiNPs and AuNPs without CS2 (right). [(1)-0.25 mL-AuNPs, (2)-0.5 mL- AuNPs, (3) -0.75 mL-AuNPs, (4)-1 mL- AuNPs). 128

Figure 4.10 Absorbance of metal fluorophore aggregates formed by mixing 20 μ L of DTC activated layered RhB doped SiNPs with varying amounts of AuNPs. Control samples were prepared by mixing the same ratios of SiNPs and AuNPs. Control

samples were prepared by mixing the same ratios of SiNPs and AuNPs without CS₂. [(1)-0.25 mL-AuNPs, (2)-0.5 mL-AuNPs, (3)-0.75 mL-AuNPs, (4)-1 mL-AuNPs] . 129

Figure 4.11 Spectral overlap of normalized fluorescence emission and absorbance of Rubpy, with normalized absorbance of 13 nm AuNP plasmon. 130

Figure 4.12 Fluorescence emission of metal fluorophore aggregates formed by mixing 10 μ L of DTC activated layered Rubpy doped SiNPs with varying amounts of AuNPs (left). Control samples were prepared by mixing the same ratios of SiNPs and AuNPs without CS₂ (right) [(1)-0.25 mL-AuNPs, (2)-0.5 mL-AuNPs, (3)-0.75 mL-AuNPs, (4)-1 mL-AuNPs). Samples excited at 450 nm at 10 nm slit width. 131

Figure 4.13 Absorbance of metal-fluorophore aggregates formed by mixing 10 μ L of DTC activated layered Rubpy doped SiNPs with varying amounts of AuNPs. Control samples were prepared by mixing the same ratios of SiNPs and AuNPs without CS₂. [(1)-0.25 mL-AuNPs, (3)-0.75 mL-AuNPs, (4)-1 mL-AuNPs.) 132

Figure 4.14 Spectral overlap of normalized fluorescence emission and absorbance of BODIPY with normalized absorbance of 13 nm AuNP plasmon. 133

Figure 4.15 Fluorescence emission of metal fluorophore aggregates formed by mixing 10 μ L of DTC activated layered BODIPY doped SiNPs with varying amounts of AuNPs (left). Control samples were prepared by mixing the same ratios of SiNPs and AuNPs without CS₂ (right). [(1) 0.25 mL- AuNPs, (2) 0.5 mL –AuNPs, (3) 0.75 mL –AuNPs, (4) 1 mL-AuNPs). Samples were excited at 490 nm at 5 nm slit width..... 134

Figure 4.16 Absorbance of metal-fluorophore aggregates formed by mixing 10 μ L of DTC activated layered BODIPY doped SiNPs with varying amounts of AuNPs without

CS2. [(1) 0.25 mL - AuNPs, (2) 0.5 mL -AuNPs, (3) 0.75 mL -AuNPs, (4) 1mL-
AuNPs)..... 135

Figure 4.17 TEM image of RhB doped layered SiNP trapped between two AuNPs.. 138

Abstract

Enhancement of molecular fluorescence is of great interest due to the widespread popularity of fluorescence-based detection techniques available today. Although fluorescence-based detection is considered to be more sensitive than other optical approaches, there is still an intense need for more photostable, high quantum yield fluorophores. In this regard, metal-enhanced fluorescence (MEF) has opened novel pathways for the development of brighter, fluorescent markers with enhanced stability.

Surface plasmon resonance of metal nanoparticles can modify the radiative properties of nearby fluorophores in ways not seen in classical fluorescence. Trapping fluorophores between coupled plasmons can further enhance the near-field interactions leading to even larger enhancements. The aim of this research was to develop a solution based approach to study MEF by aggregation of fluorophore tethered gold nanoparticles, which would ultimately lead to the development of ultra-bright fluorescent probes.

Thus, in the first part of the research we have studied place-exchange of different ligands on AuNP surface and photo-physical properties of dye capped gold nanoparticles. In this study we were able to develop a simple method to control the loading of dye (BODIPYdecylthioacetate) on gold nanoparticle surface using a competing ligand (11-mercaptoundecanoic acid). Furthermore, using this method we were able to calculate the molar fluorescence of adsorbed dye on gold nanoparticle

surface. We have also developed several ligand exchange procedures which were beneficial to the second part of the research.

A goal of studying ligand exchange was to attach a fluorophore tethered third generation dendron to AuNP surface. This was crucial to get the desired spacing between the metal and the fluorophore which would give rise to MEF. During the course of the research we moved to a simpler approach to interact fluorophore doped silica nanoparticles with AuNPs.

In the second phase of our study we have used dye doped silica nanoparticles as fluorescent nano-platforms to bind with multiple AuNPs. Utilization of dye doped silica allowed us to have the desired spacing between the metal and the fluorophore to achieve MEF. Furthermore, ease of surface functionalization of silica allowed us to try various binding methods. Initially we tried electrostatic binding which did not yield MEF. In search of a more robust method, we functionalized the SiNP surface with dithiocarbamate which has a very high affinity to bind with gold. Using DTC chemistry we have developed a facile solution based method to aggregate dye doped silica nanoparticles with AuNPs which resulted remarkable fluorescence enhancements up to a 200-fold. We observed that fluorescence enhancement would increase with increased aggregation of AuNPs on dye doped SiNPs.

In the final phase we have investigated the dependence on MEF on the spectral overlap of the fluorophores with the plasmon resonance of AuNPs. We have used three different dyes for this investigation; Rhodamine B, Rubpy [tris(bipyridine) ruthenium(II) dichloride] and carboxy-BODIPY. Our results indicated that the spectral overlap of RhB results greatest enhancement with 13 nm AuNP aggregates.

We believe this simple solution based approach we have developed to produce bright photostable metal fluorophore aggregates would have a greater potential to be used in the development of ultra-bright fluorescent tags for cellular imaging.

Chapter 1: **Introduction**

Fluorescence based detection techniques are widely used in a range of applications in biotechnology, clinical chemistry, material science and photonics due to their versatility and high sensitivity.¹ The detection sensitivity of such techniques mainly relies on the stability and the inherent brightness of the fluorophores. Thus, during the past 30 years tremendous efforts have been made to synthesize fluorophores with high extinction coefficients and quantum yields and also explore ways to improve their photo-stability; such as encapsulation of fluorophores in polymer matrices or incorporation of fluorophores in host-guest complexes. Furthermore, technology-wise there has been a massive improvement in imaging and spectroscopic techniques.² However, among the numerous applications, the need for further enhanced, photo stable, high quantum yield fluorophores is strongly felt in fields such as cellular tracking and imaging, single molecule detection and in the development of nano-optical sensors due to following limitations. In imaging technology, increasing the number of fluorophores to get a stronger signal often results self-quenching, furthermore, it would not be favorable for cellular imaging where the number of attachment sites are limited.³ Another way to increase the signal strength of fluorophores is to use a stronger excitation source, which could have adverse effects such as tissue damage or disruption of the fluorophore itself.⁴ Moreover, the reduction of sample size is critical for the miniaturization of optical devices such as microfluidics and lab on a chip clinical diagnostics. Therefore, novel approaches that could increase the signal strength with a minimum number of fluorophores would greatly enhance the effectiveness of fluorescence-based detection techniques.

Interestingly, recent findings on metal-fluorophore interactions show that noble metal particles can dramatically enhance the emission of fluorophores at close proximity in ways not seen in classical experiments. The recent advancements of this new field; metal-enhanced fluorescence (MEF), suggest that it could be a promising tool in tracking and detecting molecules at very low concentrations.^{1a, 5}

MEF arises due the near field-interaction of surface plasmon resonance (SPR) of metal colloids with nearby fluorophores. These interactions can result remarkable changes in the fluorophore, such as increased quantum yields, decreased lifetimes, and increased localized excitations improving the overall photo stability of the fluorophore. Thus, study of MEF can be very useful for the development of bright fluorescent markers with enhanced photo stability. The focus of this research is to study metal-fluorophore interactions in solution phase; in order to develop bright fluorescent markers which could be used for solution based sensing in future applications.

This chapter will include the origination of SPR, interactions of SPR with nearby fluorophores, and discuss the origin of MEF which is the basis of my research.

1.1 Origination of Surface Plasmon Resonance

Noble metal particles in the nanometer regime exhibit unusual characteristics which are not displayed by the bulk metals or by individual atoms. The most attractive of them is their color which results due to a strong absorption band in the visible region. For example, silver nanoparticles (AgNPs) absorb at 450 nm whereas gold nanoparticles (AuNPs) absorb at 520 nm. The characteristic color of metal nanoparticles results due to absorption of electromagnetic radiation which causes collective oscillations of surface electrons on nanoparticle surface which is known as surface plasmon resonance (SPR).

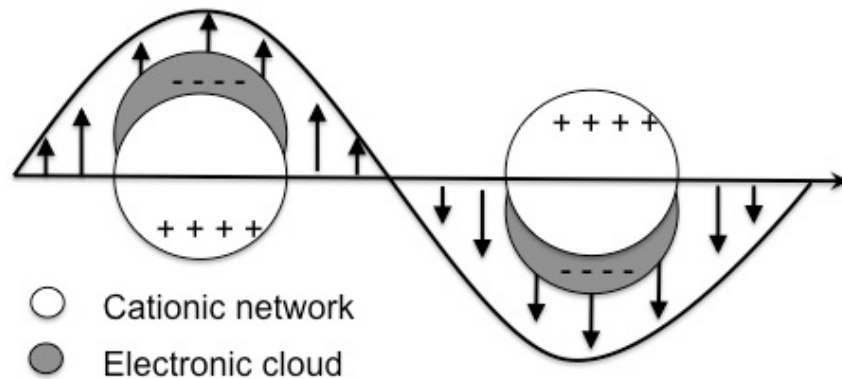


Figure 1.1 Origination of surface plasmon oscillation under the effect of an electromagnetic field. [6]

Origin of SPR can be understood by considering the electronic structure of metal nanoparticles. Metal nanoparticles consist of an immobile positively charged core (lattice) and a cloud of mobile conduction electrons on the surface (Figure 1.1). When the nanoparticles are exposed to electromagnetic radiation having larger wavelengths than the particle size, mobile electrons on the surface can move freely due to the

influence of the oscillating electromagnetic field of the incident light. A strong absorbance band is observed when the frequency of incident light matches the natural frequency of oscillating surface electrons against the restoring force of the positive nuclei. This resonance is called surface plasmon resonance. The movement of the electrons between the positively charged immobile metal core and the mobile electron cloud create oscillating dipoles which can produce electromagnetic radiation to the far-field, providing a channel for radiative decay.^{2b} However, the ability to create an oscillating dipole depends on the polarizability of the nanoparticle surface. Therefore, varying the dielectric constant of the surrounding material or surface can also affect the oscillation frequency of the surface plasmon.⁷

The optical properties of metal colloids were first theoretically modeled by Mie in 1908.¹⁰ This theory is still used to interpret plasmonic interactions. According to the Mie theory extinction of metal nanoparticles is a combined effect of both absorption and scattering. This theory shows that absorption component of the extinction results due to plasmons that cannot radiate to the far, which dissipates as heat, and the scattering component results due to radiating plasmons.^{2b, 8}

The strength of the electromagnetic field of the plasmon depends on the size, shape and the type of metal. For example gold spheres will have a single plasmon band around 520 nm, whereas, gold nanorods will have two plasmon bands due to longitudinal and transverse oscillations of surface electrons.⁷ Theoretical calculations and simulations show that nanoparticles with sharp edges such as triangles or spheroids result stronger electromagnetic fields rather than nanoparticles with smooth surfaces.⁹ Moreover, plasmons of nearby metal particles or metal aggregates can couple with each

other creating more intense electric fields in the coupled region,¹⁰ which would be discussed in more detail in chapter 3.

It is noted that not only metal particles but also metal surfaces or thin metal films can create surface plasmons or collective oscillations of surface electrons.¹¹ However, surfaces or films possess propagating plasmon modes along a broad range of wavelengths.⁸ To induce a plasmon on thin films it is necessary to use a prism and also irradiate the surface with the precise angle. On the other hand plasmons of nanoparticle have discrete modes, thus they can be easily induced by wavelengths greater than the nanoparticle size.⁸

The tunable properties of the surface plasmons, have paved their way to be utilized in various chemical and biological sensors.^{5a, 6} Mostly silver and gold nanoparticles are used in sensor development due to their easier tunability and known surface chemistry. Recently plasmon properties of other metals such as tin, iron, aluminum and zinc have also been explored.¹²

1.2 Metal-Fluorophore Interactions

When an excited fluorophore is placed in the vicinity of a metal nanoparticle, the spectral properties of the fluorophore would change dramatically due to the interactions of the SPR of the metal.¹³ These interactions are highly sensitive to the distance between the metal surface and the fluorophore. Metals were observed to be fluorescent quenchers. Quenching is dominant when the fluorophore is less than 5 nm away from the metal surface.

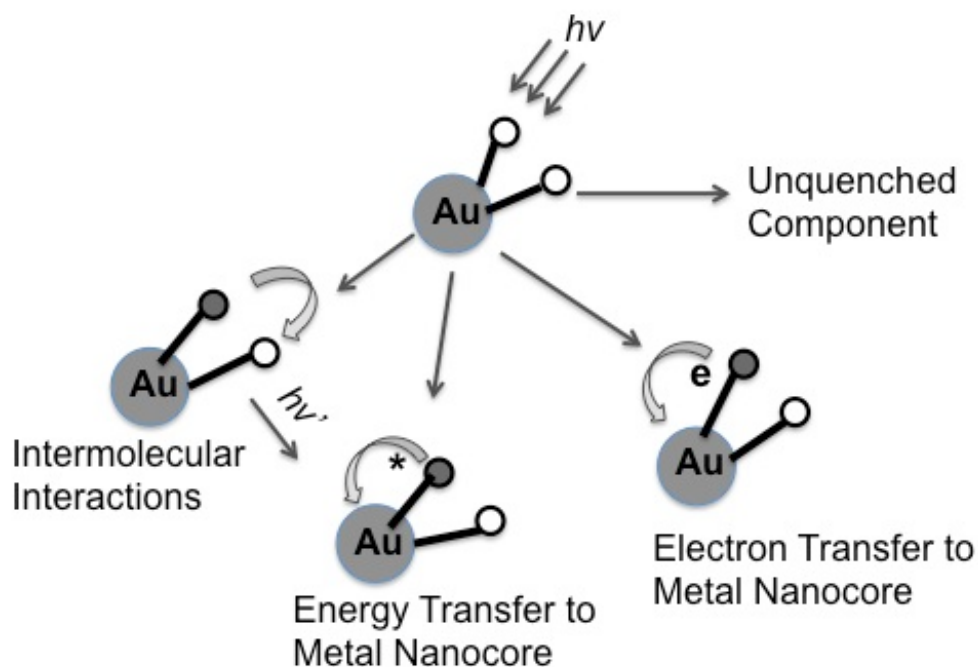


Figure 1.2 Deactivation pathways of an excited fluorophore near a gold nanoparticle. [13]

Figure 1.2 illustrates the deactivation pathways of an excited fluorophore near a metal nanoparticle. If the excited fluorophore is less than a few angstroms away from the metal surface, it can deactivate non-radiatively by passing the excited electrons directly to the metal. Furthermore, the excited fluorophore can deactivate non-radiatively by resonance energy transfer to the metal. It has been shown that the distance for the resonance energy transfer can increase above 10 nm in presence of the metal.^{1c} Moreover, if the fluorophores are tightly packed on the metal surface there could be inter-molecular quenching which is not due to any interaction with LSPR.¹³ In above three pathways excited fluorophore will deactivate non-radiatively, causing the fluorophore to quench. There are many reports on sensor design using fluorescence quenching near a metal.¹⁴ However, if the fluorophore is placed more than 5 nm away from the metal, the non-radiative pathways due to SPR would be minimized. As detailed in the next section metal-fluorophore interactions at this distance can result large enhancements in fluorescence. Thus, to observe metal enhanced fluorescence it is critical to move the fluorophore away from the quenching region.

1.3 Metal-Enhanced Fluorescence

Most fluorescence based applications used today involve measurement of spontaneous emission of fluorophores into “free space”.^{1b} These applications are based on far-field interactions where fluorophores are excited from photons coming from a far field (at least several wavelengths away) source, and detection of isotropically emitted radiation, by a detector placed several wavelengths away from the fluorophore. Furthermore, in classical fluorescence, the extinction coefficients and the radiative decay rates of fluorophores are considered to be constants and not change substantially with changing environments. Thus, changes in emission are mostly accounted for changes in nonradiative processes, such as collisional quenching, resonance energy transfer, and on environmental factors such as solvent polarity and viscosity.^{1b, c}

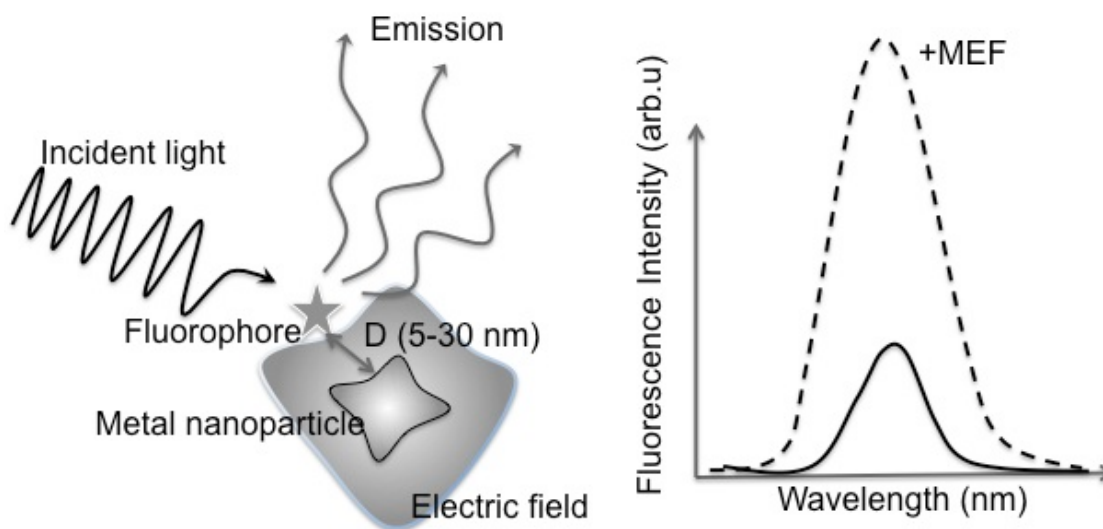


Figure 1.3 Schematic representation of the near-field interactions modifying the free space condition of the fluorophore causing metal-enhanced fluorescence (MEF).

In near-field fluorescence, properties of the fluorophores are modified by changing the “free space” condition of the fluorophore. Near-field interactions occur at distances less than a wavelength away from the metal. In near-field fluorescence, the emission or the brightness of the fluorophore can be modified by changing the radiative decay rates and the rate of excitation.^{1d} When the metal and the fluorophore are at the optimal distance, the near-field interactions can lead to dramatic changes in the fluorophores emission such as increased quantum yields, decreased lifetimes, and increased photostability.^{1b, 1d, 2a} This new approach has changed the classical perceptions of fluorescence spectroscopy, giving rise to a new regime in fluorescence based techniques known as “metal-enhanced fluorescence”.

Since metals were first known as fluorescence quenchers it is interesting to know how metals would enhance fluorescence. Metal colloids can enhance the fluorescence of nearby fluorophores in several ways.¹⁵ Metal colloids in resonance with the incident light can enhance the optical intensity around the fluorophore through near-field enhancement causing increased excitations of the fluorophore, furthermore, metal colloids can modify the radiative decay rates of the fluorophore by increasing the coupling efficiency of fluorescence to the far field through nanoparticle scattering.^{8, 15} The effect of near-field metal-fluorophore interactions can be better understood by considering the quantum yield and the Jablonski diagrams of a fluorophore with and without the presence of metal. Figure 1.4 shows the energy flow of a fluorophore at free space condition and that with the near-field interactions caused due to presence of metal.

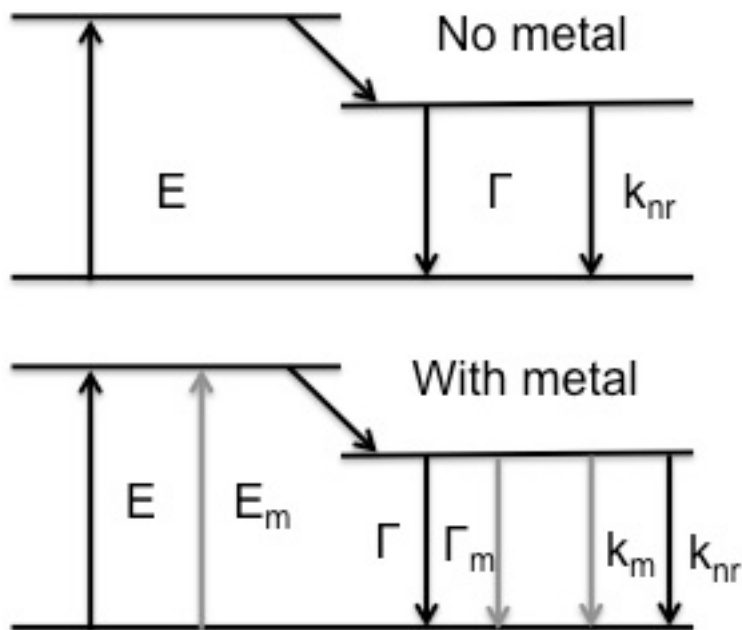


Figure 1.4 Jablonski diagrams of fluorophore at free space condition (top), additional excitation and emission pathways produced by the near-field interactions due to the presence of the metal nanoparticles (bottom).

The fluorophore at free space condition is excited by the excitation source at rate (E), from the ground state (S_0) to the singlet excited state (S_1) and then it is deactivated by emitting photons radiatively, or non-radiatively. The rate of emitting photons (radiative decay rate) is denoted by Γ and the non-radiative decay rates are shown as (k_{nr}).

The quantum yield gives the competition of radiative decay rate to all possible decaying pathways. Equation 1. shows quantum yield of a fluorophore at free space condition.

$$Q_0 = \frac{\Gamma}{\Gamma + k_{nr}} \quad (1)$$

The life time (τ_0) gives the mean time that a molecule would spend in the excited state before deactivation. The life time is the inverse of all possible decay rates (Eq 2.).

$$\tau_0 = \frac{1}{\Gamma + k_{nr}} \quad (2)$$

In classical fluorescence, the radiative decay rate of a molecule is considered to be a constant that depends on the extinction coefficient of the fluorophore.¹⁶ Thus, in classical fluorescence the quantum yield and the lifetime of a fluorophore would only depend on the non-radiative decay rates. If the non-radiative decay rates increase the lifetime of the fluorophore would decrease resulting a decrease in quantum yield. Therefore, in classical fluorescence the quantum yield and the life time would move in the same direction.

1.3.1 Effect of Concentrated Localized Fields on MEF

When a fluorophore is placed in the close proximity to a metal it can have increased excitations and radiative decay rates due to near field interactions of LSPR. These near field interactions cause dramatic changes in fluorophores emission. Figure 1.4 (bottom) shows the modified Jablonski diagram of a fluorophore in presence of a metal.

Metals have a large absorption cross section which is about 10^5 greater than that of a fluorophore.^{1d} Thus, metals can strongly interact with incident light. When a fluorophore is placed near a metal; it could also feel the effect of the concentrated fields and have increased excitations (Figure 1.5).

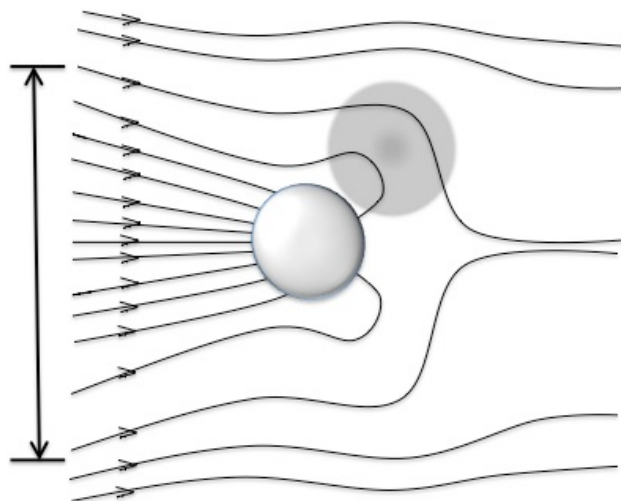


Figure 1.5 Representation of interaction of resonant metal colloid with the electric field of incident light. The lines represent the direction of electric fields. Fluorophore is shown in the near -field of the colloid. [1d]

The increased excitations would result increased emission. This near field effect is also known as “lighting rod effect”.^{1b} In classical experiments if higher emission intensity is required, the intensity of the lamp or the slit width would have to be increased. In biological experiments this approach could increase the auto fluorescence (background) as well as cause tissue damage.⁴ Due to “lightening rod” effect one could achieve massive enhancements with the little amount of excitation energy from the source, thus it could be very useful in clinical diagnostics. It has been reported that the local electric field near a silver nanoparticle can increase up to 140 fold compared to the electric field of the incoming light.⁵ This would increase the local intensity and the rate of excitation about 20,000 fold.^{2a} However the effect of the increased field strength due to the plasmon, decays rapidly with increasing distance, thus the fluorophore should be placed within 15 nm from the metal surface to have increased excitations.^{1b, 17} Another single molecule study had been conducted using fluorescently labeled silver nanoparticles of different sizes (5-100 nm).¹⁸ In this study the electric field intensity around silver nano

particles was calculated using FDTD method (finite-difference time-domain). Their results show that the electric field intensity on 8 nm circle from the metal core would increase with particle size from 5-70 nm and then drop at 100 nm. The fluorescence enhancement follows the same trend indicating that the increased emission could be partly due to the increased field intensity. It should be noted that the “lightning rod” effect does not change the quantum yield of the fluorophore although it increases the emission.⁵ Increased emission is due to the increased excitation of molecules per unit time. Due to “lightning rod” effect the fraction of excited molecules decaying radiatively is not changed.

1.3.2 Effect of Modification of Radiative Decay rate on MEF

Another important near-field interaction that is observed near a metal is the change in radiative decay rate, which increase or decrease the photonic-mode density of the fluorophore.^{1b} If the fluorophore is placed less than 5 nm away from the metal, the metal can strongly quench the fluorophore by direct electron transfer or by resonance energy transfer. Thus, presence of metal can add additional non-radiative pathways, and decrease the quantum yield of the fluorophore. However, if the fluorophore is away from the quenching region of the metal, the near-field interactions could modify the radiative decay rates.^{1d, 8} The experimental evidence show that samples with increased emission show decreased lifetimes. This effect could only result due to increased radiative decay rates. This effect has been predicted theoretically, in Gestern-Nitzan model, for spectroscopic properties of molecules interacting with small dielectric particles.^{2b} This model predicts that the radiative decay rate of a fluorophore can

increase up to a 1000 fold near a metal spheroid. Thus, due to near-field interactions of the metals, fluorophore will have a metal induced radiative decay rate (Γ_m). Furthermore the metal can induce non-radiative decay rate (k_m) if the fluorophore is located within 0-5 nm from the metal surface.

$$Q_m = \frac{\Gamma + \Gamma_m}{\Gamma + \Gamma_m + k_{nr} + k_m} \quad (3)$$

$$\tau_m = \frac{1}{\Gamma + \Gamma_m + k_{nr} + k_m} \quad (4)$$

Equations 3 and 4 show the quantum yield (Q_m) and the life time (τ_m) in presence of the metal. Introduction of the additional radiative decay rate would increase the quantum yield and decrease the life time. Thus, in contrast to classical fluorescence, in MEF, quantum yield and life time would move in opposite directions; as the quantum yield increase the life time would decrease. Additional metal induced radiative decay rate will increase the brightness of the fluorophore (Figure 1.4).

Increased radiative decay rates will result increased photonic-mode density or photon flux of the fluorophore. Therefore, changes in radiative decay rates can result, non-fluorescent species to be highly fluorescent. It has been shown that low quantum yield species such as DNA would be highly fluorescent in presence of metal.^{1b} Furthermore, decreased lifetimes would increase the photostability of the fluorophore. Photochemical degradation depends on the amount of time the fluorophore spends in the excited state. Therefore, if the fluorophore spends less time in the excited state it would minimize the opportunity for photo-degradation. This would be very useful for

single molecule imaging, where the detection of a species is limited by the photon emission rate and the photo stability.^{2a}

Another potentially useful near-field effect that arises due to metal-fluorophore interactions is the plasmon coupled directional emission. Directional emission can improve the collection efficiency of photons about 10 fold greater than the isotropic emission.^{1d}

Furthermore, the increased excitations caused by the near-field interactions can be very useful in imaging techniques that use two-photon excitation. For two-photon excitation, a very high intensity pulsed laser such as Ti- sapphire laser is required. Since metals can increase the local intensity up to 10^4 fold, two photon-excitation should be made easier in presence of the metal.⁵

Most of the initial work in MEF was done by Joseph R. Lakowicz, Chris D. Geddes, and their colleagues. They have published a number of manuscripts and review articles on MEF as cited above.

1.3.3 Distance Dependency between Metal and Fluorophore on MEF

Since MEF is highly sensitive to distance between the metal and the fluorophore, in order to observe these interesting effects it is critical to move the fluorophore away from the quenching region of the metal, which is about 5 nm from the metal surface. Furthermore, to experience the near-field effects of the plasmon, the fluorophore should be placed not more than 30 nm away from the metal surface as well. Thus, most MEF techniques require a 5-10 nm thick spacer between the metal and the fluorophore.¹⁹ This is mostly achieved by the deposition of a silica layer or any other polymer matrix

between the metal and the fluorophore, such as physisorption of dye on to silica or polymer coated metal colloids deposited on a solid surface. To further investigate the optimal distance required for enhancement, a number of studies have been conducted.⁹ ¹⁹⁻²⁰ Tovmachenko et al. have conducted an interesting experiment using gold and silver nanoparticles (AgNPs), coated with a silica spacer shell and a dye labeled silica shell to study the distance dependence.¹⁹ They have observed maximum MEF with AuNPs (6.8) and AgNPs (12.5) at 25 nm distance. Their theoretical calculations show that the optimal spacer thickness to be 20-30 nm.

1.3.4 Radiative Plasmon and Plasmon Scattering

The remarkable optical modifications observed in MEF such as increased quantum yields, decreased lifetimes, increased localized excitations, and increased photo stability, make us wonder what optical or geometric properties of the metal-fluorophore system are responsible for these useful near-field interactions.^{1c, 2a} However, the exact mechanism for MEF is still under investigation. First it was simply defined that it is the surface plasmon which is responsible for radiating to the far-field, this simple explanation did not explain much about the interactions. In 2005 Joseph R. Lakowicz and his colleagues explained these interactions using radiative plasmon (RP) model.⁸ This new field of study is known as radiative decay engineering. Although this model is not conclusively proven, it is generally accepted due to its reasonability.^{1c}

RP model uses Mie theory to explain radiative properties of the metal colloids.¹⁰ Mie theory does not explain metal fluorophore interactions, however, it explains the optical properties of conducting metal spheres. According to Mie theory the extinction

cross section C_E , is composed of two components, the absorption cross section C_A , and scattering cross section C_S .¹⁰

$$C_E = C_A + C_S$$

It is predicted that scattering cross section of the metal represents the ability of a metal nanoparticle to be an oscillating dipole which can radiating electromagnetic waves to the far-field, whereas, absorbed radiation is dissipated as heat, opening paths of non-radiative decay. Mie theory shows that absorption cross section is proportional to the third power of the radius whereas the scattering cross-section is proportional to the sixth power of radius. Furthermore, it has been reported that extinction of smaller colloids about 20 nm, comprise of a larger absorption cross-section and a reasonably smaller scattering cross-section.⁸ As the particle size increase, the scattering cross section would increase. Furthermore, silver nanoparticles with the same size as AuNPs have a larger scattering cross-sections than AuNPs, making silver a better plasmon scatterer than gold.¹⁰ However, scattering of incident light from plasmons is not very useful in identification; moreover, in fluorescence scattering is a property that one would want to eliminate. But for metal nanoparticles it is the scattering component which is responsible for far-field emission. If the nanoparticle is in resonance with the incoming light, both the scattering and the absorption cross-section increase beyond the physical parameters.^{5b} The arrow in figure 1.5 represents the size of the absorption cross-section of a nanoparticle in resonance. Although resonant nanoparticles radiate or scatter the same wavelength as the incident light, when a fluorophore is placed in the close proximity to a metal, the metal can scatter light with a Stokes shift.^{5b}

The radiative plasmon model suggests that an excited fluorophore near a metal can induce plasmons on the metal nanoparticle.^{5b, 21} The fluorophore induced plasmons can radiate to the far-field at the same wavelength as the fluorophore, creating observable emission, this plasmon is called a radiative plasmon. However, it has been observed that the excited state lifetime of the fluorophore decreases drastically in this process. Since plasmon decay rates are rapid (about 50 fs)^{1d} it is thought that the excited fluorophore transfers energy to the plasmon and it is the plasmon that emits to the far-field.^{1a, 5b} Since the plasmon emits the same wavelength as the fluorophore, it is referred to as metal induced radiative decay rate of the fluorophore. Thus, in MEF the emitting species is considered as the metal-fluorophore complex or the plasmophore. Since the emission wavelength matches that of the fluorophore, the quantum yield of the metal-fluorophore complex is interpreted considering the fluorophore. The RP model suggests that if the absorption of the metal particle is dominant over scattering, the fluorophore would quench, whereas, if scattering is dominant the fluorophore would enhance.⁸ Thus, small metal particles would quench fluorescence since absorption is dominant over scattering and large metal particles would enhance fluorescence, since extinction is dominated by scattering.

Thus, to observe MEF it is predicted that the absorbance and the emission of the fluorophore should overlap with the scattering cross-section of the metal. Some reports suggest that overlap of scattering cross-section with the emission band would result enhancement.¹⁵ This is not very well understood. Furthermore, the geometric structure is also important in determining the scattering efficiency. It is reported that rough metal

surfaces or shapes with sharp edges would scatter more light, than smooth surfaces. Therefore, to observe MEF metal nanoparticles with larger scattering potentials are desired.

1.3.5 Effects of Coupled Plasmons on MEF

Another way to promote MEF is through coupled plasmons. It has been predicted that very large enhancement in the electromagnetic field can be obtained when two resonant metal nanoparticles are brought close to each other.²² If a fluorophore is trapped between a coupled plasmon it can be dramatically enhanced due to increased field strength within the coupled plasmon. Furthermore, aggregation of particles would increase the scattering cross-section of the metal fluorophore complex. Reports show that the enhancement due to aggregation could be possible due to increased scattering as well. Thus metal fluorophore aggregation can facilitate MEF in both ways by increased excitations as well as modifying radiative decay rates. These effects will be discussed in detail in chapter 3.

1.4 Research Focus

Researchers have developed various techniques to optimize MEF using metal-fluorophore aggregation. However, most MEF techniques require solid phase attachments, coupled with specialized imaging tools which could be only practical for surface assays. So far very few studies have been performed in solution phase and the reported enhancements for solution based methods are relatively lower than surface immobilization techniques. Since most detection targets are developed in liquid or

aqueous media, study of MEF in solution phase has very high significance. Furthermore, bright fluorescent markers viable in solution media would greatly enhance cellular tracking and imaging in biomedical applications.

The aim of this research is to study metal enhanced fluorescence in solution phase in order to develop bright fluorescent markers, using metal-fluorophore aggregation.

A key issue in MEF is the need to increase the distance between the fluorophores and the metal surface so that the metal would not quench the fluorophore. In our initial method, we decided to cap the AuNPs with a dendron to achieve the desired spacing between the dye and the metal. Therefore, in the first part of the research, we studied the place exchange of different ligands on AuNP surface. However, to place the fluorophore away from the quenching region of the metal, a third generation dendron was needed. Thus, we moved to a new approach to provide desired spacing using dye doped silica nanoparticles with multiple AuNPs aggregated around them. By this approach we expected the dye away from the quenching region of the metal would enhance. This seems to be a synthetically approachable way than the previous method and will be discussed in detail in chapter 3 and 4.

1.5 Chapter 1 References

1. (a) Aslan, K.; Gryczynski, I.; Malicka, J.; Matveeva, E.; Lakowicz, J. R.; Geddes, C. D., Metal-enhanced fluorescence: an emerging tool in biotechnology. *Current Opinion in Biotechnology* **2005**, *16* (1), 55-62; (b) Geddes, C. D.; Lakowicz, J. R., Editorial: Metal-enhanced fluorescence. *Journal of fluorescence* **2002**, *12* (2), 121-129; (c) Lakowicz, J. R., Plasmonics in biology and plasmon-controlled fluorescence. *Plasmonics* **2006**, *1* (1), 5-33; (d) Lakowicz, J. R.; Ray, K.; Chowdhury, M.; Szmecinski, H.; Fu, Y.; Zhang, J.; Nowaczyk, K., Plasmon-controlled fluorescence: a new paradigm in fluorescence spectroscopy. *Analyst* **2008**, *133* (10), 1308-1346.
2. (a) Geddes, C. D.; Gryczynski, I.; Malicka, J.; Gryczynski, Z.; Lakowicz, J. R., Metal-enhanced fluorescence: potential applications in HTS. *Combinatorial Chemistry & High Throughput Screening* **2003**, *6* (2), 109-117; (b) Gersten, J.; Nitzan, A., Spectroscopic properties of molecules interacting with small dielectric particles. *The Journal of Chemical Physics* **1981**, *75*, 1139.
3. Mitchell, P., Turning the spotlight on cellular imaging. *Nature biotechnology* **2001**, *19* (11), 1013-1018.
4. Frangioni, J. V., In vivo near-infrared fluorescence imaging. *Current opinion in chemical biology* **2003**, *7* (5), 626-634.
5. (a) Anker, J. N.; Hall, W. P.; Lyandres, O.; Shah, N. C.; Zhao, J.; Van Duyne, R. P., Biosensing with plasmonic nanosensors. *Nature materials* **2008**, *7* (6), 442-453; (b) Aslan, K.; Lakowicz, J. R.; Geddes, C. D., Plasmon light scattering in biology and medicine: new sensing approaches, visions and perspectives. *Current opinion in chemical biology* **2005**, *9* (5), 538-544.
6. Caro, C.; Castillo, P. M.; Klippstein, R.; Pozo, D.; Zaderenko Ana, P., Silver nanoparticles: sensing and imaging applications. *Silver nanoparticles* **2010**.
7. Eustis, S.; El-Sayed, M. A., Why gold nanoparticles are more precious than pretty gold: Noble metal surface plasmon resonance and its enhancement of the radiative and nonradiative properties of nanocrystals of different shapes. *Chemical Society Reviews* **2006**, *35* (3), 209-217.
8. Lakowicz, J. R., Radiative decay engineering 5: metal-enhanced fluorescence and plasmon emission. *Analytical biochemistry* **2005**, *337* (2), 171-194.
9. Zhang, J.; Lakowicz, J. R., Metal-enhanced fluorescence of an organic fluorophore using gold particles. *Optics express* **2007**, *15* (5), 2598.

10. (a) Quinten, M.; Leitner, A.; Krenn, J.; Aussenegg, F., Electromagnetic energy transport via linear chains of silver nanoparticles. *Optics Letters* **1998**, *23* (17), 1331-1333; (b) Su, K. H.; Wei, Q. H.; Zhang, X.; Mock, J.; Smith, D.; Schultz, S., Interparticle coupling effects on plasmon resonances of nanogold particles. *Nano letters* **2003**, *3* (8), 1087-1090.
11. Zhang, J.; Fu, Y.; Ray, K.; Chowdhury, M. H.; Szmecinski, H.; Nowaczyk, K.; Lakowicz, J. R., Single molecule photophysics near metallic nanostructures. *Progress in biomedical optics and imaging* **2008**, 68620S. 1-68620S. 10.
12. (a) Zhang, Y.; Dragan, A.; Geddes, C. D., Metal-enhanced fluorescence from tin nanostructured surfaces. *Journal of Applied Physics* **2010**, *107*, 024302; (b) Aslan, K.; Previte, M. J. R.; Zhang, Y.; Geddes, C. D., Metal-enhanced fluorescence from nanoparticulate zinc films. *The Journal of Physical Chemistry C* **2008**, *112* (47), 18368-18375; (c) Chowdhury, M. H.; Ray, K.; Gray, S. K.; Pond, J.; Lakowicz, J. R., Aluminum nanoparticles as substrates for metal-enhanced fluorescence in the ultraviolet for the label-free detection of biomolecules. *Analytical Chemistry* **2009**, *81* (4), 1397-1403.
13. Thomas, K. G.; Kamat, P. V., Chromophore-functionalized gold nanoparticles. *Accounts of chemical research* **2003**, *36* (12), 888-898.
14. De Santis, G.; Fabbrizzi, L.; Licchelli, M.; Poggi, A.; Taglietti, A., Molecular recognition of carboxylate ions based on the metal–ligand interaction and signaled through fluorescence quenching. *Angewandte Chemie International Edition in English* **1996**, *35* (2), 202-204.
15. Tam, F.; Goodrich, G. P.; Johnson, B. R.; Halas, N. J., Plasmonic enhancement of molecular fluorescence. *Nano letters* **2007**, *7* (2), 496-501.
16. Strickler, S.; Berg, R. A., Relationship between absorption intensity and fluorescence lifetime of molecules. *The Journal of Chemical Physics* **1962**, *37*, 814.
17. Zhang, Y.; Dragan, A.; Geddes, C. D., Wavelength dependence of metal-enhanced fluorescence. *The Journal of Physical Chemistry C* **2009**, *113* (28), 12095-12100.
18. Zhang, J.; Fu, Y.; Chowdhury, M. H.; Lakowicz, J. R., Single-molecule studies on fluorescently labeled silver particles: Effects of particle size. *The Journal of Physical Chemistry C* **2008**, *112* (1), 18-26.
19. Tovmachenko, O. G.; Graf, C.; van den Heuvel, D. J.; van Blaaderen, A.; Gerritsen, H. C., Fluorescence Enhancement by Metal-Core/Silica-Shell Nanoparticles. *Advanced materials* **2006**, *18* (1), 91-95.

20. (a) Kümmerlen, J.; Leitner, A.; Brunner, H.; Aussenegg, F.; Wokaun, A., Enhanced dye fluorescence over silver island films: analysis of the distance dependence. *Molecular Physics* **1993**, *80* (5), 1031-1046; (b) Ray, K.; Badugu, R.; Lakowicz, J. R., Distance-dependent metal-enhanced fluorescence from Langmuir-Blodgett monolayers of alkyl-NBD derivatives on silver island films. *Langmuir* **2006**, *22* (20), 8374-8378.
21. Hartlen, K. D.; Athanasopoulos, A. P. T.; Kitaev, V., Facile preparation of highly monodisperse small silica spheres (15 to > 200 nm) suitable for colloidal templating and formation of ordered arrays. *Langmuir* **2008**, *24* (5), 1714-1720.
22. Zhang, J.; Fu, Y.; Chowdhury, M. H.; Lakowicz, J. R., Metal-enhanced single-molecule fluorescence on silver particle monomer and dimer: coupling effect between metal particles. *Nano letters* **2007**, *7* (7), 2101-2107.

Chapter 2: Study of Place Exchange of Alkanethiol Tethered Fluorescent Dyes and Ligands on Gold Nanoparticle Surface

2.1 Chapter Overview

This chapter presents the place exchange studies conducted by tethering fluorescent dyes and ligands on gold nanoparticle (AuNP) surfaces. A method designed to synthesize bright fluorescent markers using metal-enhanced fluorescence (MEF) was based on capping gold nanoparticles with a dendron to get the desired spacing between the metal surface and the fluorophore. For the attachment of the dendron, it was necessary to study the place exchange of ligands on AuNP surface. Therefore, an initial study was conducted to gain knowledge and experience of AuNP synthesis, ligand exchange and to study the photophysical properties of dye capped AuNPs. Although we eventually used a different approach to observe MEF, this study gave us some deep insight into place exchange procedures as well as to the plasmon interactions of fluorophores directly attached to the metal surface.

In this study, place exchange of ligands on AuNP surface was monitored by tethering a neutral fluorescent dye (BODIPYdecylthioacetate) to AuNP surface. As a result, we were able to establish a method to control the density of dye loaded on the nanoparticle surface using a competing ligand. We have also calculated the molar fluorescence, which is an intrinsic property of the adsorbed dye, and studied how it would vary with the packing density of dye on AuNP surface. Furthermore, we were able to figure out the amount of alkanethiols required to saturate the nanoparticle

surface experimentally, and match the experimental values with the estimated numbers. This chapter includes the synthesis of AuNPs, tethering of fluorescent dye neutral BODIPYdecylthioacetate to AuNP surface by alkanethioacetate cleavage, stability of fluorophore capped AuNPs in different solvent systems and the place exchange procedures developed for capping AuNP surface with anionic and neutral alkanethiols.

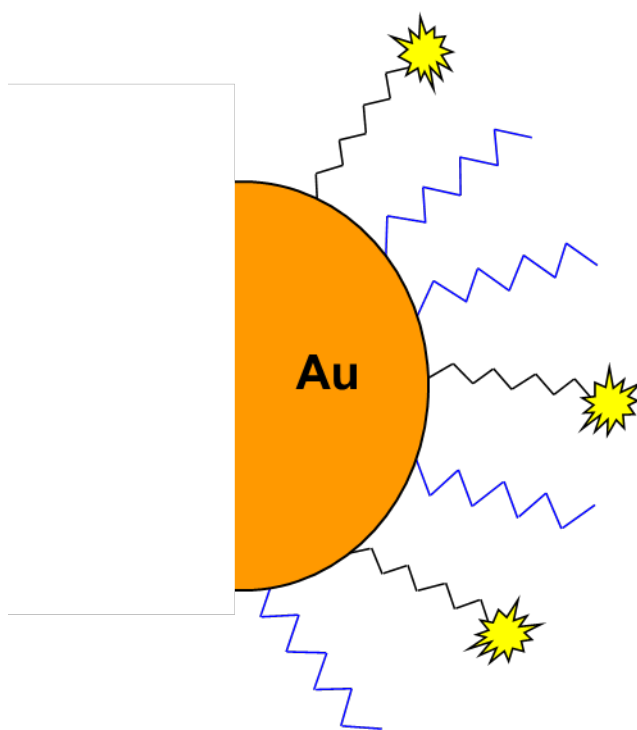


Figure 2.1 Place-exchange of tethered fluorescent dyes and ligands on AuNP surface.

2.2 Introduction

During the past few decades there has been a growing interest among scientists to harvest optical properties of noble metal particles in the nanometer regime (1-100 nm).¹ Nanostructures are distinguished from bulk materials from the fact that a high percentage of the constituent atoms are found at a surface. Thus, it is said that in the nano regime, the surface represents the fourth state of matter, where the gradient of properties are the greatest.^{1c} Modification of the nanoparticle surface with organic fluorophores is an emerging field which can be very useful in the development of optoelectronic devices, efficient light-energy conservation systems, data storage systems and optical sensors.^{1b, 2} The interactions of fluorophores with a bulk metal surface have been studied to some extent in the past. Tethering them to metal nanoparticles is a fairly new field, found to give a lot of interesting aspects to explore. The focus of this research is to develop a solution based approach to study metal-enhanced fluorescence (MEF) by aggregation of fluorophore tethered gold nanoparticles. Although metal-enhanced fluorescence was first observed with silver nanoparticles, recently, gold colloids are more attractive for solution based experiments due to their known surface chemistry and stability.^{1d, 3}

Gold nanoparticles (AuNPs) are considered as the most stable metal nanoparticles on earth.^{2b} Colloidal gold was first used to make ruby glass and for coloring ceramics in the 5th to 4th century B.C. In the middle ages soluble gold was famous for its curative powers for various diseases.⁵ In 1857 Michal Faraday first

reported that the color of gold results due finely divided colloidal gold particles.^{1d}

Recently, AuNPs have attracted photo-chemists and biologists due to their interesting plasmonic properties caused by the collective oscillations of surface electrons on nanoparticle surface and also due to biological inertness and stability.

What make AuNPs special among other metals is their known surface chemistry and the ease of surface functionality. The surface of metal nanoparticles has a higher affinity to adsorb organic materials since they facilitate to lower the free energy of the interface between the metal and the surrounding environment.^{1c} The organic adsorbents can prevent nanoparticle aggregation, decrease reactivity of surface atoms and act as an insulating film. However, coating the surface with a random mixture of organic materials is not very useful in the development of nano devices. Organic molecules can also form highly ordered structures on metal surfaces spontaneously, which are known as self-assembled monolayers (SAMs).^{1c}

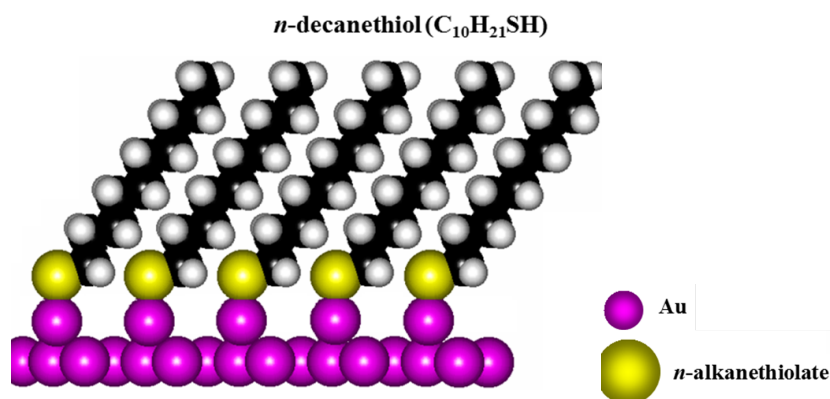


Figure 2.2 Self assembled monolayer of alkanethiols on gold surface. (Diagram produced by Lloyd Bumm)

Molecules that form SAMS possess a functionality which has a very high affinity for the metal surfaces, thus, they can displace the loosely bound adsorbents and arrange uniformly on metal surface. The most commonly used ligands for formation of SAMS are alkanethiols. Thiols have a very high affinity for metals, thus alkanethiols can be attached to the nanoparticle surface by Au-S chemisorption and further stabilized by intermolecular interactions of the hydrocarbon chains. Our group, with collaboration of Dr. Bumm's group in the physics department has also published on formation of highly ordered SAMS on Au substrates by cleavage of alkanethioacetate at bench top conditions.^{1b, 4}

Monolayer protected AuNPs are highly desirable since they provide a platform to carry out the desired chemistry on a nanoparticle surface in the solution phase. Photophysical properties of AuNPs can be controlled by tailoring the capping group of the nanoparticle. The composition of the capping or the monolayer can be fabricated in three ways. First is synthesizing the nanoparticle with a capping with the desired functionality. Second is ligand exchange and the third is modification of original capping to achieve the desired functionality by an interfacial reaction.^{1c}

In this study we have used ligand exchange or place exchange, where one ligand is displaced by another to modify the surface of AuNPs. Ligand exchange is used for surface modification when the ligand is not compatible with the reductive environment of the nanoparticle surface or when the ligand is not commercially available to be used in excess. Furthermore, ligand exchange is very useful when partial or random modification of the monolayer is desired. Place exchange by thiols is possible when nano particles are capped with weakly bound ligands such as citrates or phosphines.

Simple thiols can also be exchanged by high concentrations of more complex thiols or with disulfides which have an even higher affinity for gold surface than simple thiols.

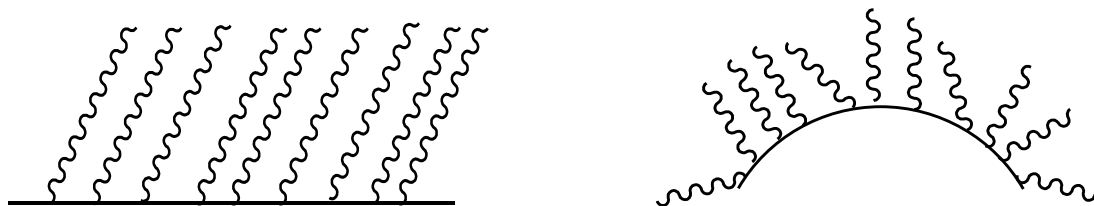


Figure 2.3 Well-ordered SAM on a flat surface (left), and non-ordered SAM on curved surface (right).

It has been reported that the ligand exchange would also depend on the curvature of the AuNP surface; particles less than 4.4 nm diameter would accommodate a higher density of ligands than a flat surface.⁵ As the size increases nanospheres will have similar characteristics as SAM on planar surfaces. Molecular dynamic simulation study of SAMs with alkanethiol surfactants show, that alkanethiols would result in larger tilt angles on spherical AuNPs than flat gold nanoparticles due to the effect of curvature.⁵ Thus SAMs on spherical metal clusters would create clefts or crevices on AuNP surface. Studies show that place exchange would maximize at these edges and the rate of exchange would decrease with increasing chain length of the capped ligand.

Fluorescent dyes can be attached to AuNPs using functional groups such as thiols, amines and thiocyanates.^{1b, 2} Dyes directly attached to the AuNP surface are usually quenched, due to electron transfer or resonance energy transfer. Number of studies has been carried out to study the fluorescence quenching mechanisms of dye attached on AuNPs. Murray and co-workers have published about quenching of fluoresceine by AuNPs, Dulkieth et al. and S.K gosh et al. have also studied fluorescence quenching of

dye attached to differently sized AuNPs.^{1a, 6} Furthermore, Kammat and co-workers have observed optical enhancements when Rhodamine 6G coated AuNPs form clustered aggregates.⁷ The same group have studied fluorescence of pyrene derivatives on gold surface and observed suppression in quenching.⁸

Study of fluorophore-bound gold nanoparticles provides an efficient route to examine mechanistic information of various deactivation pathways on nanoparticle surface. Furthermore, they can be used to monitor place-exchange reactions on nanoparticle surface. In this study we have used fluorophore-bound AuNPs to monitor place-exchange reactions on AuNP surface and develop new place-exchange procedures.

Although quenching properties of gold have been studied to some extent, very little is known about the photophysical properties of dye adsorbed on AuNPs surface. In this study we have also investigated the change in molar fluorescence of the dye adsorbed on AuNP surface.

2.3 Results and Discussion

2.3.1 Synthesis of Gold Nanoparticles

AuNPs of various shapes and sizes are synthesized by reduction of a gold salt (HAuCl_4) to form colloidal gold. There are number of different techniques to synthesize AuNPs. The most commonly used method to produce size controlled, spherical AuNPs is citrate reduction. This method was introduced by Turkevich in 1951, where gold salt is reduced by trisodium citrate at high temperature in aqueous solutions.⁹ In other techniques, gold salt is first reduced by a strong reducing agent such as sodium borohydride to produce small spherical particles or seeds. Next seeds are transferred to a growth solution where size controlled growth takes place. The growth solution contains more metal ions, surfactants and a weak reducing agent, where particles are grown slowly on the seeds capped with the surfactant. Two phase reactions have also been used to produce thiol capped AuNPs in 1-5 nm range. Furthermore, inverse micelles have been used to generate different sizes and shapes of AuNPs. In any method to obtain mono-disperse particles it is necessary to have rapid nucleation below saturation and controlled growth until all precursors are consumed.^{1c}

For our study AuNPs were synthesized by standard citrate reduction method introduced by G. Frens which is a modified version of Turkevich's prep.¹⁰ In this method monodisperse gold nanoparticles are prepared by reduction of HAuCl_4 by trisodium citrate in boiling water. This method is suitable when a rather loose shell of ligands is required around the gold core. In citrate reduction the size of the

nanoparticles can be controlled by the amount of citrate added to the boiling solution of HAuCl_4 . By decreasing the amount of citrate, larger nanoparticles can be produced but the size distribution of these nanoparticles would be greater. This method is most suitable to synthesize nanoparticles below 20 nm diameter. In citrate reduction, citrate ions serve as a reducing agent as well as a capping agent. Negatively charged citrate capping will stabilize gold nanoparticles in water, preventing aggregation. A solution of suspended AuNPs is called a “sol” rather than a solution.

It is interesting to know how citrate ions facilitate the reduction process of gold salt. Sanjeeve Kumar et al. have modeled the formation of AuNPs by citrate reduction.¹¹ According to their study, the first step is the oxidation of citrate to form dicarboxy acetone, releasing carbon dioxide and two electrons. In the second step auric salt consumes the electrons and converts to aurous salt. The next step is disproportionation of aurous species to gold atoms. In this step dicarboxy acetone facilitates in forming a complex to combine three aurous molecules to form gold particles or to initiate nucleation. The study shows that at least two dicarboxy acetone molecules are required to combine three aurous ions. Furthermore, at high temperatures dicarboxy acetone decomposes to acetone and carbon dioxide. This model indicates that it is the balance between the rate of nucleation and the decomposition of dicarboxy acetone that determines the particle size. Therefore, the particle size would depend on the citrate to HAuCl_4 ratio.

For our study we used the amount of citrate required to synthesize 16 nm AuNPs. During the process, when trisodium citrate is added to boiling HAuCl_4 solution, within one minute the solution turn from colorless to pale blue indicating the formation of gold

nuclei. Within three minutes the boiling solution changes color to brilliant red indicating completion of formation of AuNPs. The characteristic color of the particles results from the localized surface plasmon resonance. Nanoparticles within 10 to 20 nm diameter would appear as bright red, transparent solutions. As the particle size increases the color would change from bright red to murky brown and also the solution would be more translucent due scattering of light from larger nanoparticles. For the AuNP synthesis in our study, although we used the amount of citrate required to produce 16 nm AuNPs, the TEM studies show that average particle diameter to be 13 nm.

Figure 2.4 shows the broad absorption spectra of synthesized AuNPs ranging from 400-600 nm with an absorbance maximum at 520 nm. The solution appears to be bright red, due to absorption of green light.

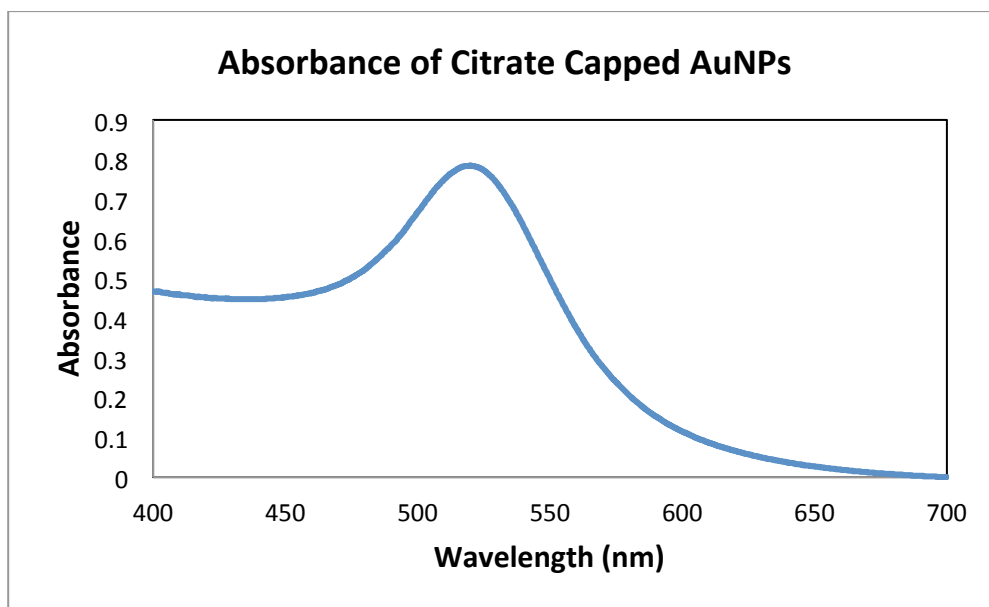


Figure 2.4 Absorbance spectra of citrate capped 13 nm diameter AuNPs in water.

2.3.1.1 Estimation of Concentration of AuNPs

Concentration of the AuNPs can be calculated using the extinction coefficient of AuNPs. Xiong Lui et al. have studied the extinction coefficients of AuNPs with different sizes ranging from 4-40 nm, capped with three types of ligands in different solvents; citrate stabilized AuNPs in water, decanethiol-protected AuNPs in toluene and oleylamide-protected AuNPs in THF.¹² Their findings indicate that, despite different cappings and different solvents, for most AuNPs a linear relationship exist between the double logarithm plot of the extinction coefficient against the nanoparticle diameter. This finding somewhat contradicts the Mie theory which suggests that plasmon resonance absorbance depends on the dielectric of the surrounding media which includes both capping ligands as well as the solvent. However, their values appear to be closer to the theoretical values predicted by El-Sayed et al.¹³ We used this linear relationship to calculate the extinction coefficient of the citrate capped AuNP solution. The linear relationship is given as,

$$\ln \varepsilon = k \ln D + a$$

Where, ε is the extinction coefficient in $M^{-1}cm^{-1}$, D is the particle diameter in nm, $k=3.32111$ and $a=10.80505$. In this study particle diameters were determined by high resolution transmission electron (TEM) microscopy.

The TEM studies show that average particle diameter to be 13 nm. Therefore, we assumed D to be 13 nm in calculating the extinction coefficient. The extinction coefficient was found to be $2.47 \times 10^8 M^{-1}cm^{-1}$. The concentration was calculated using the Beer's law,

$$A = \epsilon b c$$

Where, A is the absorbance (0.785) obtained from figure 2.4, ϵ is the extinction coefficient in ($\text{cm}^{-1}\text{M}^{-1}$), b is the path length in (1 cm) and c is the concentration (M). The concentration of the citrate capped sol was found to be $3.3 \times 10^{-9} \text{ M}^{-1}$ which is 3.3 nM. We have calculated the concentration of citrate capped AuNPs, by starting with the amount of HAuCl_4 used, assuming 100% of the gold salt to be converted to AuNPs. By this mathematical estimation we found the concentration should be 2.3 nM, which is considerably close to the actual value obtained using the extinction coefficient.

2.3.2 Capping Gold Nanoparticles with Fluorescent Dyes

Two dyes, BODIPY and rosamine were modified with decylthioacetate tethers to be attached on AuNP surface using thiolate affinity. The synthesis of BODIPYdecylthioacetate and tethering of both dyes with alkanethioacetate tethers were carried out by Anuradha Singh in Dr. Halterman's lab. BODIPY is a neutral dye whereas rosamine is a cationic dye. Since AuNPs are stabilized in solution with a negatively charged citrate capping, if we tether a positively charged dye it would cause aggregation. Therefore, the neutral dye, BODIPY with an absorbance maximum of 521 nm, was chosen for our initial experiments. The fluorescence emission maximum of this dye is at 530 nm. Figure 2.5 shows the structure of the dye.

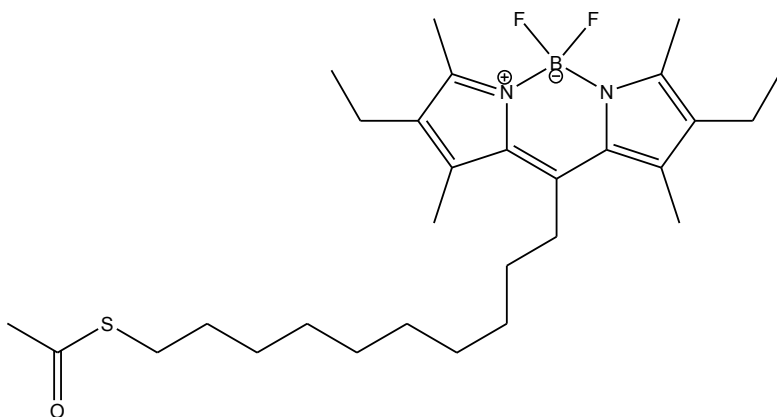


Figure 2.5 Structure of BODIPY decylthioacetate.

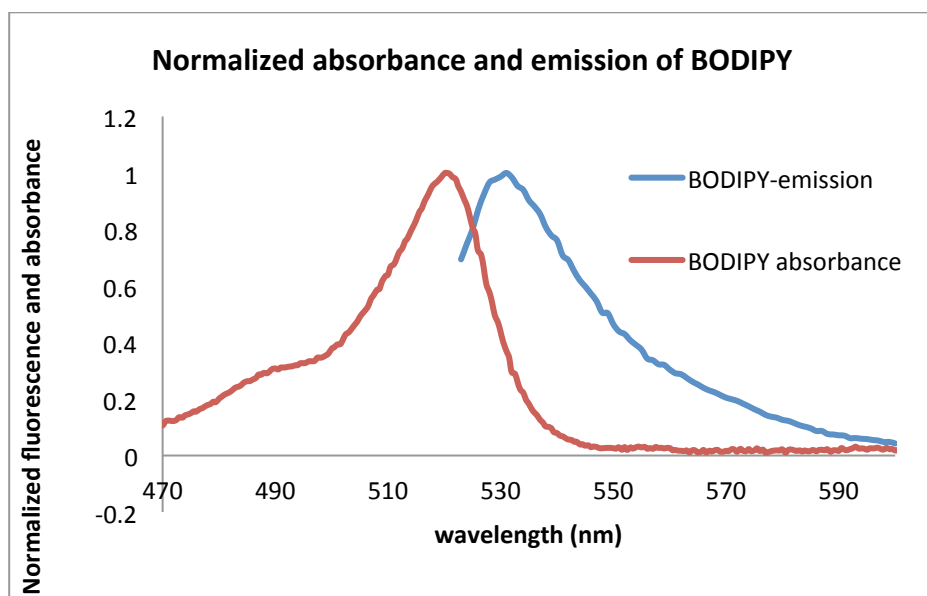


Figure 2.6 Normalized absorbance and emission of BODIPY decylthioacetate.

Previous work from our group with collaboration of Dr. Bumm's research group suggest that pre-cleaving alkenethioacetate to alkenethiol using a suitable base such as KOH would result highly ordered SAMS on gold surfaces. Thus, the acetate group of BODIPY was pre-cleaved with an equivalent amount of KOH, 30 minutes before mixing with AuNPs. Upon addition of AuNPs, the loosely bound citrate capping would be displaced by the thiolate group and attach BODIPY to the AuNP surface. To obtain

the amount of dye that was adsorbed on AuNPs, the dye capped sols were centrifuged at 15,000 rpm for 15 minutes in a micro centrifuge and the supernatants were collected. The amount of dye adsorbed on AuNPs was calculated by subtracting the supernatant absorbance from the initial dye absorbance.

2.3.3 Stability of Sol/Dye Mixtures

In our initial studies sol/dye mixtures were prepared in water since AuNPs are synthesized in water. One drawback of this method was that the dye fluorescence would extremely diminish in water, since BODIPY is not very soluble in water, it would aggregate and quench its fluorescence. Therefore, the stability of AuNPs was investigated in ethanol. Although the sol was unstable in absolute ethanol, we found that it could exist in 85% ethanol without aggregation. Thus, the sol/dye mixtures were diluted with 95% ethanol so that the dye could regain its fluorescence.

Improving the Stability of the Sol/Dye Mixture by Ligand Exchange

For our initial experiments in stability studies, 3 mL of citrate capped sol was used and samples were diluted to 10 mL with 95% ethanol. The concentration of BODIPY was kept to be 1 μ M. When nanoparticles were close to saturation with neutral dye the aggregation was rapid with large aggregates forming within 30 min. The reason for aggregation could be due to the replacement of negatively charged citrate capping with neutral dye. The stability studies helped us to realize that we could minimize the amount of aggregation by decreasing the amount of AuNPs. Thus, we reduced the amount of AuNPs to 1.5 mL. It was observed that even in dilute solutions, partially

dye saturated nanoparticles were subjected to aggregation within a few hours. Therefore, to prevent further aggregation a negatively charged ligand with a thiol head group was introduced to the sol/dye mixture.

The purpose of introducing a negatively charged ligand is that it could compete with the dye to attach on gold surface. Since the ligand is negatively charged it would help to prevent aggregation. Furthermore, this would allow us to study the place exchange of ligands on nanoparticle surface. The ligand we used was 11-mercaptoundecanoic acid (Figure 2.7). The acid was deprotonated before adding to the sol/dye mixture to make it negatively charged.

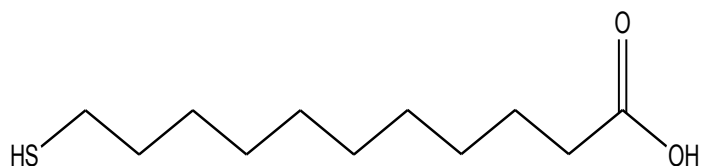


Figure 2.7 11-Mercaptoundecanoic acid.

After introducing this ligand we were able to regain the stability of sol, and also attach neutral dye to AuNP surface successfully. Furthermore, it was observed that less than 0.25 μM concentration of dye was enough to saturate 1.5 mL citrate capped sol. However, calculating the amount of dye using the absorbance data was not very efficient because the difference in the absorbance of the free dye and that of the supernatants was not very significant. Thus, we reduced the concentration of dye to 0.4 μM . The absorbance of 0.4 μM dye was less than 0.05 absorbance units. Therefore, the dye was dilute enough to calculate the adsorbed dye concentration using fluorescence.

Finally, we were able to come up with a method to control the density of dye loaded onto nanoparticle surface.

2.3.4 Controlling the Density of Dye Loaded on the Nanoparticle Surface

The stability studies led us to develop a method to control the loading of dye on a nanoparticle surface using a competing ligand. This method was very helpful to study the place-exchange on AuNP surface and develop several useful procedures to cap AuNPs with other ligands. Furthermore, we were able study some interesting photo-physical properties of the adsorbed dye using this method.

In this method the dye was pre-mixed with a competing ligand where the dye concentration was kept constant and the ligand concentration was varied. To each sample same amount of citrate capped AuNPs (1.5 mL) were added. We assumed, by keeping the amount of dye constant (0.4 μM) and varying the concentration of competing ligand (0-10 μM) we could change the amount of dye that packs on nanoparticle surface. The amount of unbound dye was obtained by measuring the fluorescence of the supernatants collected after centrifuging the samples. Subtraction of the amount of unbound dye from the initial amount of dye added to each sample allowed us to estimate the amount of adsorbed dye.

Initially, control experiments were carried out to check whether the dye emission absorbance would change by introducing the competing ligand, which is the deprotonated form of 11-mercaptoundecanoic acid (figure 2.8). Thus, varying amounts of ligand were titrated with constant amount of AuNPs to see whether the plasmon absorbance would change with the addition of the ligand (figure 2.9).

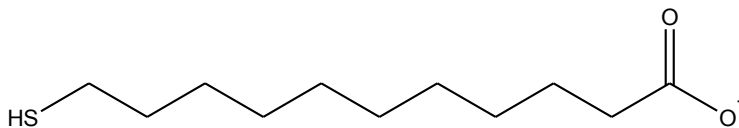


Figure 2.8 Competing ligand- (11-mercaptoundecanoate)-(MUA)

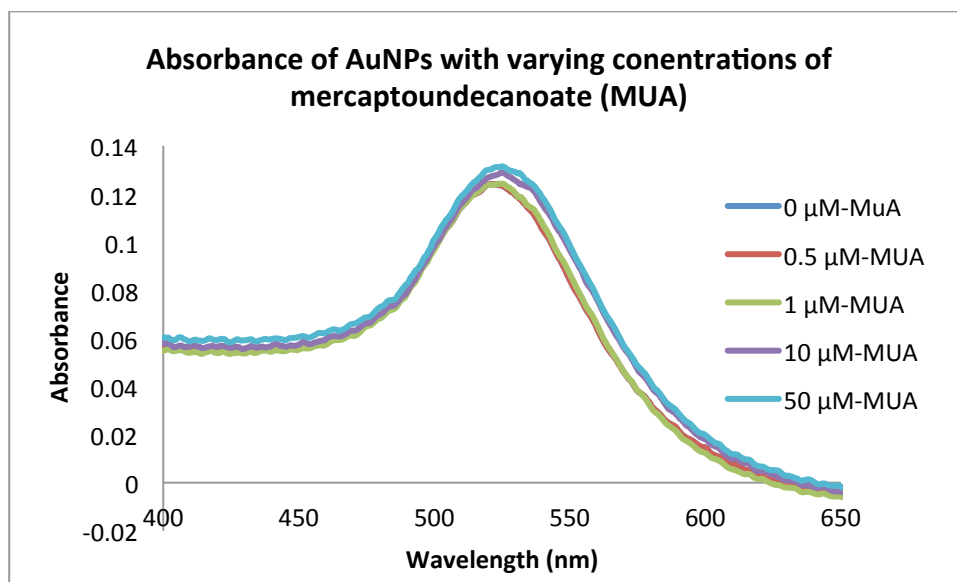


Figure 2.9 Absorbance of 1.2 nM AuNPs after ligand exchange with varying concentrations (0-50 μM) of MUA.

Figure 2.9 shows that the plasmon absorption has not considerably changed upon addition MUA below of 1μM concentration. However, at higher concentration the plasmon had red shifted slightly.

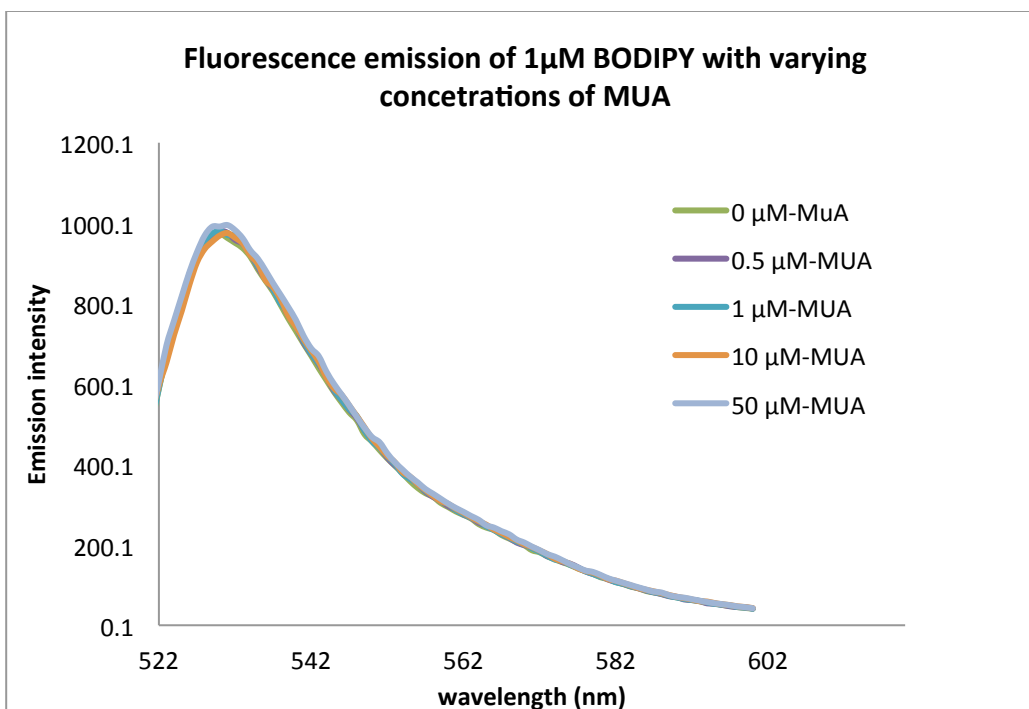


Figure 2.10 Fluorescence emission of 1 μ M BODIPY decylthioacetate with varying MUA (mercaptoundecanoate) concentrations (0-50 μ M) in 85 % ethanol. Samples excited at 521 nm.

Figure 2.10 shows that the fluorescence emission of the dye had not changed by the presence of the ligand. Since the ligand has no effect on emission of the dye, fluorescence data was used for analysis. This was possible because the absorbance of 0.4 μ M dye was below 0.05 absorbance units.

2.3.4.1 Investigation of Spectral Properties of Dye Loaded Gold Nanoparticles

In preparing the samples, constant amount of BODIPYdecylthioacetate was premixed with varying amounts of MUA, and next a constant amount of AuNPs (1.5 mL) were added to each sample, finally the samples were diluted with 95 % ethanol to 10 mL in volumetric flasks and the mixtures were kept in the dark for 24 h for place exchange. Thus, each sample contained 0.4 μ M BODIPY and 1.5 mL of AuNPs. The amount of MUA was varied from 0-10 μ M. All samples were prepared in triplicate. After 24 h, 1.5 mL aliquots of each sample was removed and centrifuged to spin down the AuNPs and the supernatants were collected. Fluorescence of the sol/dye mixtures and the supernatants was measured by exciting the samples at 520 nm.

The Following graphs show the averaged fluorescence emission spectra of sol/dye mixtures (Figure 2.11) their supernatants (Figure 2.12) and the isotherms generated using fluorescence maxima of sol/dye mixtures and their supernatants (Figure 2.13).

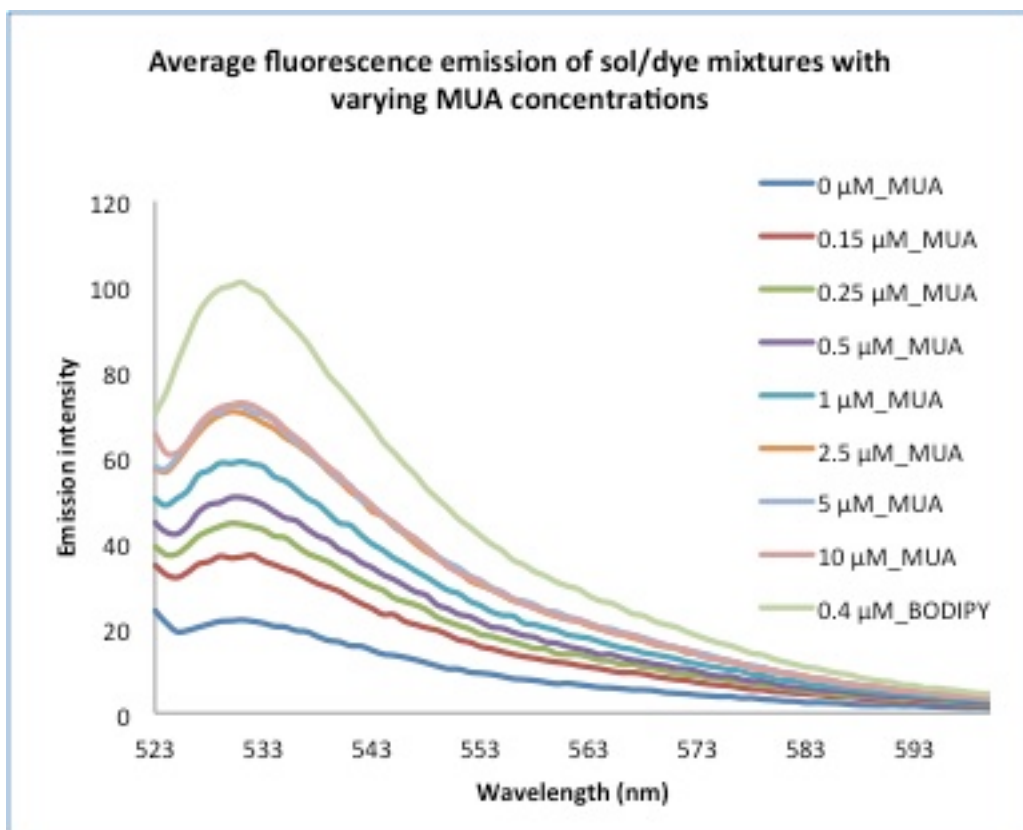


Figure 2.11 Average fluorescence emission of sol/dye mixtures containing 0.4 uM BODIPY, 1.5mL AuNPs with varyong concentrations of MUA 0-10 uM (a-h) and the fluorescence emission 0.4 uM dye without AuNPs (free-dye). Samples were excited at 521 nm.

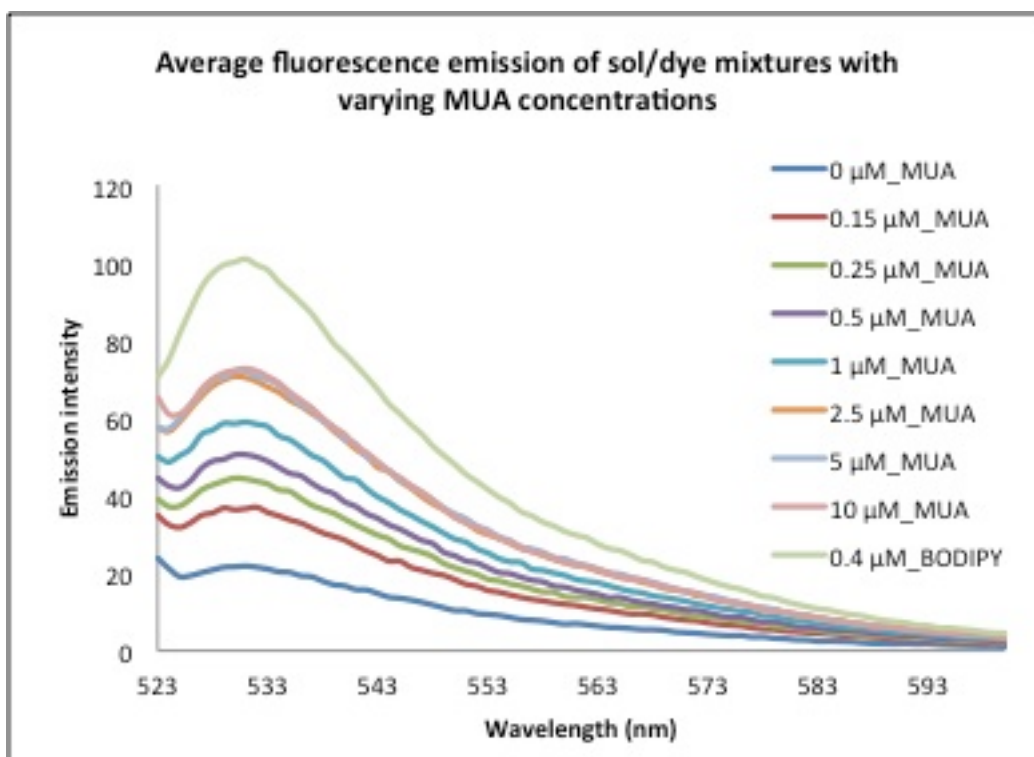


Figure 2.12 Fluorescence emission of supernatants of sol/dye mixtures containing 0.4 μM BODIPY, 1.5 mL AuNPs and varying concentrations of MUA (0-10 μM) and fluorescence emission of 0.4 μM dye without AuNPs (free-dye). Samples were excited at 521 nm.

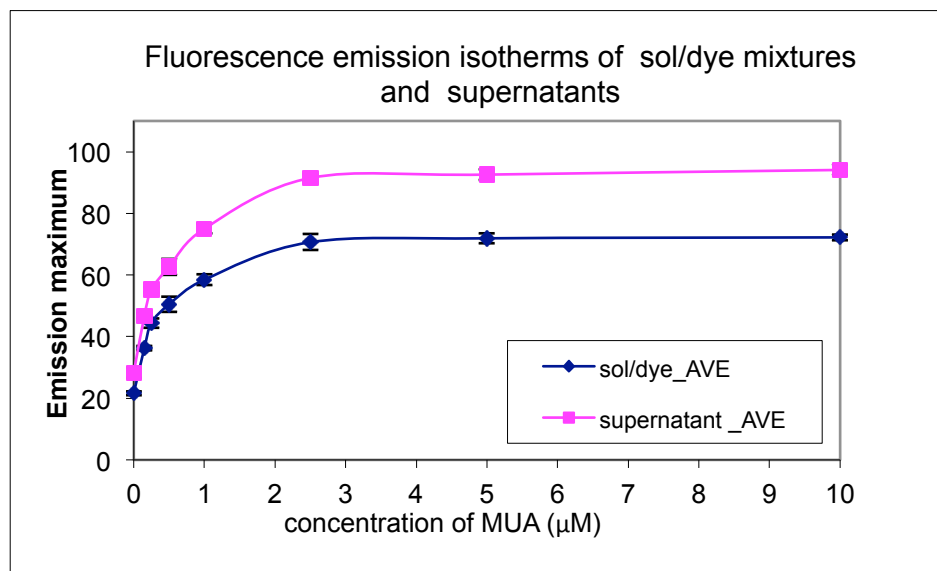


Figure 2.13 Fluorescence isotherms of sol/dye mixtures and supernatants, generated by plotting the average fluorescence emission maxima of sol/dye mixtures and supernatants against the MUA concentration (Fluorescence maxima was measured at 530 nm).

The emission spectra in figure 2.11 indicate that the fluorescence emission maximum of sol/dye mixtures have the same emission maxima at 530 nm as the free dye without AuNPs. Therefore, there is no significant shift in λ_{max} of dye with and without AuNPs. However, we observe an interesting trend in fluorescence emission intensity of sol/dye mixtures and supernatants, with increasing MUA concentration. The lowest fluorescence emission is observed for the sol/dye mixture with 0 uM MUA. With no MUA in solution, the dye can easily access the AuNP surface. Therefore, we can see that the dye attached to the AuNP surface is greatly quenched. As we increase the MUA concentration, both dye and MUA would compete for the nano-particle surface, thus, we observe a gradual increase in the emission intensity up to 1 μM concentration and then reach saturation at 5 uM concentration. This trend is observed because the amount

of free dye in solution would increase as we increase the concentration of MUA and once the surface is completely saturated with MUA the curves would level off, indicating that almost all of the dye remains free (unattached) in solution.

Although we would expect the MUA saturated sol/dye mixtures to have the same emission intensity as the 0.4 μM BODIPY without AuNPs, their emission seem to be lower than that of BODIPY without AuNPs in solution. This could be due to inner-filter effects of AuNPs present in solution. Emission spectra of supernatants (Figure 2.12) show the same trend as the emission of the sol/dye mixtures. But the overall emission intensity is higher than that of the sol/dye mixtures, also the fluorescence of the supernatants of saturated solutions have reached the emission intensity of 0.4 μM BODIPY without AuNPs. This indicates that the overall decrease in fluorescence of sol/dye mixtures could be due inner-filter effects caused by the absorbance of excitation light and the emitted light by AuNPs present in solution. Thus, emission of sol/dye mixtures was corrected for inner-filter effects (a detailed description will be included in the experimental part). Figure 2.14 shows the fluorescence isotherm of sol/dye mixtures generated after correcting for the inner-filter effects. It was observed that after the correction, the emission intensity of sol/dye mixtures has increased above the supernatants.

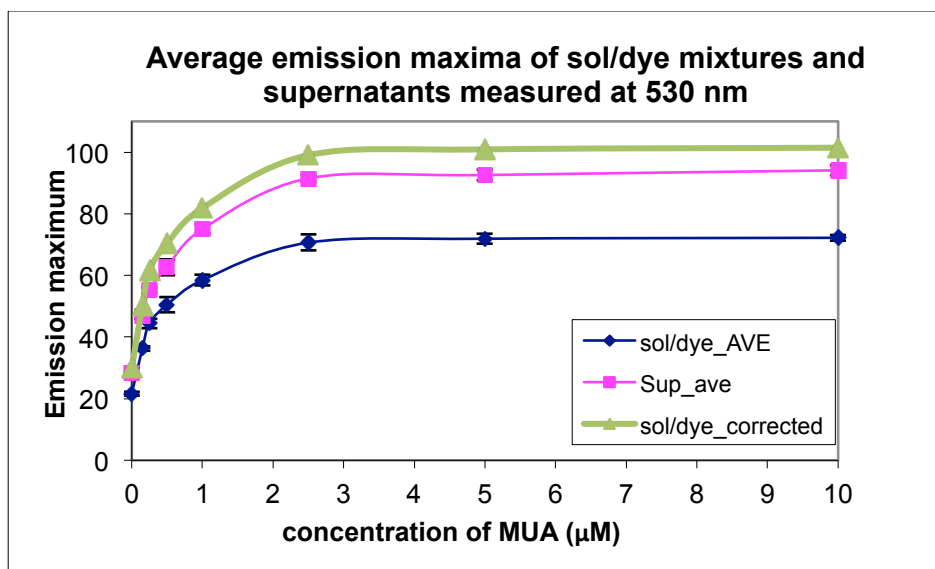


Figure 2.14 Fluorescence isotherms of sol/dye mixtures and supernatants, and sol/dye mixtures corrected for the inner-filter effects, generated by plotting the average fluorescence emission maxima of sol/dye mixtures and supernatants against the MUA concentration.

The two isotherms in figure 2.13 and 2.14 show the variation of the observed and corrected fluorescence emission maxima at 530 nm of sol/dye mixtures and the supernatants against MUA concentration. The fluorescence emission titrations indicate that we have been able to control the loading of dye on AuNP surface by varying the concentration of the competing ligand. The isotherms indicate that the AuNPs reach saturation limit at above 1 μM MUA concentration and total saturation at 5 μM concentrations.

2.3.4.2 Calculation of Concentration of Adsorbed Dye

Concentration of the adsorbed dye in each sample was calculated using molar fluorescence of BODIPY. This was possible since the absorbance of 0.4 μM BODIPY was below 0.05 absorbance units. The molar fluorescence of BODIPY in the given water/ethanol mixture was found to be $439 \mu\text{M}^{-1}$. The amount of the adsorbed dye was calculated by subtracting the fluorescence of the supernatants of each mixture from the fluorescence of 0.4 μM BODIPY and then dividing by the molar fluorescence. Figure 2.14 shows the variation of adsorbed dye on AuNPs with changing MUA concentration.

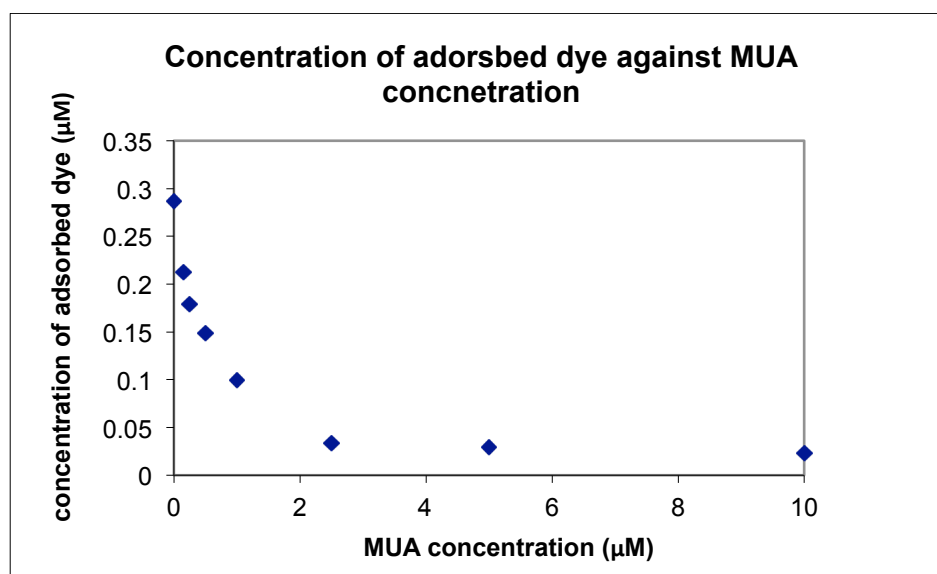


Figure 2.15 Concentration of adsorbed dye on AuNP surface against the MUA concentration.

A decrease in the concentration of adsorbed dye is observed with increasing the concentration of competing ligand (MUA). This graph further confirms that the loading of dye on AuNPs can be systematically reduced by increasing the concentration of the competing ligand concentration.

2.3.5 Estimation of Amount of Alkanethiols Required For Saturation

The data from the place exchange study were useful to gather information about the conditions required to saturate AuNP surface with alkanethiols. The isotherms show that the AuNPs in the sample would saturate with MUA above 1 μM concentrations. To predict the validity of our results, the amount of alkanethiols required to saturate the same amount of AuNPs was calculated. For this estimation it was necessary to know the average diameter of AuNPs, and the concentration of AuNPs, in the citrate capped stock solution. A TEM study showed that the average diameter of the particles was about 13 nm. Since 1.5 ml of citrate capped AuNPs were added to each sample, the total surface area of AuNPs were calculated first, and then we were able to calculate the number of thiols required to saturate the estimated surface area. For this estimation we used the surface density of thiols on a gold surface to be 4.5×10^{14} molecules/ $\text{cm}^{2(1c)}$. The table below shows the numbers we have estimated.

Table 1 Estimation of amount of Alkanethiols required for surface saturation of AuNPs.

Concentration of AuNP stock solution	3.26 nM
Number of moles of AuNPs in 1.5 ml sol	4.89×10^{-3} nmol
Number of 13 nm spheres in 1.5 ml sol	2.95×10^{12} spheres
Surface area of a sphere	5.31×10^2 nm ²
Surface density of thiols on gold surface	4.5×10^{14} molecules/ cm ²
Number of thiols needed to saturate a single sphere	2390 molecules/ sphere
Number of thiols required to saturate all the spheres in 1.5 ml sol	7×10^{15} thiol molecules
Number of thiols need to saturate 1.5 ml sol in moles	1.13×10^{-2} μ mol
Concentration of thiols required for saturation when total volume is 10 ml	> 1.13 μM

The estimated values show that the amount of alkanethiols required to saturate the total surface area of 1.5 mL of citrate capped sol to be 0.011 μM , thus the required concentration of MUA to saturate 1.5 mL sol should be greater than 1.1 μM . The estimated value shows nice agreement with the experimentally observed value. The place exchange study shows that the MUA concentration required to saturate the sol would linearly increase up to 1 μM MUA concentration and then level off or reach complete saturation at 5 μM (Figure 2.13). Thus, estimated values provide evidence for the validity of the experimentally observed data.

Next we were interested to use the fluorescence data to calculate the molar fluorescence of the adsorbed dye. We were interested to know whether the molar fluorescence of the adsorbed dye is the same as that for the free dye in solution

2.3.6 Molar Fluorescence of Adsorbed Dye

In the final step the molar fluorescence of adsorbed dye was calculated. Molar fluorescence is an intrinsic property like the extinction coefficient. This is usually a constant for a given dye in a given solvent system at low concentrations. In this study molar fluorescence was obtained by dividing the fluorescence of adsorbed dye by their concentration. The fluorescence of the adsorbed dye was determined by subtracting the supernatant fluorescence maximum from the corrected fluorescence maximum of sol/dye mixtures. The graph below shows the change in relative molar fluorescence of adsorbed dye with respect to the amount of dye loaded on the nano-particle surface.

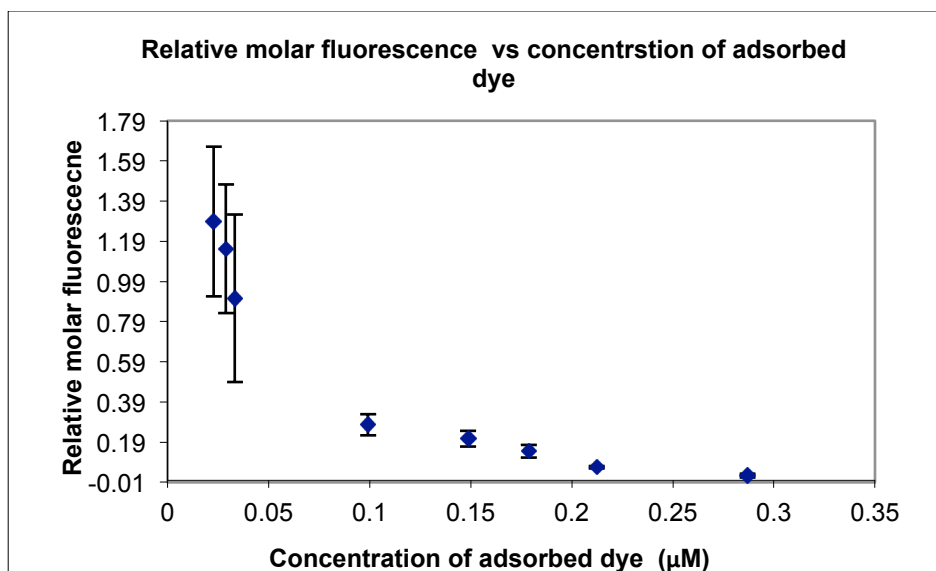


Figure 2.16 Variation of relative molar fluorescence of the adsorbed dye against the concentration of the dye adsorbed dye on AuNP surface.

If there was no change in enhancement or quenching of BODIPY fluorescence, we would expect that the molar fluorescence of adsorbed dye to remain constant despite of the amount of dye loaded on the surface. However, we observed a gradual decrease in the molar fluorescence as we increase the amount of dye loaded on the nanoparticle surface. The experiment was repeated several times and the same trend was observed each time.

Since the dye is directly attached on AuNP surface and AuNPs would quench the dye; therefore, we expected the molar fluorescence to be less than that of free dye (less than unity). However if the metal is the only source of quenching it would remain a constant. We believe the reason for the decrease in molar fluorescence with increasing adsorbed dye, could be due to the increased dye-dye interactions, which could result inter-molecular quenching when more dye is loaded on AuNP surface. We observe a

unity relative molar fluorescence within experimental error at very low adsorbed dye concentrations.

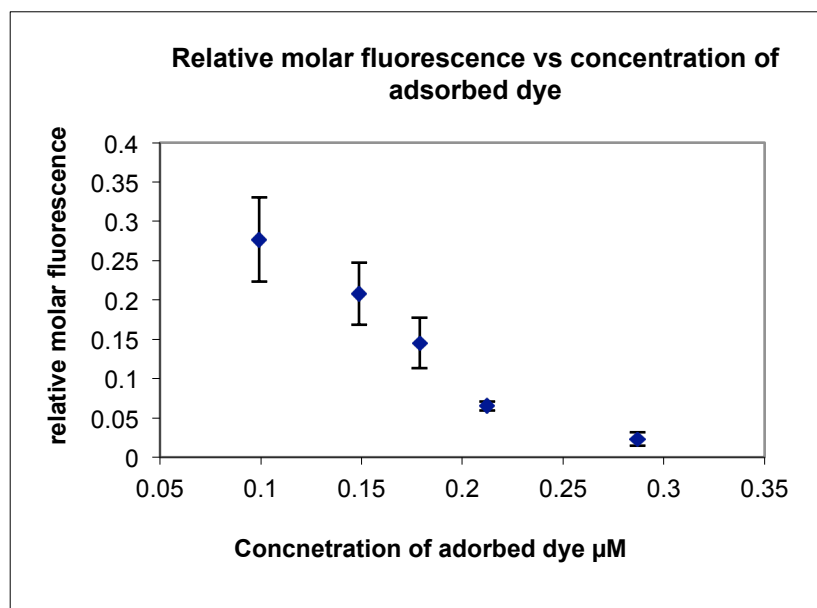


Figure 2.17 Variation of relative molar fluorescence of the adsorbed dye against the concentration of the dye adsorbed dye on AuNP surface (0.1-0.3 μM).

A closer look at the region from 0.1-0.3 μM shows that when the adsorbed dye concentration increases from 0.1 to 0.2 μM, the molar fluorescence seems to decrease linearly by 0.2 units, whereas, from 0.2-0.3 μM range it remained almost unchanged or decreases slightly 0.05 units. We believe the change in the trend of fluorescence decrease could arise due to relative orientation of dye molecules on AuNP surface. With no MUA on surface the dye molecules would lie flat or parallel on AuNP surface being completely quenched by the metal. So the molar fluorescence would be mostly dominated by quenching due to the metal and remain almost unchanged. As the competing ligand is introduced, the dye molecules would orient perpendicular to AuNP surface. Thus, intermolecular interactions would also play a role in quenching process.

With increasing MUA density on AuNP surface, dye-dye interactions would minimize, thus the molar fluorescence would increase linearly due to minimized intermolecular quenching.

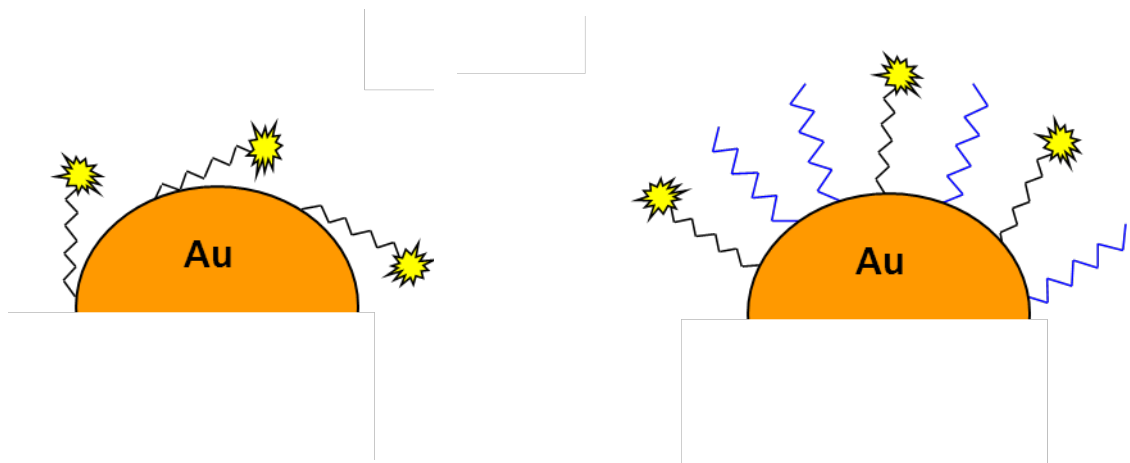


Figure 2.18 Orientation of tethered dye on AuNP surface without the competing ligand (left) and with the competing ligand (right).

2.3.6 Study of Place Exchange of Alkanethiols on AuNP Surface

In the previous ligand exchange study, mercaptoundecanoate (MUA) and acetate cleaved BODIPYdecylthioacetate were pre-mixed, and AuNPs were added later on so that the two different ligands would compete for the AuNP surface and exchange with the citrate capping simultaneously. In this study place exchange was studied by pre-capping AuNPs with thiol tethered BODIPY and then exchanging BODIPY with varying concentrations of alkanethiols. Therefore, we were able to study the place exchange of a thiol capped BODIPY by another alkanethiol. Two alkanethiols were used in this study; MUA which is a negatively charged ligand, and $(\text{CH}_3\text{O}(\text{CH}_2\text{O})_2\text{C}_{10}\text{SCOCH}_3)$ which is a neutral ligand.

2.3.6.1 Exchange of Thiol Tethered BODIPY By 11-Mercaptoundecanoate (MUA)

In this experiment 1.5 mL of citrate capped AuNPs were first exposed to 0.4 μM thiol tethered BODIPY so that the AuNPs would be pre-capped with BODIPY. After 2 hours, varying amounts of mercaptoundecanoate (MUA (0-10 μM)) were added and the solutions were diluted with 95 % ethanol to 10 mL so that the BODIPY would place exchange with MUA in solution. Fluorescence emission was measured at different time intervals; immediately after mixing MUA, after 4 h and after 24 h. Figure 2.18 shows the fluorescence isotherms of fluorescence emission maxima of sol/dye mixtures (measured at 530 nm) against MUA concentration over time.

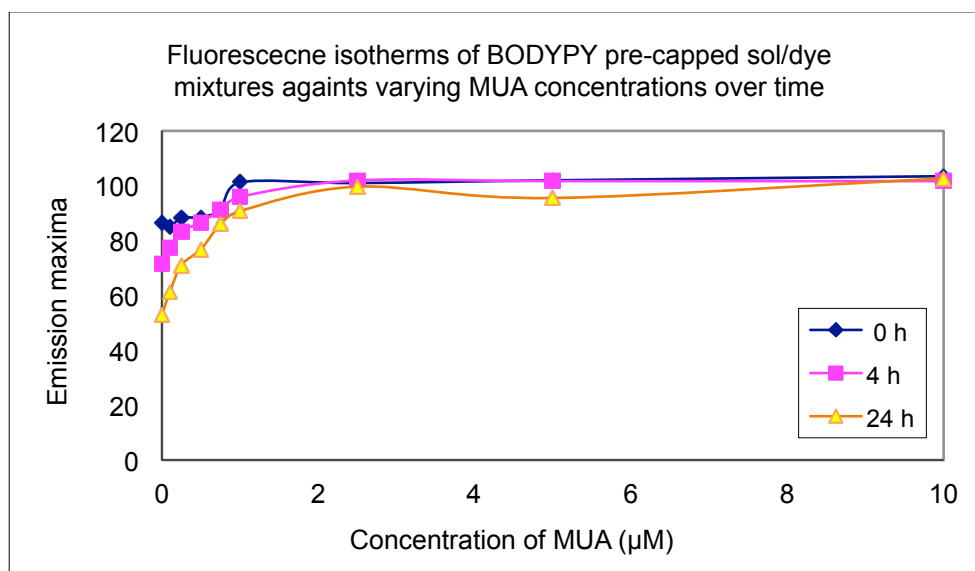


Figure 2.19 Fluorescence isotherms of BODIPY pre-capped sol/dye mixtures against varying MUA concentrations. Fluorescence of the samples were measured at immediately after mixing MUA (0h), after 4 h and after 24 h.

Our previous study showed that a ligand concentration greater than $1\mu\text{M}$ is required to saturate 1.5 mL AuNPs. Similar trend was observed in this study as well. However, the amount of BODIPY initially added to pre-cap the sol was $0.4\mu\text{M}$, which is less than the limit of saturation. This concentration was chosen because complete saturation of AuNPs with neutral BODIPY results heavy aggregation of AuNPs.

Interestingly, emission intensity of samples with high amounts of MUA, above the limit of saturation (2.5, 5 and $10\mu\text{M}$), has not changed considerably over time. This shows that BODIPY has rapidly exchanged with MUA in solution, immediately after adding high concentrations above the saturation limit. The concentration of dye in solution has remained unchanged over time indicating that dye in these solutions had not place exchanged at this limit.

Another interesting trend is observed at MUA concentrations below the saturation limit (below $1\mu\text{M}$). Although the emission of sol/dye mixture has increased from $0\mu\text{M}$ to $1\mu\text{M}$ MUA, indicating that BODIPY attached to AuNPs have exchanged with increasing amounts of MUA in solution, the emission intensity of each sample has decreased over time. This indicates that more dye has been attached to gold surface and quenched over time. This indicates that at concentrations below the saturation limit (below $1\mu\text{M}$), there is opportunity for both ligands to exchange, and the exchange is not so rapid. Even the fluorescence emission of samples without MUA has decreased from 85 to 50 units, within 24 hours. This shows that exchange of BODIPY alone with citrate capped AuNPs is also not complete even after 4 hours. This study reveals that AuNPs can be saturated with MUA at concentrations above the saturation limit rapidly, however, at low concentrations, place-exchange needs more time.

2.3.6.2 Exchange of Thiol Tethered BODIPY by $\text{CH}_3\text{O}(\text{CH}_2\text{CH}_2\text{O})_2\text{C}_{10}\text{SH}$

In the previous place-exchange experiment, BODIPY capping was exchanged with a negatively charged ligand. In this study BODIPY is exchanged with a neutral ligand, which is a thiol tethered diethyleneglycol ($\text{CH}_3\text{O}(\text{CH}_2\text{CH}_2\text{O})_2\text{C}_{10}\text{SCOCH}_3$) shown below.

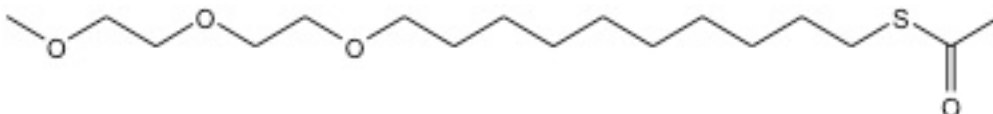


Figure 2.20 Structure of $\text{CH}_3\text{O}(\text{CH}_2\text{CH}_2\text{O})_2\text{C}_{10}\text{SCOCH}_3$

This ligand was also synthesized by Anuradha Singh in Dr Haltermans lab. The significance of this ligand is that although it is neutral, it has a hydrophilic tail with ethyleneglycol groups which make it more water soluble than a simple decanethiol. Furthermore, the electrostatic repulsion of oxygen atoms prevents AuNPs from aggregation to some extent. This experiment was also conducted by pre-capping the AuNPs with the dye as described in the previous study. Thus, first AuNPs were pre-capped with 0.4 μM BODIPYdecylthioacetate and after 2 hours varying amounts of acetate clefted ligands (figure 2.19) were added. This capping is referred as the “ether capping” since the terminal subunit is an ether group

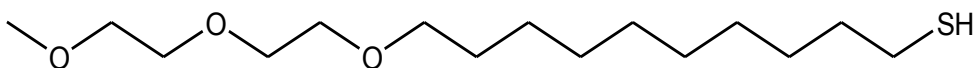


Figure 2.21 Structure of the thioacetate clefted ligand-"ether capping"

Figure 2.21 shows the fluorescence isotherms of emission maxima of sol/dye mixtures (at 530 nm) against the ligand concentration over time. Fluorescence emission of sol/dye mixtures were measured at 4 h and 48 h after addition of the ether ligand.

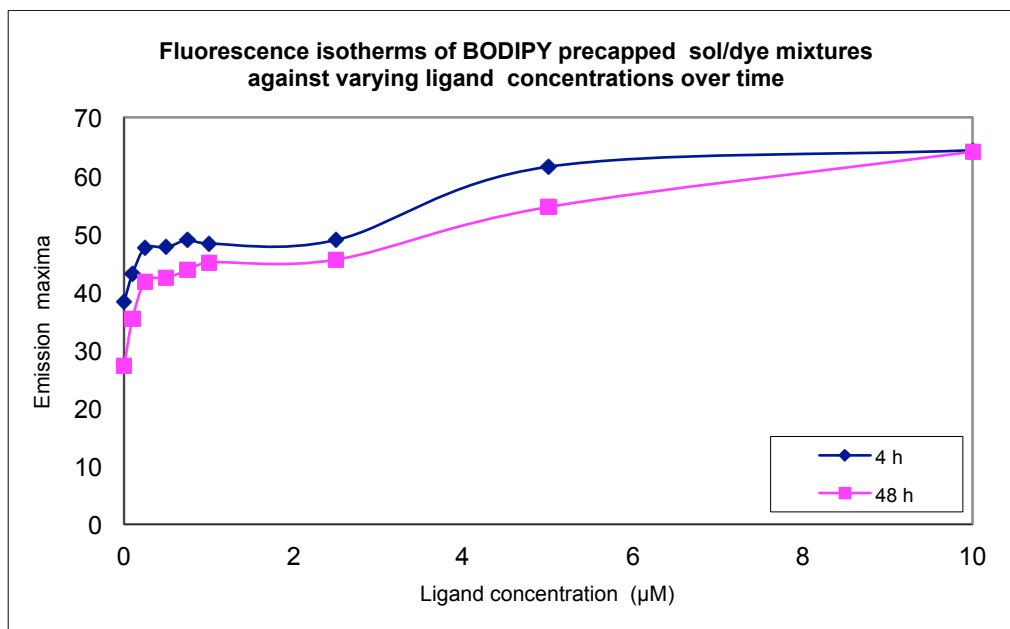


Figure 2.22 Fluorescence isotherms of BODIPY pre-capped sol/dye mixtures against varying $\text{CH}_3\text{O}(\text{CH}_2\text{CH}_2\text{O})_2\text{C}_{10}\text{SH}$ concentrations. Fluorescence of the samples was measured at 4 h and 48 h after addition of the ligand.

This experiment follows the same trend as the exchange of MUA with BODIPY pre-capped AuNPs. The amount of free dye in solution has increased with increasing ligand concentration. However, the fluorescence of each sample has decreased over time up to 5 µM ether concentration. This indicates that the ether can be exchanged with BODIPY in solution passed the expected saturation limit which is 1µM. The rapid saturation is achieved only at 10 µM ether concentration.

Comparison of the two studies suggests that the rate of place exchange of MUA is more rapid and stable than that of the ether. This could be attributed to the difference in spatial distribution of the two ligands in solution. The literature shows that MUA would remain as a linear tether whereas the ether would spiral at the end. Therefore, it could be easier for MUA to penetrate through the citrate capping or the BODIPY capping and bind with gold surface efficiently. Furthermore, the inter-molecular interactions between the linear hydrocarbon tethers would make the MUA capping more ordered and more stable on the gold surface than the spiral ether capping. Thus, BODIPY can be exchanged with the ether capping more easily even past the limit of saturation contrast to MUA.

These studies were helpful to develop procedures to coat citrate capped AuNPs with MUA and ether. MUA saturated AuNPs can survive in 100% water without aggregation, whereas, ether capped sol would aggregate in pure water. To preserve the monodispersity of ether capped sol, at least 9:5, water:95% ethanol, ratio is required (34% ethanol). These procedures are discussed in the experimental section.

2.3.6.3 Place-Exchange of Thiols by Disulfides on AuNP Surface

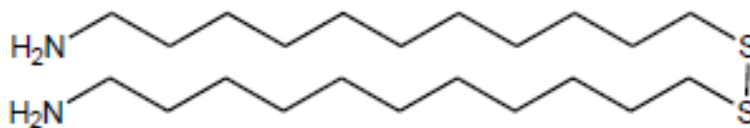


Figure 2.23 Structure of the disulfide

In this study ether capped AuNPs were exchanged with a disulfide which has two hydrocarbon chains with amine functionality at the tail (11-(2-(11-aminoundecyl)disulfanyl)undecan-1-amine) (Figure 2.22). This ligand was also synthesized by Anuradha Singh. However, saturating AuNPs with amines causes severe aggregation of AuNPs since gold has a high affinity for amines. Therefore, the number of amines per AuNP is critical to control aggregation. Calculations show that a 13 nm diameter AuNP can accommodate about 2300 thiols. We expected to have 10 to 20 disulfides per AuNP to prevent AuNPs from aggregation.

For this study ether capped sol was titrated with varying amounts of disulfide and the absorbance was measured to monitor aggregation. The concentration of ether capped AuNPs was kept at 0.6 nM, and the disulfide concentration was varied from 0-350 nM, to get the desired AuNP: disulfide ratio. Figure 2.23 shows the absorbance spectra of ether capped AuNPs with varying disulfide concentrations. The estimated number of thiols that accommodate 13 nm AuNP surface is 2300. For disulfides it should be about 1150 molecules. These results indicate that a gold nanoparticle can accommodate up to 60 disulfide molecules and remain unaggregated. However, it was

observed that disulfides exchange rapidly with thiols even at concentrations well below the limit of saturation.

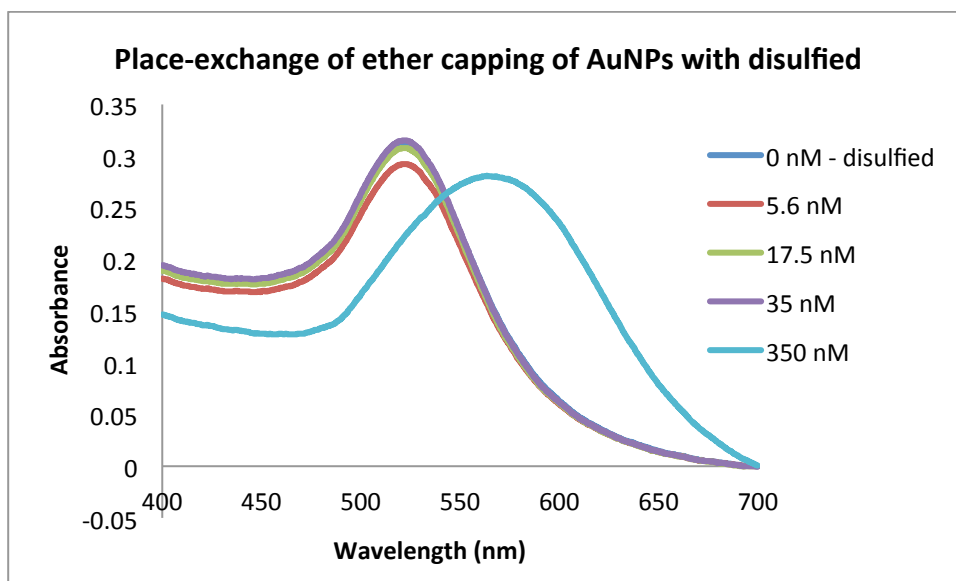


Figure 2.24 Absorbance spectra of ether capped AuNPs (0.6nM) with varying amounts of disulfide.

Table 2 Estimated amount of disulfide molecules per AuNP.

Concentration of disulfide (nM)	AuNP: disulfide ratio
5.6	1: 10
17.5	1:30
35	1:60
350	1: 580

2.4 Chapter Summary

In this chapter we have investigated place exchange of thiol tethered dyes with other alkanethiols on AuNP surface. We were able to develop a method to control the loading of the dye on the nanoparticle surface using a competing ligand. Furthermore, we were able to study the variation of the molar fluorescence of the adsorbed dye on AuNP surface. The knowledge gathered in this study was helpful to develop several place exchange procedures to cap AuNPs with different ligands (MUA, ether and disulfide). These procedures were extremely useful in the second part of the research.

2.5 Experimental

2.5.1 Preparation of 13 nm Diameter AuNPs by Standard Citrate Reduction

All glass wares were rinsed with aqua-regia ($\text{HNO}_3:\text{HCl}$, 1:3) and washed thoroughly with soap and water before preparation of all solutions.

A stock solution of chloroauric acid (HAuCl_4) (0.25mM) was prepared by dissolving HAuCl_4 (23.46 mg) in milipore water (238ml). A solution of trisodium citrate ($\text{Na}_3\text{C}_6\text{H}_5\text{O}_7$) (34 mM) was prepared by dissolving $\text{Na}_3\text{C}_6\text{H}_5\text{O}_7$ (2.25 g) in milipore water (228 mL). To prepare a 16 nm mono-dispersed AuNP solution, 0.25 mM HAuCl_4 (50 mL) was brought to boil while stirring and 34 mM $\text{Na}_3\text{C}_6\text{H}_5\text{O}_7$ (1 mL) was added to the boiling solution and the solution was continued to boil gently for another 10 min. After addition of $\text{Na}_3\text{C}_6\text{H}_5\text{O}_7$ the color of the solution was turned pale blue within 2 min, and after 6 min it was turned bright red indicating the completion of reaction. The mixture was cooled to room temperature, and the final volume was brought to 50 mL by transferring the red color AuNP solution to a volumetric flask and adding sufficient milipore water to reach 50 mL mark. A readily prepared sol would be kept for 24 h, before being used for any experiment.

2.5.2 Experimental Procedure for Preparation of sol/dye/MUC Series, for Controlling the Density of Dye Loaded on AuNP Surface.

Stock solutions of 1 mM BODIPY was prepared by dissolving 5.45 mg of BODIPY in 95% ethanol in a 10 mL volumetric flask. A 1 mM solution of 11-Mercaptoundecanoic acid was prepared by dissolving 5.46mg of MUA in 25 ml volumetric flask. 1 mM KOH solution at pH 11 was also prepared prior to the experiment. The thioacetate group of the dye needs to be cleaved 30 minutes before the experiment. Therefore, 125 μ L of 1 mM BODIPY was mixed with 125 μ L of 1 mM KOH (pH 11) in a 10 mL volumetric flask. After 30 minutes the resulting solution was diluted to 10 mL with 95% ethanol so that the final concentration of dye would be 12.5 μ M. Furthermore, a 10 μ M and 100 μ M deprotonated MUA solutions were prepared by adding equivalent amount of KOH. Care was taken to use these solutions within 30 min since they can form disulphide over time.

First 320 μ L aliquots of thioacetate cleaved 12.5 μ M BODIPY solutions were pre-mixed with varying amounts of deprotonated MUA to result 0, 0.15, 0.25, 0.5, 0.75, 1, 2.5, 5, 50 μ M concentrations of MUA in 10 mL volumetric flasks. Then 1.5 mL gold sol and 0.75 mL of 1 mM Na₃Cit were added to each mixture and the resulting mixtures were diluted up to 10 mL with 95% ethanol. Sol controls were prepared for each sample having same amount of MUA and AuNPs but not BODIPY. Controls with BODIPY only were prepared by having same constituents but 1.5 mL of deionized water instead of AuNPs. All samples were prepared in triplicate. These samples were

stored in the dark for the ligand exchange. After 24 h, 1.5 mL aliquots from each sample was removed and they were centrifuged at 14000 rpm for 30 min in a micro-centrifuge and their supernatants were collected. The fluorescence and absorbance of each sample was measured. Samples were excited at 521nm to measure the fluorescence.

2.5.3 Place Exchange of Citrate Capping of AuNPs with 11-Mercaptoundecanoate (MUA)

AuNP solution with 13 nm diameter was prepared by standard citrate reduction method described in chapter 2.5.1. A mixture of 1 mM MUA (250 μ L) was deprotonated by adding an equivalent amount of 1 mM KOH (250 μ L at pH-11) in a 20 mL scintillation vial. Next citrate capped sol (8 mL) was added to the mixture and it was kept in the dark for 2 hours for place exchange. To remove excess MUA, aliquots (1.5 mL) of the mixture were transferred micro-centrifuge tubes and centrifuged at 10,000 rpm for 8 minutes. Excess MUA was removed with the supernatants by pipette. The AuNPs in each centrifuge tube were re-suspended in milipore water (1.5 mL) by sonication. All re-suspended fractions were collected in a glass vial to form the MUA capped AuNP stock solution which was characterized by optical measurements.

2.5.4 Place Exchange of Citrate Capping of AuNPs with



AuNPs with 13 nm diameter were synthesized using standard citrate reduction method described in section 2.5.1. The neutral alkanethioacetate $\text{CH}_3\text{O}(\text{CH}_2\text{CH}_2\text{O})_2\text{C}_{10}\text{H}_{20}\text{SOCH}_3$ was synthesized by Anuradha Singh. First the thioacetate group of the neutral ligand was cleaved to yield $\text{CH}_3\text{O}(\text{CH}_2\text{CH}_2\text{O})_2\text{C}_{10}\text{H}_{20}\text{SH}$ by mixing 1 mM $\text{CH}_3\text{O}(\text{CH}_2\text{CH}_2\text{O})_2\text{C}_{10}\text{H}_{20}\text{SOCH}_3$ (200 μL) with an equivalent amount of 1 mM KOH (200 μL at pH-11) in a 10 mL volumetric flask. After 30 minutes the mixture was diluted up to the 10 mL mark with 95% ethanol. Next the solution was split into two portions (5 mL) in two glass scintillation vials. To each 5 mL portion, citrate capped AuNPs (9 mL) were added. The mixtures (total volume in each, 14 mL) were kept in the dark for 24 h for the place exchange. The percentage of ethanol in the final mixture was 34 % (9:5, water: 95% ethanol). The solutions were optically characterized by measuring the UV absorption. (Ether capped sol cannot be resuspended after centrifugation, excess ether cannot be removed from solution).

2.5.6 Correction for Inner-filtering Effects

Correction for inner-filtering effects was necessary to correct the fluorescence of sol/dye mixtures for the re-absorption of excited and emitted radiation by AuNPs. Since the absorption spectra of the sol/dye mixtures represents the absorption of AuNPs, the absorption due to dye was neglected. There are two types of inner-filtering effects the primary inner-filter effect and the secondary inner-filter effect.¹⁴

Primary Inner-filter effect (f_{prim})

The intensity of the fluorescence emission of a samples can be affected by the decrease in the intensity of the excitation beam (λ_{ex}), which was 521 nm for BODIPY, from the front window of the cell to the beginning of the interrogation zone (X), and by the decrease in excitation beam intensity that occurs in the interrogation zone (X to Y). This is called the primary inner filter effect.

Secondary Inner-filter effect (f_{sec})

The emitted light intensity at 90° can also be diminished by absorbance (at λ_{em}) in the interrogation zone (V to U) and from the edge of the interrogation zone to the exit window (U). This is known as the secondary inner filter effect. The Emission can be corrected by considering both inner filtering effects as shown below.

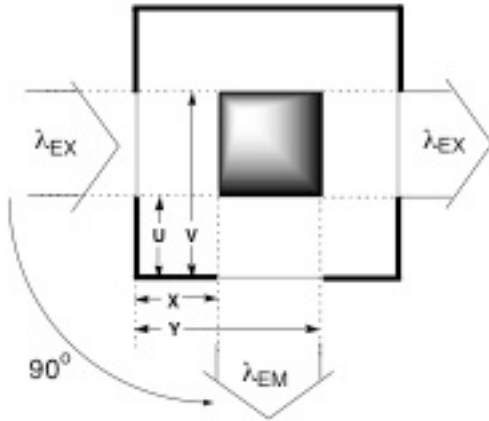


Figure 2.25 Typical cell configuration for right angle fluorometry. Window parameters (X,Y and U,V). [14]

$$f_{\text{prim}} = I_{\text{F}}^{\text{corr}} / I_{\text{F}}^{\text{obs}} = \{2.303 A (Y - X)\} / \{10^{-AX} - 10^{-AY}\}$$

$I_{\text{F}}^{\text{corr}}$ = corrected emission signal

$I_{\text{F}}^{\text{obs}}$ = observed emission signal

A = absorbance (b = 1 cm) at λ_{ex}

$$f_{\text{sec}} = I_{\text{F}}^{\text{corr}} / I_{\text{F}}^{\text{obs}} = \{(V - U)(1/b) \ln T\} / \{T_{\text{at } V/b} - T_{\text{at } U/b}\}$$

$I_{\text{F}}^{\text{corr}}$ = corrected emission signal

$I_{\text{F}}^{\text{obs}}$ = observed emission signal

T = transmittance across cell pathlength at λ_{em}

$T_{\text{at } V/b}$ and $T_{\text{at } U/b}$ are transmittance values at the interrogation zone boundaries and are calculated using Beer's law and the known molar absorptivities at λ_{em}

$$I_{\text{F}}^{\text{corr}} = f_{\text{prim}} f_{\text{sec}} I_{\text{F}}^{\text{obs}}$$

To apply above correction factors, the length of the excitation and emission window was measured. It was found that (V-U) and (Y-X) were both equal to 0.9 mm. Since the path length of the cell was 10 mm the whole volume of the cuvette could be considered as the interrogation zone. Therefore, a simpler approach was used for the correction.

Correction Used for the Experimental Data

For this correction, absorbance of MUA capped sol at different concentrations (0-10 μM) was measured (Figure 2.25) The absorbance at 521 nm of each mixture was converted to transmittance (Table 2.3). Next the fluorescence maximum of each sol/dye mixture was divided by the transmittance of each mixture (Table 2.4)

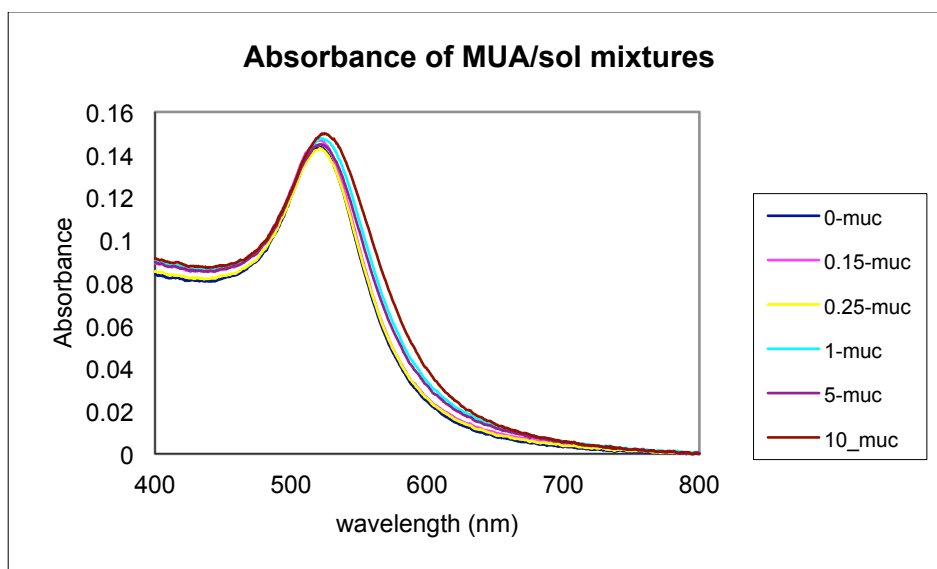


Figure 2.26 Absorbance of AuNPs capped with varying amounts of MUA.

Table 3 Absorbance and transmittance of sol/dye mixtures at 250 nm

MUA (μM)	0	0.15	0.25	0.5	1	2.5	5	10
Absorbance at 521 nm	0.140	0.1413	0.1422	0.144588	0.146275	0.146704	0.147133	0.147633
Transmittance	0.7232	0.7222	0.7207	0.7168	0.7140	0.7133	0.7126	0.7118

Table 4 Corrected values of sol/dye fluorescence for inner filter effects

MUA	Average sol/dye fluorescence	T	(sol/dye)/T Corrected sol/dye fluorescence	Average fluorescence of supernatants
0	21.60533	0.723269	29.87177	28.21767
0.15	36.30867	0.722271	50.27016	46.829
0.25	44.44733	0.720775	61.66599	55.18867
0.5	50.467	0.716824	70.40362	62.68767
1	58.47767	0.714044	81.89644	75.042
2.5	70.63967	0.713339	99.02681	91.48533
5	71.90767	0.712634	100.904	92.587
50	72.21467	0.711814	101.4516	94.1

2.6 Chapter 2 References

1. (a) Kamat, P. V., Photophysical, photochemical and photocatalytic aspects of metal nanoparticles. *The Journal of Physical Chemistry B* **2002**, *106* (32), 7729-7744; (b) Thomas, K. G.; Kamat, P. V., Chromophore-functionalized gold nanoparticles. *Accounts of chemical research* **2003**, *36* (12), 888-898; (c) Love, J. C.; Estroff, L. A.; Kriebel, J. K.; Nuzzo, R. G.; Whitesides, G. M., Self-assembled monolayers of thiolates on metals as a form of nanotechnology. *Chemical Reviews-Columbus* **2005**, *105* (4), 1103-1170; (d) Eustis, S.; El-Sayed, M. A., Why gold nanoparticles are more precious than pretty gold: Noble metal surface plasmon resonance and its enhancement of the radiative and nonradiative properties of nanocrystals of different shapes. *Chemical Society Reviews* **2006**, *35* (3), 209-217.
2. (a) Thomas, K. G.; Ipe, B. I.; Sudeep, P., Photochemistry of chromophore-functionalized gold nanoparticles. *Pure and Applied Chemistry* **2002**, *74* (9), 1731-1738; (b) Daniel, M. C.; Astruc, D., Gold nanoparticles: assembly, supramolecular chemistry, quantum-size-related properties, and applications toward biology, catalysis, and nanotechnology. *Chemical Reviews-Columbus* **2004**, *104* (1), 293.
3. Zhang, J.; Lakowicz, J. R., Metal-enhanced fluorescence of an organic fluorophore using gold particles. *Optics express* **2007**, *15* (5), 2598.
4. Singh, A.; Dahanayaka, D. H.; Biswas, A.; Bumm, L. A.; Halterman, R. L., Molecularly Ordered Decanethiolate Self-Assembled Monolayers on Au(111) from in Situ Cleaved Decanethioacetate: An NMR and STM Study of the Efficacy of Reagents for Thioacetate Cleavage. *Langmuir* **2010**, *26* (16), 13221-13226.
5. Ghorai, P. K.; Glotzer, S. C., Molecular dynamics simulation study of self-assembled monolayers of alkanethiol surfactants on spherical gold nanoparticles. *The Journal of Physical Chemistry C* **2007**, *111* (43), 15857-15862.
6. (a) Dulkeith, E.; Morteani, A.; Niedereichholz, T.; Klar, T.; Feldmann, J.; Levi, S.; Van Veggel, F.; Reinhoudt, D.; Möller, M.; Gittins, D., Fluorescence quenching of dye molecules near gold nanoparticles: radiative and nonradiative effects. *Physical Review Letters* **2002**, *89* (20), 203002; (b) Ghosh, S. K.; Pal, T., Photophysical aspects of molecular probes near nanostructured gold surfaces. *Phys. Chem. Chem. Phys.* **2009**, *11* (20), 3831-3844.
7. Chandrasekharan, N.; Kamat, P. V.; Hu, J.; Guilford Jones, I., Dye-capped gold nanoclusters: Photoinduced morphological changes in gold/rhodamine 6G nanoassemblies. *The Journal of Physical Chemistry B* **2000**, *104* (47), 11103-11109.
8. Ipe, B. I.; Thomas, K. G., Investigations on nanoparticle-chromophore and interchromophore interactions in pyrene-capped gold nanoparticles. *The Journal of Physical Chemistry B* **2004**, *108* (35), 13265-13272.

9. Turkevich, J.; Stevenson, P. C.; Hillier, J., A study of the nucleation and growth processes in the synthesis of colloidal gold. *Discuss. Faraday Soc.* **1951**, *11* (0), 55-75.
10. Frens, G., Controlled nucleation for the regulation of the particle size in monodisperse gold suspensions. *Nature* **1973**, *241* (105), 20-22.
11. Kumar, S.; Gandhi, K.; Kumar, R., Modeling of formation of gold nanoparticles by citrate method. *Industrial & engineering chemistry research* **2007**, *46* (10), 3128-3136.
12. Liu, X.; Atwater, M.; Wang, J.; Huo, Q., Extinction coefficient of gold nanoparticles with different sizes and different capping ligands. *Colloids and Surfaces B: Biointerfaces* **2007**, *58* (1), 3-7.
13. Link, S.; El-Sayed, M. A., Spectral Properties and Relaxation Dynamics of Surface Plasmon Electronic Oscillations in Gold and Silver Nanodots and Nanorods. *The Journal of Physical Chemistry B* **1999**, *103* (40), 8410-8426.
14. Tucker, S. A.; Amszi, V. L.; Acree, W. E., Primary and secondary inner filtering. Effect of K₂Cr₂O₇ on fluorescence emission intensities of quinine sulfate. *Journal of Chemical Education* **1992**, *69* (1), 8.

Chapter 3: **Metal-Enhanced Fluorescence of Dye Doped Silica Nanoparticles by Metal-Fluorophore Aggregation**

3.1 Chapter Overview

This chapter presents our attempts to develop a solution based approach to form metal-fluorophore aggregates with enhanced fluorescence. For this study we have used Rhodamine B (RhB) doped silica nanoparticles (SiNPs) as suspended fluorescent nano-platforms that would bind with multiple AuNPs in solution phase. This method allows trapping fluorophores between multiple AuNPs, so that the dye molecules away from the quenching region would greatly enhance emission due the interaction of the coupled plasmons. Furthermore, we wanted to optimize MEF by varying nanoparticle ratios or by varying the amount of aggregation.

We have tried two methods for metal-fluorophore aggregation. The first study describes our attempts to aggregate anionically capped AuNPs and cationically SiNPs using electrostatic interactions, which did not result in controlled aggregation of enhanced fluorescence. The second study describes our attempts to form metal-fluorophore aggregates using dithiocarbamate capped SiNPs to covalently bind multiple AuNPs. By this covalent method we were able to form metal-fluorophore aggregates with up to a remarkable 200-fold enhancement. These extremely bright fluorescent markers that can be produced in solution phase have a greater potential to be used as bright fluorescent tags in cellular imaging.¹

3.2 Introduction

Recent advancements in MEF suggest that it could be a very useful tool in creating ultra-bright fluorescent probes with enhanced photostability.^{1a, 2} The development of these ultra-bright probes relies on the optimization of near-field interactions of the metal-fluorophore complex so that the fluorophore would gain the maximum opportunity to radiate to the far-field.^{1b, 2a, 2c} One possible way of approaching this optimization is trapping fluorophores within coupled plasmons, or formation of clusters of metal-fluorophore aggregates.

Metal nanoparticles can enhance the local electromagnetic field surrounding a fluorophore due to strong interaction of incoming light which causes collective oscillations of surface electrons. The local electric fields created by the plasmons can be many orders higher than the incident field.³ However, these enhanced fields are confined to a nanometer scale region, surrounding the particle surface, and their intensities would decay significantly with increasing distance.⁴ Recent findings show that overlap of multiple plasmons of nearby metal colloids would even strongly intensify the electromagnetic field in the overlapped region, this is known as plasmon coupling.^{3, 5} Coupling effects of plasmons have been studied by several groups in the past.^{4a, 6} One of the early studies conducted on plasmon coupling has predicted that light can be transmitted by electrodynamic coupling through a chain of resonant silver nanoparticles.⁷ They indicate that the optimum inter-particle distance required for transmission would be 25 nm, and the field intensity would decay continuously with increasing distance. In most studies frequency domain (FDTD) method has been used to calculate the strength of the electromagnetic field of the coupled

plasmons.^{3-4, 6a, 6c, 7} Another study conducted using elliptical gold nanoparticles showed that the near-field coupling would become negligible when the gap between the nanoparticles exceeds 2.5 times the short length axis of the particles.^{4a} Their results also demonstrate that the resonant peak of two interacting particles was red shifted due to the coupling of near-field interactions. A similar study conducted on aggregation of 13 nm gold nanoparticles showed that as larger aggregates form the plasmon would redshift and the scattering component of the extinction would increase.⁸

A fluorophore trapped within a coupled plasmon can enhance due to two effects; it can feel the intensified electromagnetic field and have further increased probability for excitations, moreover, the fluorophore can radiate to the far field by coupling to the enhanced plasmon scattering. Therefore, metal-fluorophore aggregate can result even greater enhancements than single metal-fluorophore complexes. Effects of coupled plasmons on fluorophores have been studied theoretically and experimentally, during the past years.^{3, 5, 7-9} An interesting experimental evidence of fluorescence enhancement due to plasmon coupling using bio-molecular tethering has been demonstrated by Lakowicz group recently^{6b} (Figure 3.1). Their studies showed that single molecule fluorescence of Cy5 molecules gave a 7-fold enhancement when attached to a single with silver nanoparticle (monomer) and a 13-fold enhancement with silver nanoparticle dimer.

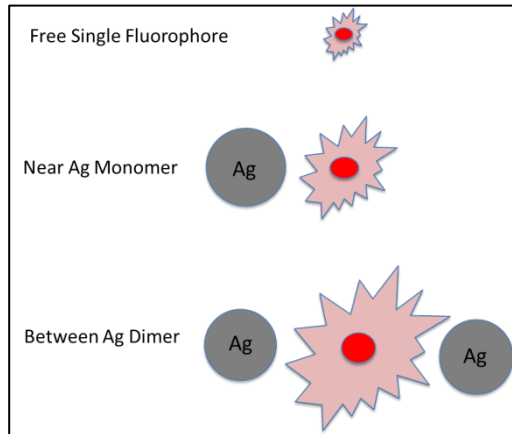


Figure 3.1 Enhanced emissions near silver nanoparticle monomer and dimer.[8]

One popular technique used in trapping fluorophores between coupled plasmons is, placing fluorophores in closely spaced nanoparticle arrays.^{6a, 6c} However, most methods used for metal-fluorophore aggregation require solid phase attachments or biomolecule tethering; very few studies have been performed in solution phase. The first solution based MEF study was reported in 2004 by Aslan et al.^{2b} In this study they have developed a solution-based sensing platform using metal-fluorophore aggregation, where SiO₂ coated silver colloids with Cy3-labelled streptavidine was aggregated with silver spheres with biotinylated-BSA, resulting in a 3-5-fold enhancement in fluorescence. Another solution based approach was reported in 2009, where silver colloids were aggregated with near IR fluorophores in a liquid-liquid droplet micro-mixer.⁹ In this nano device, silver colloids were aggregated by varying the salt concentration, and they were able to produce remarkable 35-fold enhancements in this solution based approach. However, among the few studies done in solution phase, reported enhancements are typically relatively low and less reproducible than surface immobilized techniques^{2b, 10}. Thus, more direct, simpler assembly methods are needed

for more facile study of MEF in solution phase. Furthermore, most metal-fluorophore aggregation studies have utilized silver nano particles (AgNPs). This could be due to the enhanced scattering properties of AgNPs above AuNPs (discussed in detail in chapter 1 section 1.7). However, AuNPs possess many potential advantages for MEF studies over silver nanoparticles. AuNPs are more attractive for biological studies due to their high chemical stability, it has been reported that even very small AuNPs can survive as particles with indefinite stability. Furthermore, the surface chemistry of AuNPs is well understood, thus, the binding of biomolecules and other chemical functionalities on AuNP surface can be easily accomplished.¹¹ Therefore, it would be beneficial to develop metal-fluorophore aggregation methods which lead to greater enhancements using AuNPs.

The aim of this study was to develop a solution based method to interact dye doped silica nanoparticles (SiNPs) with gold nanoparticles (AuNPs) that would result enhanced fluorescence. Our hypothesis is that trapping fluorophores, between multiple plasmons would result greater enhancements than monomer interactions.

3.3 Results and Discussion

3.3.1. Metal-Fluorophore Aggregation by Electrostatic Interactions

In an initial attempt we tried to form metal-fluorophore aggregates using electrostatic interactions. To achieve electrostatic binding, the SiNPs were to be coated with an amine which would be positively charged (ammonium) at neutral pH, and the AuNPs were to be coated with a carboxylic acid which would be negatively charged (carboxylate) at the same pH. We anticipated that these ions would salt bridge to form metal-fluorophore aggregates when particles are mixed at neutral pH. Thus, as detailed below the SiNPs were coated with 3-aminopropyltriethoxysilane (APTES), and the AuNPs were coated with 11-mercaptopundecanoic acid (MUA), and different AuNP to SiNP ratios were mixed at neutral pH to achieve electrostatic binding.

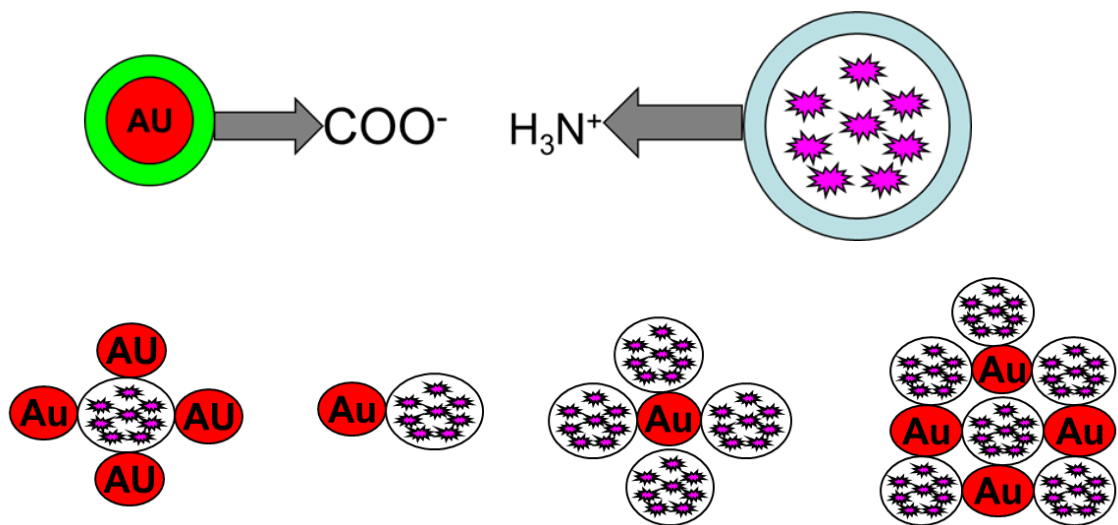


Figure 3.2 Formation of variety of metal-fluorophore aggregates through electrostatic binding between MUA coated AuNPs and APTES coated dye doped SiNPs.

According to our hypothesis, to optimize MEF a single dye doped SiNP should be trapped between multiple AuNPs. Experimentally, this would be difficult to control especially in solution phase, since particles can aggregate in a variety of clusters as

shown in Figure 3.2. However, we expected to have some control over the type of aggregates formed by varying the AuNP to SiNP ratio. Furthermore, Since MEF is very sensitive to the distance between the metal and the fluorophore, we assumed the dye located within 5 nm from the metal surface would quench and the dye away from the quenching region would enhance due to the effect of the coupled plasmons.

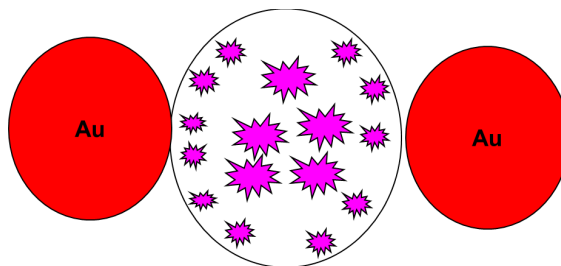


Figure 3.3 Enhanced dye molecules located beyond the quenching region of the metal.

3.3.1.1 Synthesis and Surface Functionalization of RhB Doped SiNPs

Dye doped silica nanoparticles are attractive for biomedical applications due to their bio-compatibility, water solubility, low cost and ease of functionalization.¹² Researchers have used silica as a spacer in MEF experiments.^{2b, 11, 13} Furthermore, dye doped silica or silica nanoshells have been used to coat individual metal colloids in order to study distance dependencies in MEF experiments.^{11, 13} The most common methods used to synthesize dye doped SiNPs are the Stöber method^{12c} and the micro-emulsion method.^{12b} For this study Rhodamine B (RhB) doped 70 nm diameter SiNPs were synthesized using Stöber method and their surface was functionalized with APTES, using a procedure reported in literature.¹⁴ The normalized absorbance and emission spectra of Rhodamine B are shown in Figure 3.4.

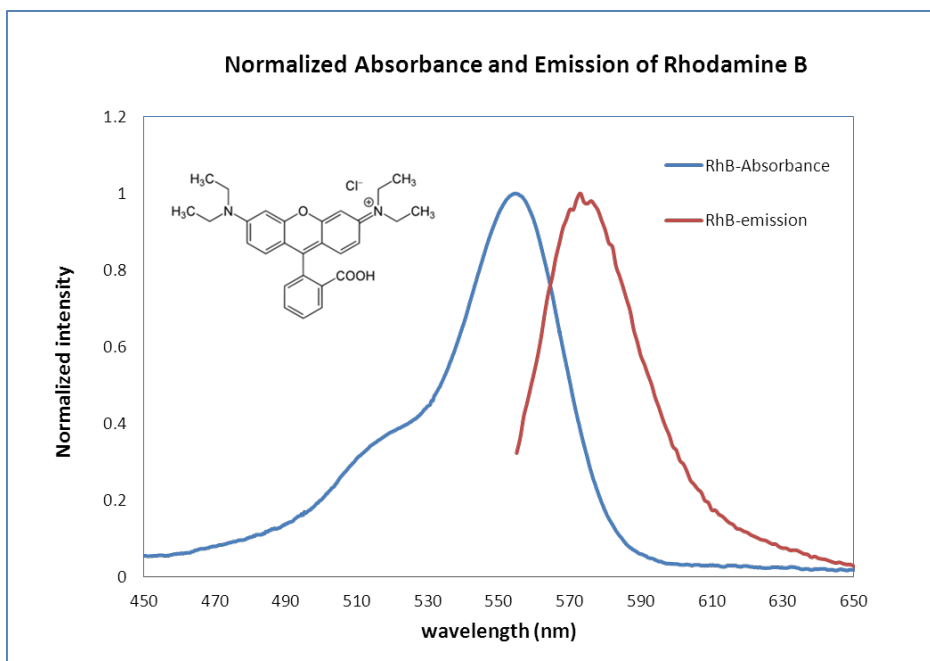


Figure 3.4 Normalized absorbance and fluorescence emission of Rhodamine B.

Using an established procedure for the synthesis of dye doped silica; the dye was covalently attached to silica using a silane coupling agent. Thus, leaking of dye from the particles to the solution could be minimized. RhB was initially covalently linked to silane coupling agent (APTES), by amide bond formation using EDC coupling.¹⁴

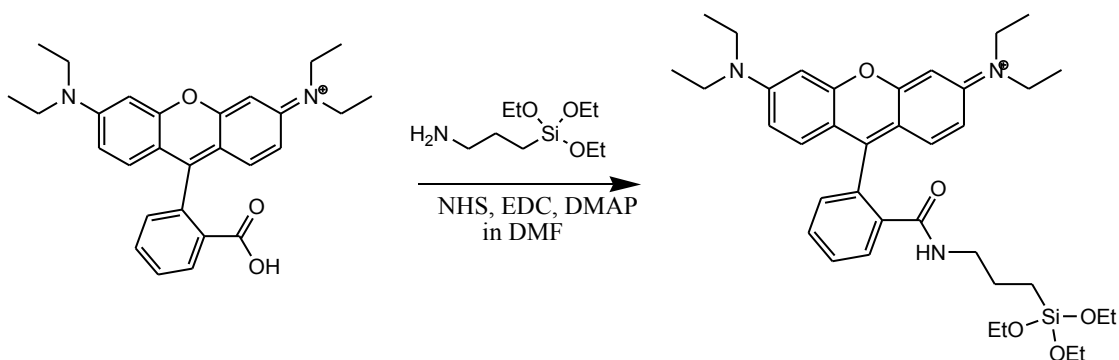


Figure 3.5 Amide coupling of APTES with RhB

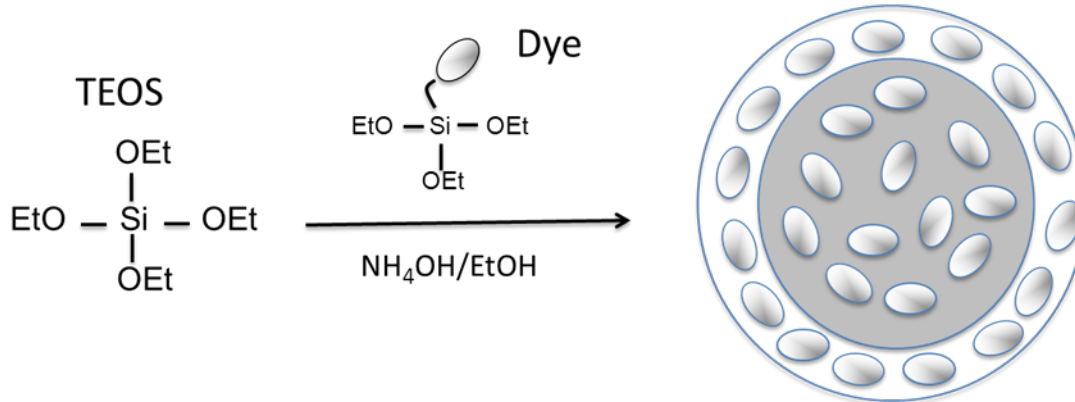


Figure 3.6 Synthesis of dye doped silica. [15]

After hydrolysis of the siloxane groups in the RhB tethered APTES, tetraethoxyorthosilicate (TEOS) was added and the mixture was stirred for another 24 h to complete the formation of RhB doped SiNPs. The reaction was quenched by centrifugation. Thus, the excess dye and the other reagents were easily removed from the pink pellet of dye doped silica collected at the bottom of the centrifuge tube. The particles were re-suspended in 95% ethanol by sonication, and washed with 95% ethanol and DI water three times each, until the supernatants were clear. The weight was determined by vacuum drying the particles at 35 °C overnight. According to literature, the size of the nanoparticles would depend on the rate of hydrolysis of the ethoxy groups.¹⁴ Thus, the particle size can be controlled by the amount of ammonium hydroxide added to the solution; smaller particles can be synthesized by decreasing the amount of ammonium hydroxide while keeping the other parameters constant. (To prepare 70 nm SiNPs, 0.640 mL of 30 % ammonium hydroxide was mixed in 8.375 mL of 95% ethanol and 0.355 mL of TEOS was added.)

Surface functionalization with propyl amine, was achieved by acid catalyzed hydrolysis of APTES in the presence of dye doped SiNPs in deionized water. Thus, to 10 mg of particles re-suspended in 1 mL of deionized water, 20 μ L of glacial acetic acid and 20 μ L of APTES were added and the mixture was stirred for 3 hours. Again the reaction was quenched by centrifugation and the particles were washed as described previously. A stock solution of APTES coated RhB doped SiNPs was prepared by dissolving 30 mg of SiNPs in 25 mL of water.

3.3.1.2 Synthesis and Surface Functionalization of AuNPs

AuNPs with 13 nm diameter were synthesized by standard citrate reduction and characterized by TEM as described in section 2.5.1. The loosely bound citrate capping present in the synthesis of AuNPs was exchanged by MUA using a place exchange procedure developed in chapter 2, section 2.5.3. In this procedure of 1 mM MUA (250 μ L) was deprotonated by an equivalent amount of 1 mM KOH. Next citrate capped sol (8 mL) was added and to the mixture and it was kept for 2 hours for place exchange. To remove excess MUA, aliquots of MUA capped sol (1.5 mL) were transferred to micro-centrifuge tubes and they were centrifuged at 10,000 rpm for 8 minutes. Excess MUA was removed with the supernatants and the sol was re-suspended water (1.5 mL) by sonication. All re-suspended fractions were collected in a glass vial to form the MUA capped AuNP stock solution which was characterized by optical measurements.

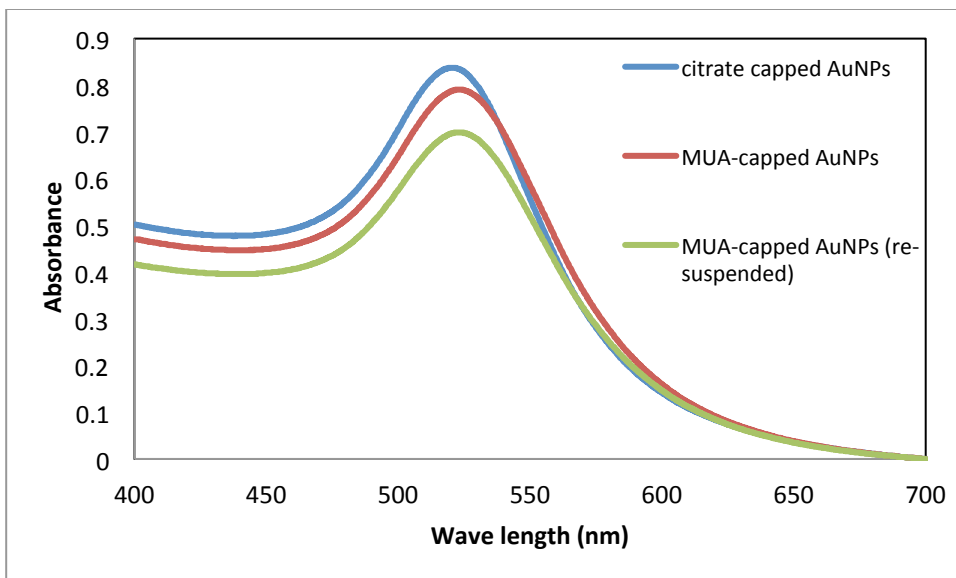


Figure 3.7 Absorbance spectra of 3.2 nM AuNPs before and after place exchange with MUA in milipore water.

The pH of this solution was measured to be 7.3. Thus, it was assumed that the carboxylic acid of MUA capping was in the deprotonated form. The solution appeared bright red indicating that there was not much aggregation among particles. Figure 3.6 Shows the absorbance spectra of and MUA capped sol before and after being re-suspended in DI water. The slight red shift and the dampening of the spectra indicate the place exchange of the capping from citrate to MUA. The decrease in peak intensity after re-suspension indicates loss of some material with the supernatant. However, the wavelength of the absorbance maximum has not changed after re-suspension, indicating spinning down the MUA capped AuNP did not cause inter-particle aggregation.

3.3.1.3 Interaction of MUA capped AuNPs with APTES coated silica

To achieve electrostatic binding between MUA capped AuNPs and APTES coated SiNPs both cappings should be in the ionic forms. Hence, the pH of both stock solutions was left near pH 7. Electrostatic binding between AuNPs and SiNPs, was studied by keeping the amount of AuNPs constant and varying the SiNP ratio. Although precise concentrations of nanoparticles were not known, but relative ratios could be prepared and studied as preliminary method to get a trend. Therefore, aliquots of AuNPs (1.5 mL) were mixed with varying amounts of APTES coated RhB doped SiNPs (4-200 μ L). Control samples were prepared by having the same amount of SiNPs but having milipore water (1.5 mL) instead of the AuNPs. Fluorescence and absorbance spectra were measured 24 h after mixing the samples. Samples were excited at 550 nm at 5 nm slit width for fluorescence measurements. Figure 3.4 shows the absorbance spectra of metal-fluorophore mixtures. The aggregation was monitored by red shifting of the absorbance spectra.

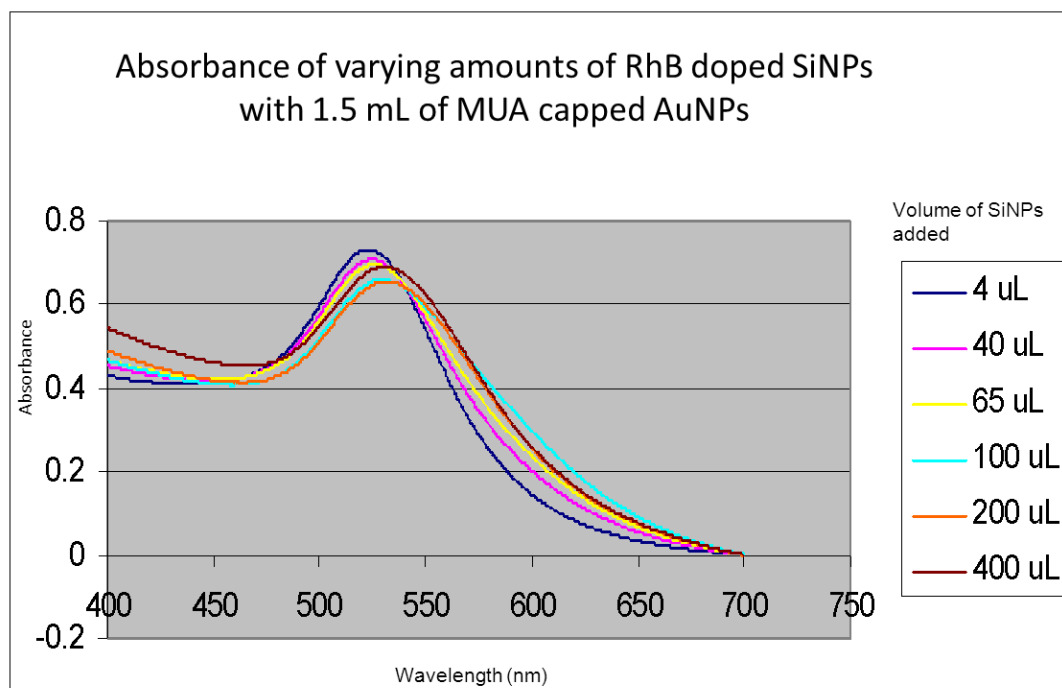


Figure 3.8 Absorbance of 1.5 mL of MUA capped AuNPs upon varying additions of RhB doped SiNPs as described in text.

Examination of absorbance spectra shows that plasmon resonance peak of MUA capped AuNPs have red shifted with increased additions of SiNPs, indicating aggregation of AuNPs. The red shifting of the plasmon could be due either undesired gold-gold aggregation or desired gold-silica aggregation.

Figure 3.8-3.10 show the fluorescence emission of control samples without AuNPs, the fluorescence emission of AuNP-SiNP aggregates and fluorescence isotherms of fluorescence maximum of control samples and AuNP-SiNP aggregates against the amount of SiNPs added.

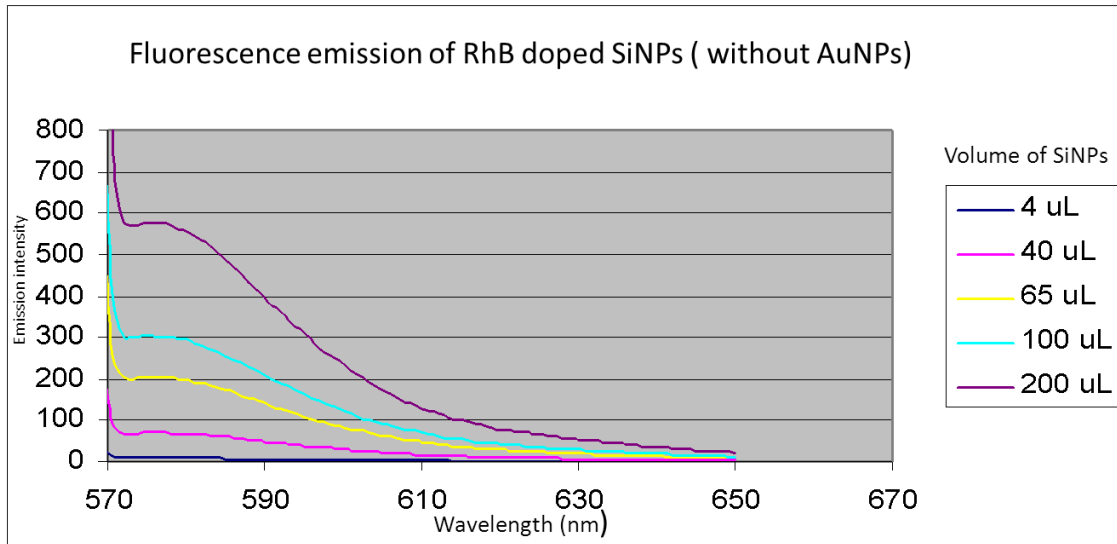


Figure 3.9 Fluorescence emission of control samples of RhB doped SiNPs (without AuNPs) in water. Samples were prepared by adding varying amounts of SiNPs to milipore water (1.5 mL). Fluorescence emission was measured by exciting the samples at 550 nm at 5 nm slit width.

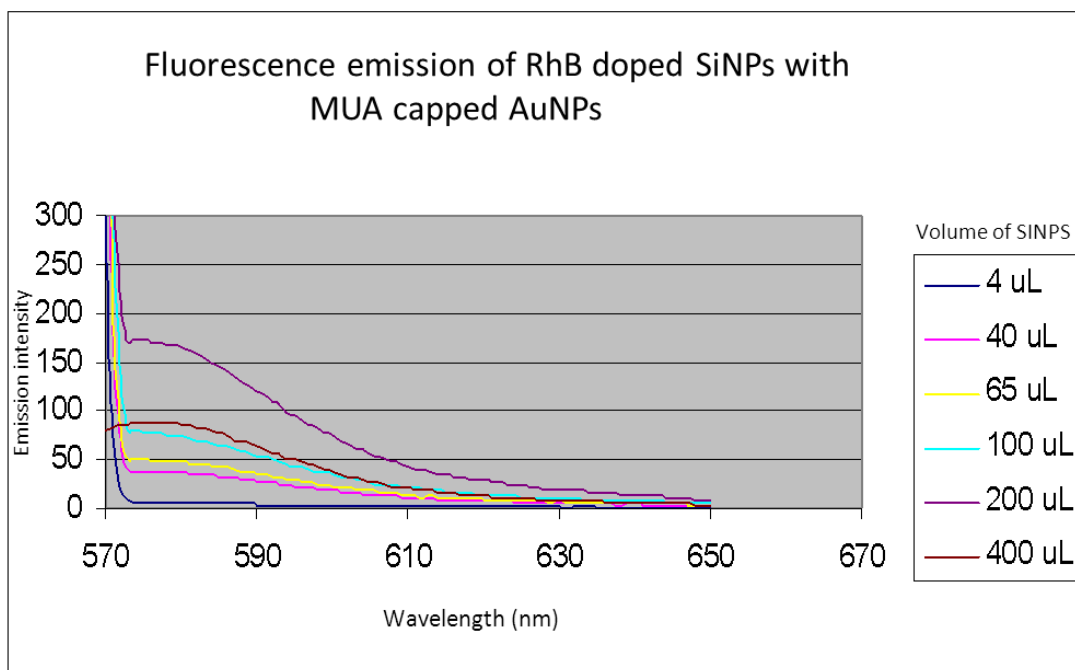


Figure 3.10 Fluorescence emission of varying additions of RhB doped SiNPs to MUA capped AuNPs (1.5 mL) in milipore water (as described in the text). Fluorescence emission was measured by exciting the samples at 550 nm at 5nm slit width.

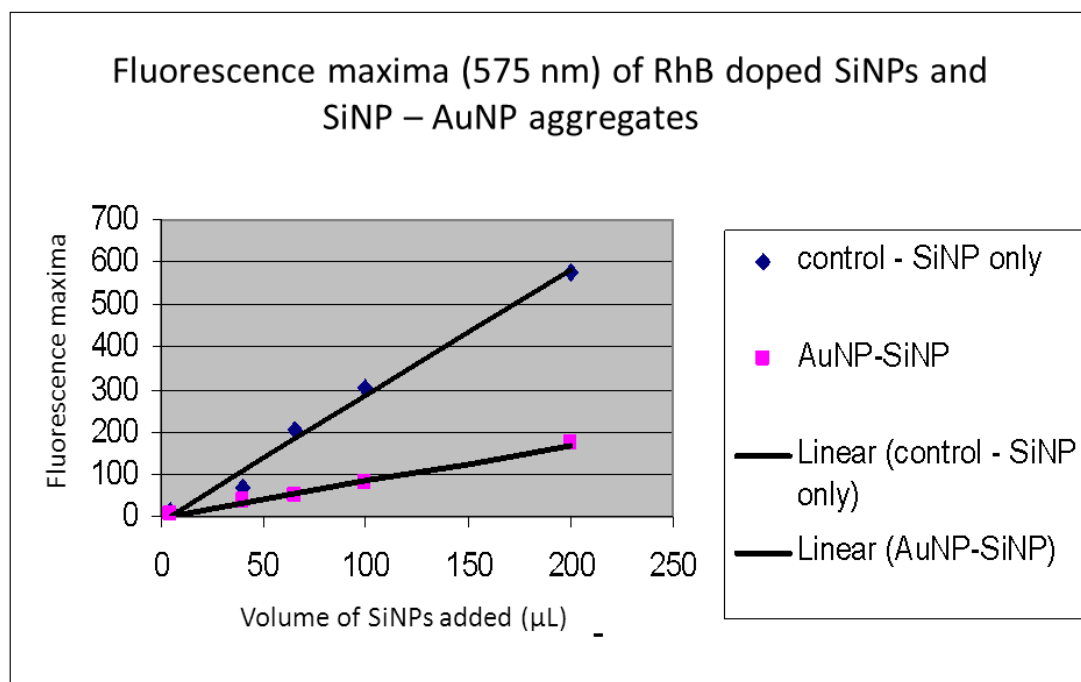


Figure 3.11 Fluorescence isotherms of fluorescence maxima of control samples (without AuNPs) and AuNP-SiNP aggregates against amount of SiNPs added. Fluorescence emission was measured by exciting the samples at 550 nm at 5 nm slit width. Emission maxima were measured at 575 nm.

The fluorescence isotherms in figure 3.11 show that fluorescence emission of control samples and mixtures linearly increase with increasing SiNP concentration. However, the fluorescence of the AuNP-SiNP aggregates are lower than that of control samples. It was suspected that this effect could be due to inner-filter effects caused due to presence of AuNPs in solution. Thus, the emission was corrected for the inner-filter effects as described in the experimental section in 2.5.6. Figure 3.12 shows the fluorescence emission maxima corrected for the inner-filter effects.

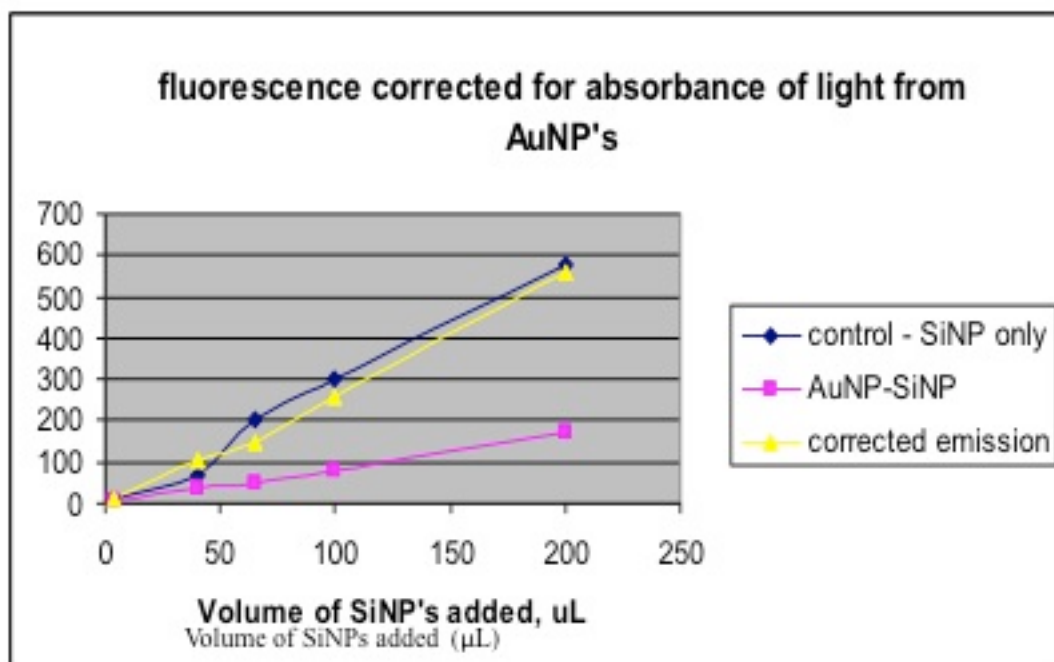


Figure 3.12 Fluorescence isotherms of fluorescence maxima of control samples and AuNP-SiNP aggregates before and after correction for inner-filter effects. Fluorescence emission was measured by exciting the samples at 550 nm at 5 nm slit width. Emission maxima was measured at 575 nm.

After the correction, it was observed that the emission maxima of mixtures almost overlapped with that of the controls, indicating that there has not been a significant change in fluorescence under these conditions. Although we were confident that AuNPs were aggregated by examining the absorbance data, we could not observe any enhancement or quenching as a result of this aggregation. We believe that the observed red-shift in the plasmons was mainly caused by increased gold-gold aggregation rather than the desired gold-silica aggregation under these conditions. Therefore, we

concluded that electrostatic binding was not a very efficient method for AuNP-SiNP aggregation. Furthermore, these results indicated the need for an improved technique to observe metal-fluorophore aggregation such as TEM (transmission emission microscope) imaging, since relying totally on absorbance measurements could be misleading.

After analyzing the results of this initial study we saw the need for stronger interactions such as covalent bonding between the two units. Since gold has a high affinity for sulfur atoms, n-alkanethiols have been widely used to functionalize gold surfaces.¹⁵ But our previous studies of thiol tethered BODIPY, showed that at high concentrations even the thiols could place exchange on gold surfaces. In search of a more robust method we noted dithiocarbamate (DTC) chemistry developed by Wie and co-workers to stabilize ligands on gold surfaces.¹⁷ It was reported that DTC does not place exchange even when exposed to very high concentrations of alkanethiols.¹⁸ Therefore, in our next phase we focused on DTC coupling for metal-fluorophore aggregation.

3.3.2 Metal-Fluorophore Aggregation by Dithiocarbamate Chemistry

In this section we report a facile solution based approach we have developed for using dithiocarbamate (DTC) chemistry to aggregate multiple gold nanoparticles around dye encapsulated in silica nanoparticles.

Recent studies show that dithiocarbamate ligand has proved to be extremely robust and versatile for metal directed self-assembly than simple thiols.¹⁶ The superiority of dithiocarbamate ligand is attributed to the inter-atomic distance between two sulfur groups in dithiocarbamate which is nearly ideal for the epitaxial adsorption onto Au surfaces.¹⁷ The DTC ligand is formed by the reaction of primary or secondary amines with carbon disulfide under basic conditions. The unstable bi-dentate DTC ligand has a very high affinity for thiophilic metals, and is thus easily stabilized by bonding to the metal.

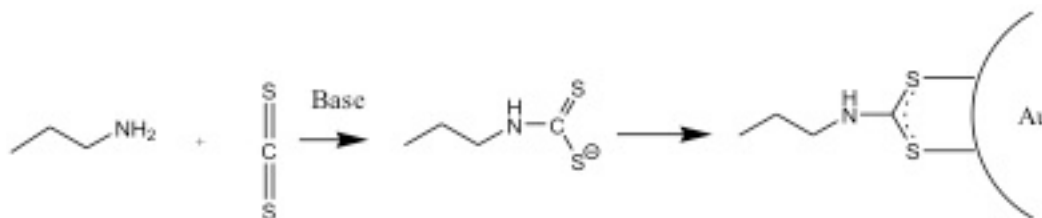


Figure 3.13 Dithiocarbamate bond formation on gold.

Recently, DTC chemistry has been used by the Rotello's group to immobilize gold nanoparticles on amine coated silica substrates using the robustness of the dithiocarbamate bond formation.¹⁸ We have modified this method and developed an

approach to covalently bind SiNPs to AuNPs in solution media which is a more convenient and direct than biomolecule tethering.

3.3.2.1 Synthesis of SiNPs and AuNPs for DTC Coupling

For this study, 70 nm diameter RhB doped SiNPs were synthesized using Stöber method and their surface was functionalized with APTES¹⁴ as described in Section 3.3.1.1. Using the density of silica and the volume of a 70 nm sphere, the concentration of the SiNPs solution was converted to nmol/L, which is about 4.3 nM.

AuNPs with 13 nm diameter were synthesized using standard citrate reduction method described in chapter 2 section 2.5.1, and they were capped with a neutral alkanethiol ($\text{CH}_3\text{O}(\text{CH}_2\text{CH}_2\text{O})_2\text{C}_{10}\text{H}_{20}\text{SH}$), using a procedure developed during our place exchange study described in 2.5.4. This ligand was synthesized by Anuradha Singh in Dr. Haltermans lab in the thioacetate form.¹⁹ We would refer to this capping group as the “ether capping” for convenience since the terminal group is an ether. In this place exchange first of 1 mM solution of the above ether (200 μL) in the thioacetate form was reacted with 1 mM KOH (200 μL) to cleave the acetate and convert it to the thiol ($\text{CH}_3\text{O}(\text{CH}_2\text{CH}_2\text{O})_2\text{C}_{10}\text{H}_{20}\text{SH}$). After 30 minutes the mixture was diluted up to 10 mL with 95 % ethanol and the solution was split into two 5 mL portions in two glass vials. To each 5 mL portion of ether, 9 mL of citrate capped sol was added. The solution was mixed and left in the dark for 24 h for the place exchange. The concentration of ether capped AuNP solution was determined using the extinction coefficient of AuNPs to be 1.2 nM.

3.3.2.2 Interaction of APTES coated SiNPs with Ether capped AuNPs using DTC

Chemistry

In this approach, APTES coated RhB doped SiNPs were mixed with 1 mM carbon disulfide (CS_2) at pH 8.5-9.5 in 95% ethanol for 30 minutes, for DTC activation (Figure 3.14). The amine functionality of APTES would readily react with carbon disulfide under basic conditions to produce dithiocarbamate ligand which has a very high affinity for gold surfaces.^{17a, 20} When ether capped 13 nm AuNPs were added to DTC activated SiNPs, tiny silica-gold aggregates were formed. Fluorescence and absorbance spectra of these samples were measured over time.

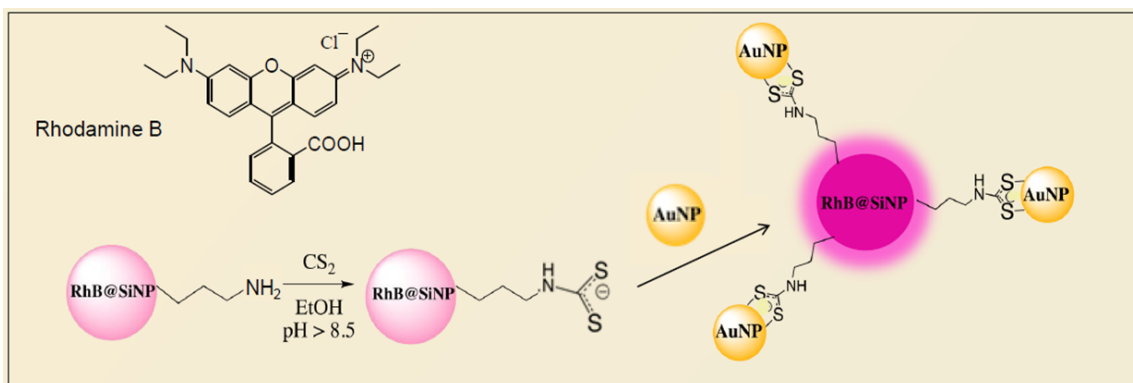


Figure 3.14 Formation of metal-fluorophore aggregates using DTC chemistry.

3.3.2.3 Development of Experimental Procedure

Finding the optimal experimental conditions that would give rise to fluorescence enhancement was challenging since this was a new approach. We had to optimize three unknown experimental conditions; the best pH range, the CS₂ concentration, and the SiNP to AuNP ratio that would give rise to fluorescence enhancement. Although in the literature the DTC reaction was carried out at high pH (above 11), we observed that with solutions above pH 10, CS₂ would apparently interact with AuNPs and cause distinct gold-gold aggregation, as determined by red shifting of the absorbance spectra. Therefore, to prevent undesired gold-gold aggregation the pH of the samples were kept were kept in the 8.5-9.5 range. This was achieved by addition of small aliquots of concentrated KOH to raise the pH to the desired range. The pH of the samples could not be controlled by buffer, since addition of extra salt also caused gold-gold aggregation. Furthermore, in literature procedures equi-molar mixtures of CS₂ and amine were used.²¹ Since the amount of amine on the surface of the SiNPs was unknown, CS₂ concentration was varied between 0.1-10 mM concentration to find the optimal concentration that would facilitate coupling SiNPs with AuNPs while preventing gold-gold aggregation. Moreover, according to literature DTC activation and the addition of AuNPs was done simultaneously^{20, 21} in one pot. We however did not see any enhancements by mixing all reagents simultaneously. Thus, in our procedure we did the DTC activation (base and CS₂) 30 min prior to the addition of AuNPs. To find the optimal AuNP: SiNP ratio that would give rise to fluorescence enhancement, initially, the amount of AuNPs was kept constant and the SiNP ratio was varied. As detailed in

the experimental section the AuNP to SiNP ratios was estimated using the nano molar concentrations of the solutions (preparation-1).

We were able to observe about 2-3 fold fluorescence enhancement when the SiNP to AuNP ratio was about 1:10, with 1 mM CS₂, indicating that enhancement was possible by this method (Figure 3.15) . Thus, the experiment was repeated by mixing varying amounts of DTC activated SiNPs with 1 mL of ether capped AuNPs. For the DTC activation 1 mM CS₂ solution was prepared in 95% ethanol. The pH of this solution was raised above 8.5 by adding KOH. Next 1 ml aliquots of the CS₂ solution were transferred to different vials and varying amounts of SiNPs (250, 25, 12.5 μL) were added to each vial. Mixtures were capped and stirred for 30 min for the DTC activation. After 30 min, 1 mL of ether capped AuNPs (1 mL) were added to each sample and the samples were stirred over time. The prepared AuNP to SiNP ratios were; 1:1, 10:1, 20:1. To test whether the DTC coupling gave rise to the enhancement, controls were made by mixing same ratios of AuNPs and SiNPs at same conditions but having 95% ethanol instead of 1 mM CS₂. Another set of controls were prepared by having the same amount of SiNPs at same conditions but having 1 ml of 9:5 water: ethanol mixture, to compensate for 1 mL of ether capped AuNPs in water/ethanol mixture. Fluorescence emission of these samples was measured by exciting the samples at 550 nm wavelength, at 5 nm slit width. The following figures (3.15-17) show the fluorescence emission of controls with and without AuNPs and DTC coupled mixtures of the above samples. Enhancement was calculated relative to the fluorescence of SiNP mixtures without AuNPs.

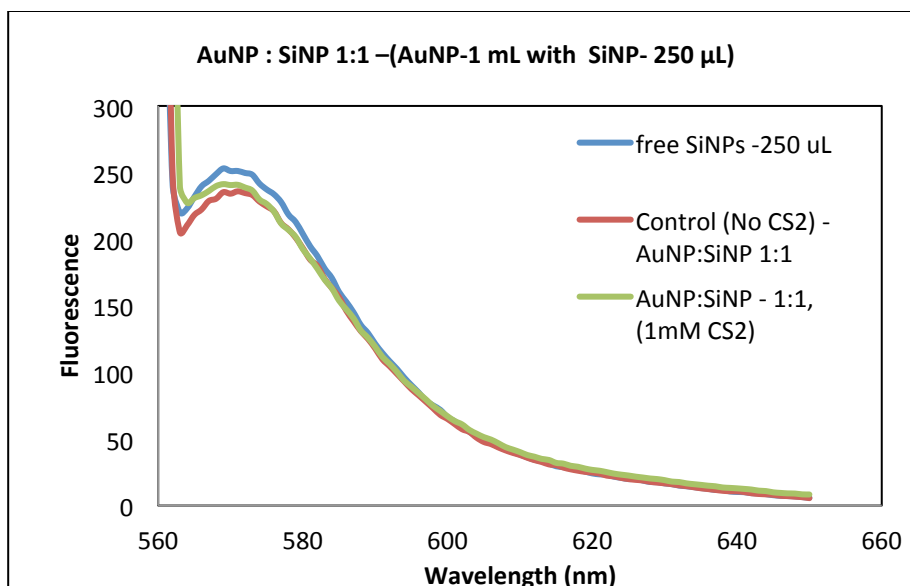


Figure 3.15 Fluorescence emission of DTC coupled 1:1 AuNP:SiNP mixtures and controls; without CS2 and without AuNPs (free SiNP). Samples were prepared as described in text, in 70% ethanol, samples were excited 550 nm at 5 nm slit width.

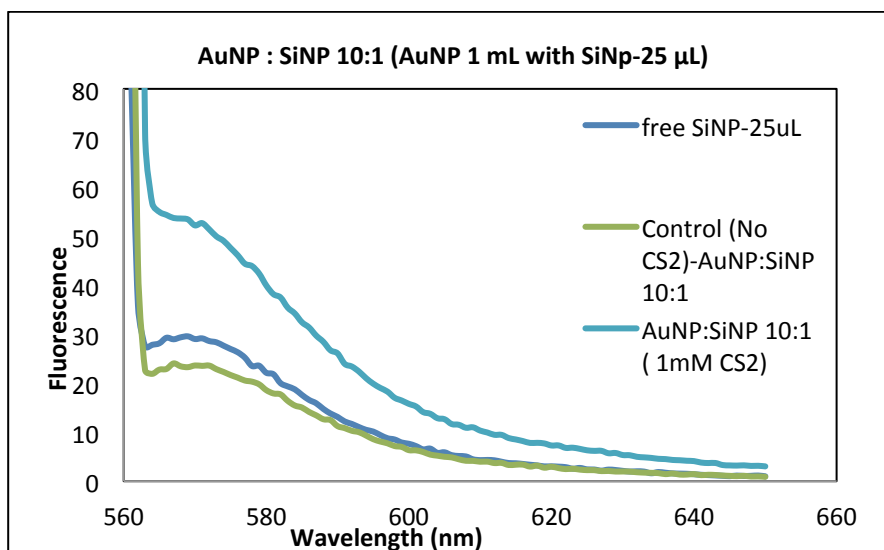


Figure 3.16 Fluorescence emission of DTC coupled 10:1 AuNP:SiNP mixtures and controls; AuNP and SiNPs without CS2 and SiNPs without AuNPs (free SiNP). Samples were prepared as described in text, in 70% ethanol and excited at 550 nm at 5 nm slit width.

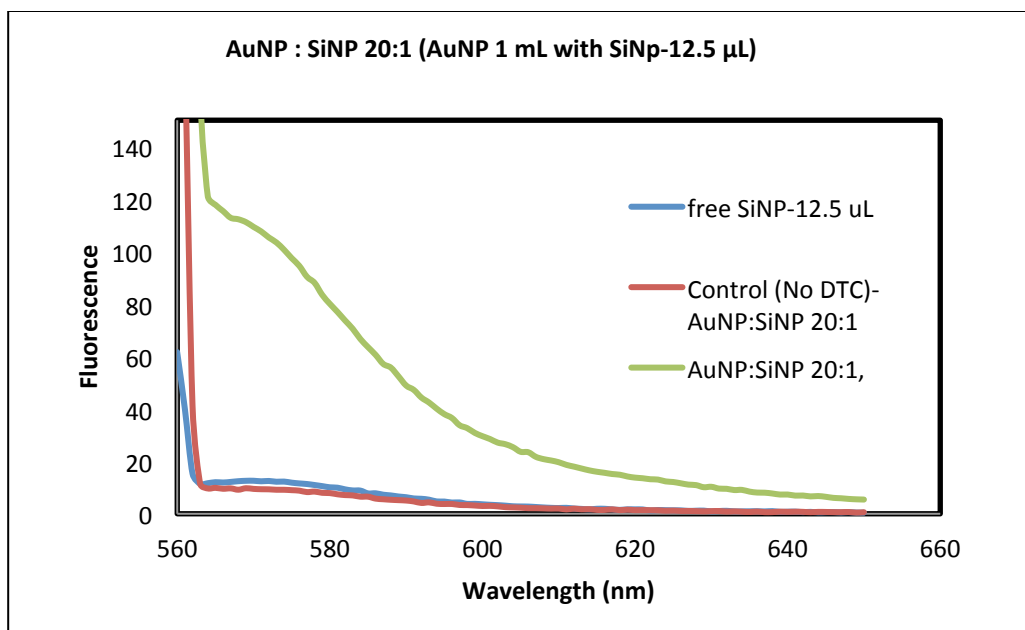


Figure 3.17 Fluorescence emission of DTC coupled 20:1 AuNP:SiNP mixtures and controls; AuNP and SiNP without CS2 and SiNPs without AuNPs (free SiNP).

Examination of the above fluorescence data indicates that fluorescence enhancement is possible by interacting multiple AuNPs with fewer dye doped SiNPs. The data indicated that the 1:1, AuNP : SiNP mixture showed no enhancement, while the 10:1 mixture showed about 2 fold enhancement and the maximum enhancement was observed with 20:1 AuNP:SiNP ratio. The absorbance spectra of the enhanced samples were also red shifted indicating aggregation of AuNPs. Since the enhancement increased with increasing AuNP ratio, these results indicate that enhancement could be due to increased aggregation.

3.3.2.4 Optimization of Enhancement by Metal-Fluorophore Aggregation

To further optimize the enhancement, next we fixed the amount of SiNPs at a very low concentration (7.5×10^{-4} mg/mL) and varied the AuNP ratio. For this study APTES

coated RhB doped SiNPs were prepared using the method described in section 3.3.1.1, but less dye was doped into the particles (preparation-2). In sample preparation, 1 mM CS₂ (3 mL) were added to 4 different glass vials and their pH was raised to about 8.5 by adding concentrated KOH. To each sample 20 μL of APTES coated RhB doped SiNPs were added and the samples were capped and stirred for 30 minutes for DTC activation. After 30 minutes, varying amounts of AuNPs (0.25, 0.5, 0.75, 1 mL) were added to each sample. To keep the final volume to a 4 mL in each sample, additional amounts of 9:5 water/ethanol mixture were added to samples having less than 1mL of AuNPs. The necks of screw capped vials were sealed with Parafilm to prevent evaporation of ethanol. Control samples were prepared by having the same constituents as the DTC coupled samples but having 95% ethanol instead of 1mM CS₂. Another control was prepared by having same conditions but only SiNPs and no AuNPs. The samples were stirred for 24 h the fluorescence and absorbance were measured. Figure 3.18 shows the fluorescence spectra of the DTC coupled samples after day 1.

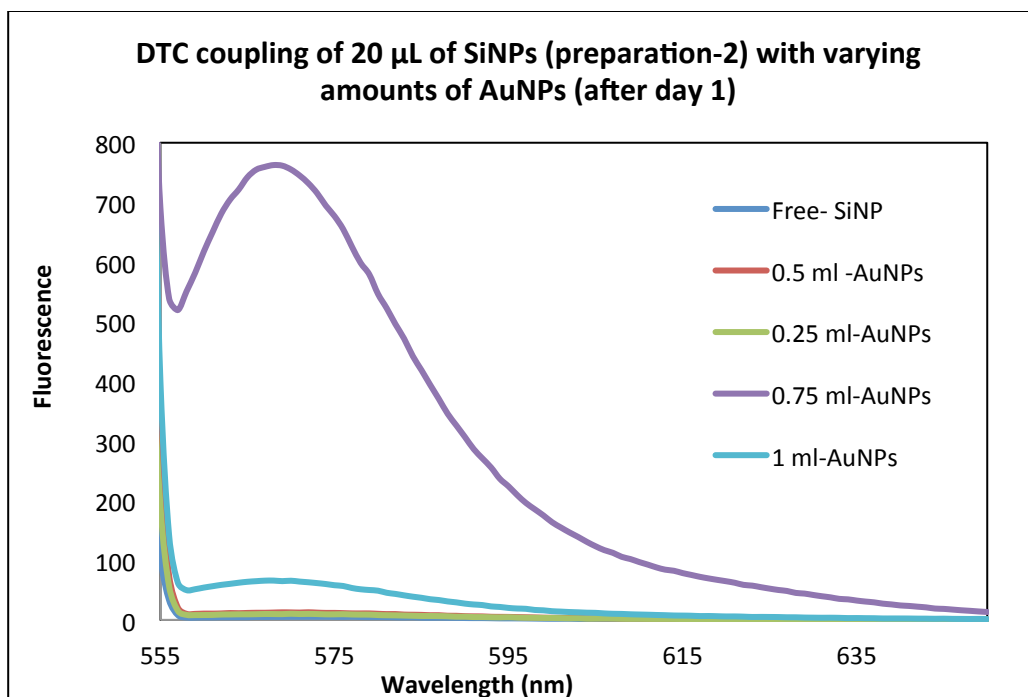


Figure 3.18 Fluorescence emission of DTC coupled RhB doped SiNPs (20 μ L) from preparation-2, with varying amount of AuNPs after day 1. Samples were prepared as in text in 85% ethanol. Samples were excited at 545 nm at 5nm slit width.

Interestingly, in this attempt we were able to produce aggregates giving large enhancements greater than 100-fold after day 1. The maximum emission was observed for the sample having 0.75 mL of ether capped AuNPs. Figure 3.19 shows the absorbance spectra of DTC coupled samples and the controls with no CS₂ after day 1. We did not observe a significant red shift in the absorbance spectra of the AuNP plasmon after the first day. This indicated that there was still a significant amount of un-aggregated AuNPs in solution. Therefore, the samples were kept stirring for a longer period of time. More red shifting and broadening of spectra was observed over time (Figure 3.20), furthermore the fluorescence enhancement also increased.

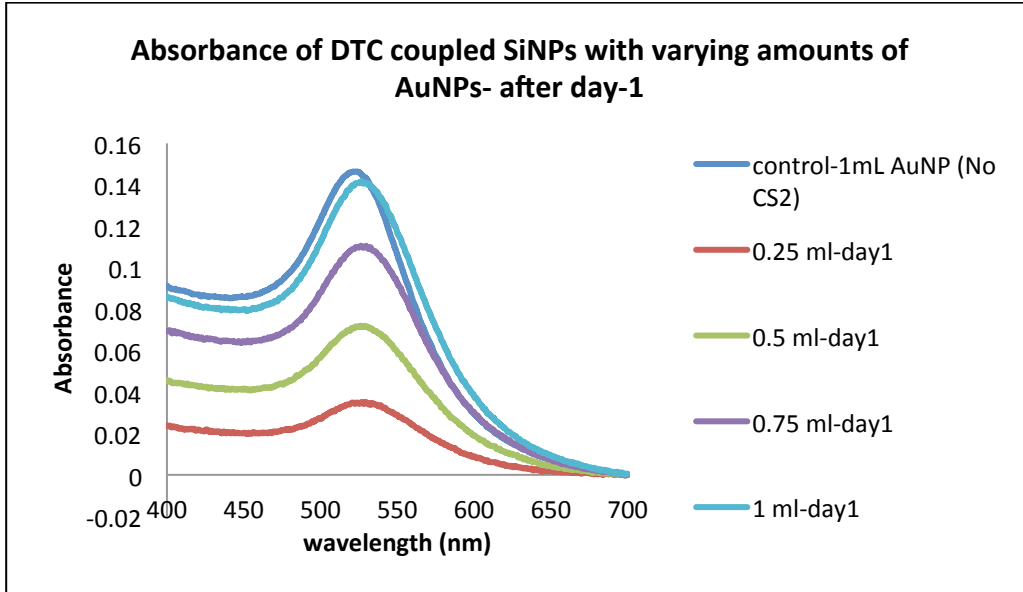


Figure 3.19 Absorbance spectra of DTC coupled metal-fluorophore aggregates and control samples (1mL AuNPs and SiNPs without CS₂ from preparation -2) after day 1.

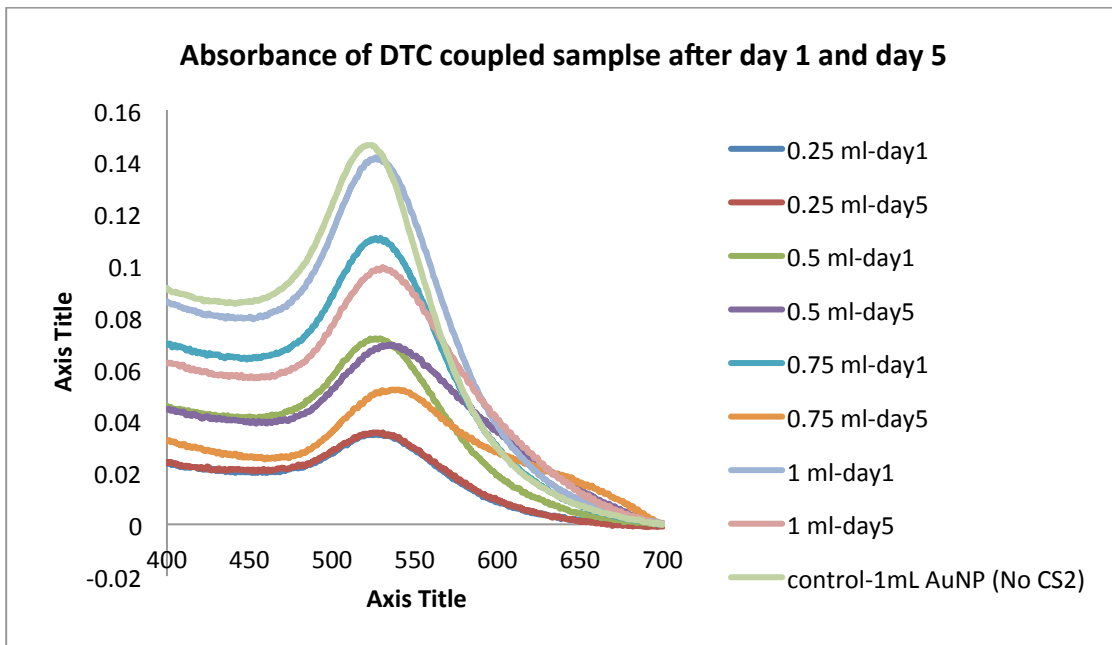


Figure 3.20 Absorbance spectra of DTC coupled metal-fluorophore aggregates from preparation -2, after day 1 and day 5.

Figure 3.21 shows the increase in fluorescence emission of the sample which gave the highest enhancement over time, and the inset shows the emission of controls; without AuNPs, and the controls with AuNPs but with no CS₂. The enhancement of this DTC coupled sample increased overtime and reached nearly 200-fold, after 7 days and then leveled off. The enhancement was calculated relative to the fluorescence of the control samples without AuNPs.

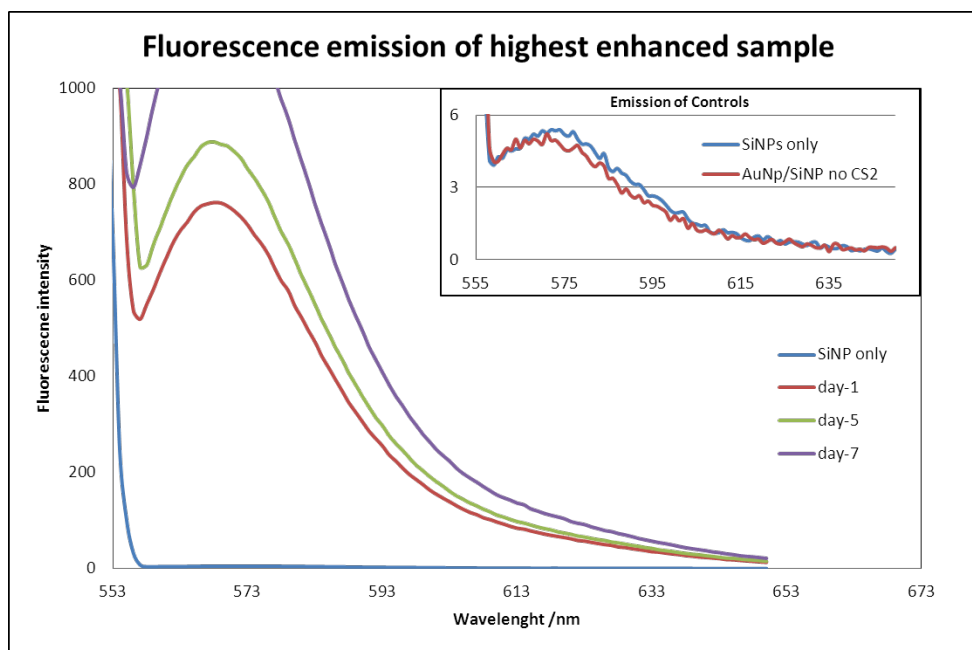


Figure 3.21 Fluorescence emission of the sample with the highest enhancement (from preparation -2) over time (inset-emission of control samples). Samples were excited at 545 nm at 5nm slit width.

Figure 3.22 shows the absorbance spectra of the same sample over time. The red shifting and the broadening of the AuNP plasmon band at day 5 and day 7 indicates the aggregation of individual AuNPs and formation of large AuNP aggregates over-time. The broadening could be attributed to the enhanced scattering from large aggregates. We believe the observed increase in enhancement over time was also caused by continuous aggregation of AuNPs on dye doped silica nano spheres.

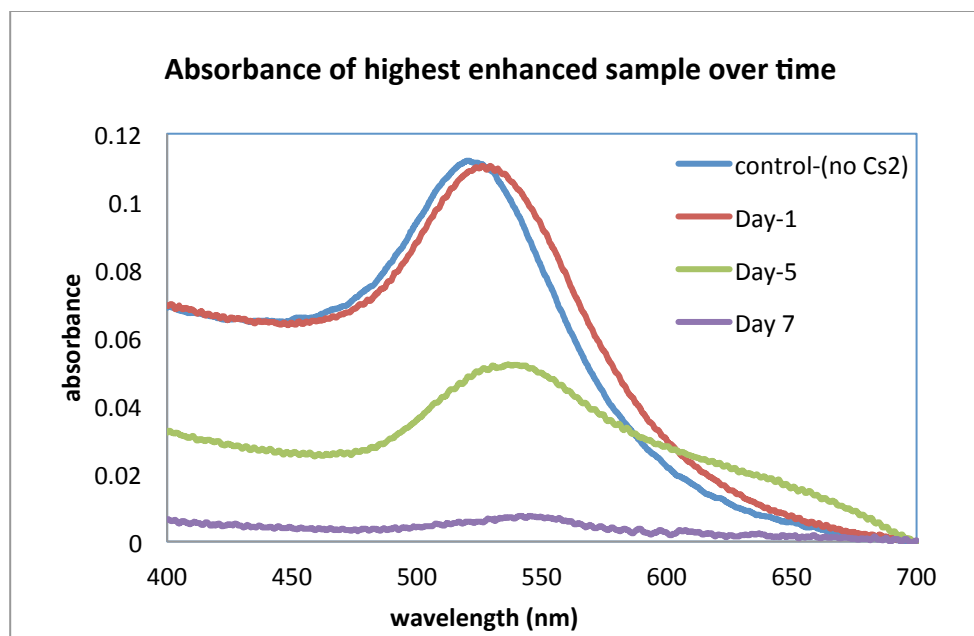


Figure 3.22 Absorbance spectra of the sample with the largest enhancement (from preparation -2) after day 1, day 5 and day 7.

3.3.2.5 TEM Study of Enhanced Samples

To get a better understanding of the metal-fluorophore aggregation pattern, the enhanced preparation-2 samples were imaged under the transmission emission microscope (TEM). For TEM analysis, 3 μ L aliquots from the highest enhanced sample from preparation-2 were drawn out at different time intervals (2 days and 14 days after preparation) and were deposited on a copper grids coated with formvar. The images provided interesting evidence for the predicted aggregation pattern. Figure 3.23 (left) shows the aggregation pattern of the enhanced sample after two days and 3.23 (right) shows the aggregation pattern after 14 days.

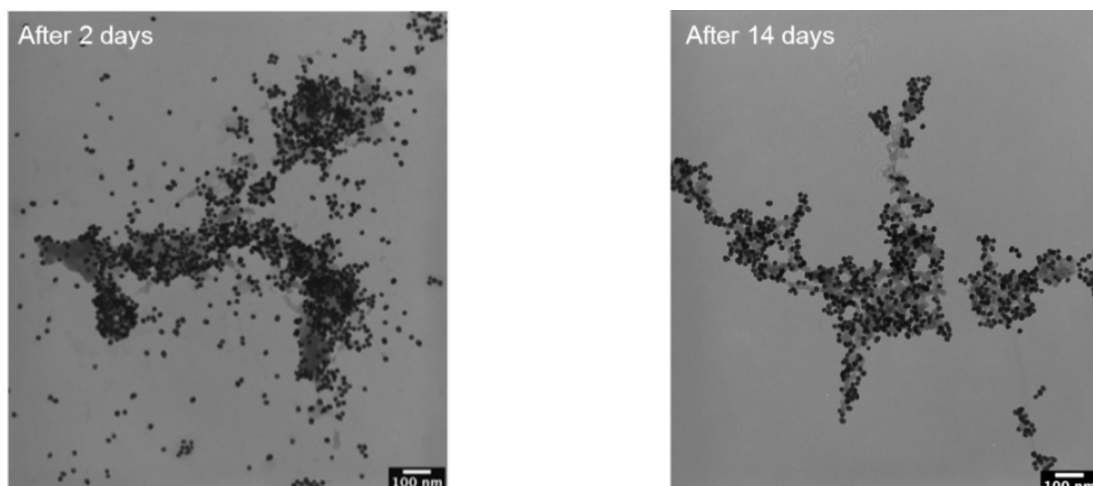


Figure 3.23 TEM images of an enhanced metal-fluorophore aggregates (SiNPs from preparation -2) over time (after 2 days -left and after 14 days-right).

In the above images the black dots are the AuNPs and the gray material is silica. The images indicate that SiNPs are webbed together in solution rather than existing as individual particles. Furthermore, they show good evidence for aggregation of AuNPs on silica. However, the 2 day old sample shows a lot of un-aggregated AuNPs around, indicating incomplete aggregation, whereas, in the 14 days old sample the aggregation seems much more complete. These images also match with the absorbance data. The absorbance spectrum after day 1, was only slightly red shifted indicating presence of a lot of un-aggregated AuNPs, whereas, the absorbance after day 7 was very much red shifted and indicating significant aggregation. These results confirm that the observed increase in enhancement over time could be probably due to continuous aggregation of AuNPs on SiNPs. The TEM imaging was done by Nathan Green in Dr. Halterman's lab.

3.3.3.6 Calculation of the Enhancement Factor

The enhancement factor was calculated by integrating the fluorescence emission of enhanced samples and dividing them by the average integrated fluorescence of control samples without AuNPs. Figure 3.24 shows the increase in enhancement of the DTC coupled samples over time and the variation in enhancement factor with increasing amounts of AuNPs added. Figure 3.25 shows the same graph in log scale.

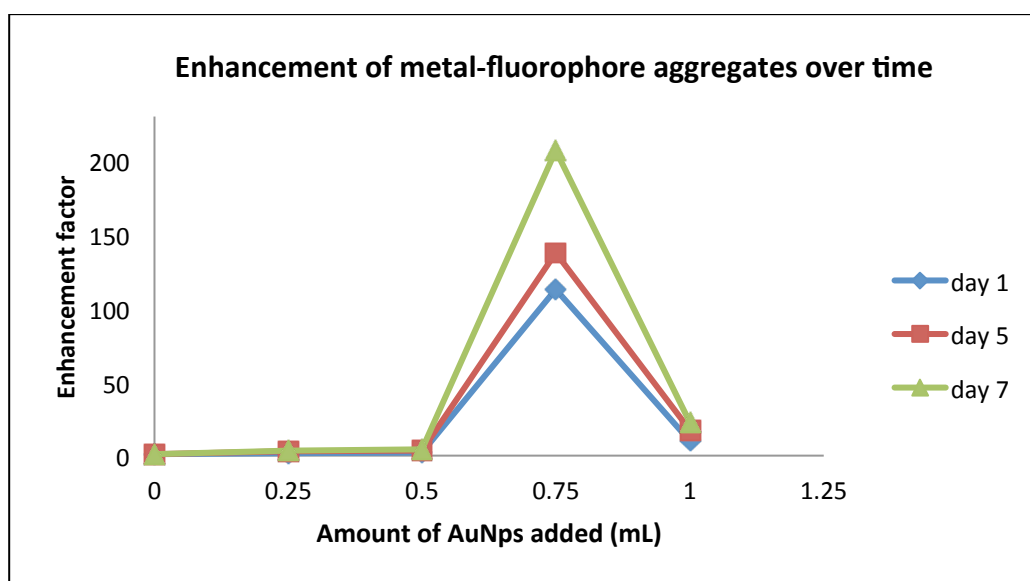


Figure 3.24 Variation of the enhancement factor with increasing amounts of AuNPs over time (preparation-2)

We observed that the enhancement factor increased with increasing additions of AuNPs up to 0.75 mL and then dropped with further additions. Furthermore, the enhancement of each sample increased over time. Both effects could be possible due to increased AuNP-SiNP aggregation, which resulted location of fluorophores between coupled plasmons.

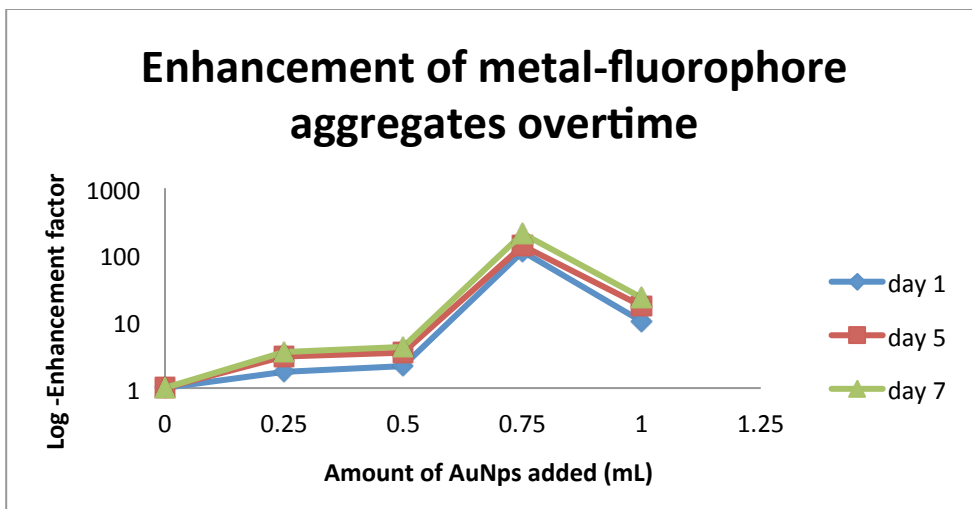


Figure 3.25 Variation of the enhancement factor with increasing amounts of AuNPs, over time (SiNPs from preparation -2)

3.3.4 Reproducibility of the Technique

To check the reproducibility of the technique, we repeated the experiment in the same manner, by keeping the SiNP ratio constant and varying the AuNP ratio. Samples were prepared in duplicates (a & b). Figure 3.26 shows the variation of the enhancement factor upon increasing additions of AuNPs after day 3.

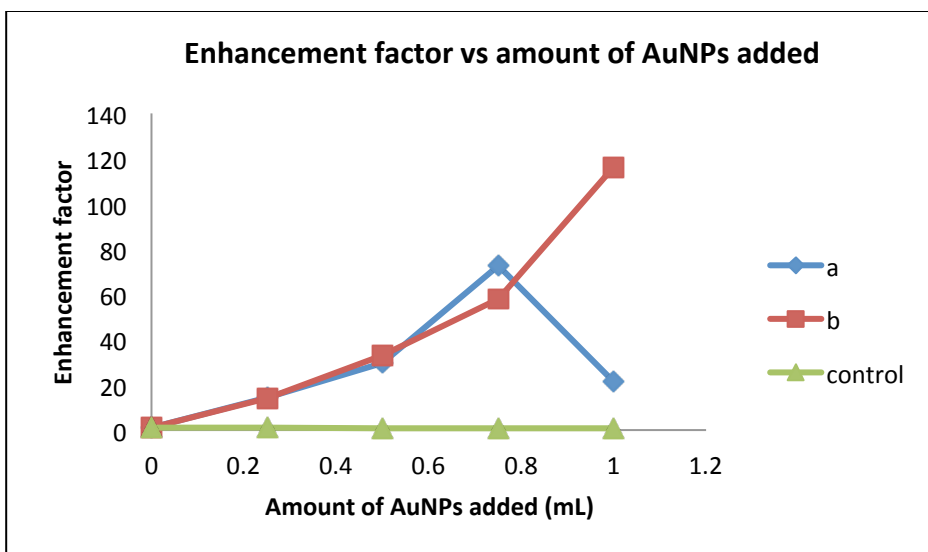


Figure 3.26 Variation of enhancement factor with increasing amount of AuNPs (preparation-3).

At this attempt, we were able to repeat the same trend as we observed at the first attempt except for the duplicates containing the highest amount of AuNPs (1 mL). Furthermore, higher enhancements were observed with the samples having less amount of gold than the previous attempt. While the 200-fold enhancement was not reproduced, maximum enhancement of was 120-fold was observed. As before the enhancement increased with increasing amount of AuNPs. For the samples with the highest amounts of AuNPs, one of the duplicates showed 120 fold enhancement (highest) while and the other showed only 20 fold enhancement. A closer look at the TEM images (Figure 3.27) and information from these observations indicate that there could be a competition between two possible events of aggregation in solution phase, metal-fluorophore and metal-metal aggregation. As we increase the AuNP concentration the enhancement would increase and reach a maximum until metal-fluorophore aggregation is dominant.

After further additions of AuNPs the enhancement would decrease if metal-metal aggregation is dominant.

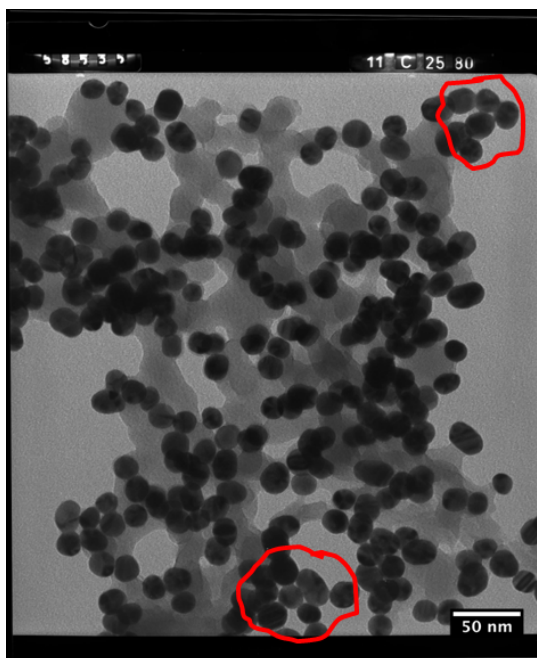


Figure 3.27 TEM image of gold silica aggregates at higher magnification (SiNPs from preparation -2).

A closer look at the TEM image (Figure 3.27) shows that although AuNP-SiNP aggregation is dominant there are some areas showing gold-gold aggregation as well. Thus, if the gold-gold aggregation dominates without attachment to SiNPs, the enhancement would not increase as much. Furthermore, if the amount of dye molecules incorporated per particle was significantly different, it would cause inconsistency in the data as well.

3.3.5 Calculation of Dye Molecules Incorporated per Particle

The number of dye molecules per particle was calculated assuming that the RhB in silica matrix would emit at the same intensity as the free dye would emit in a given ethanol/water mixture. Therefore, dilution series of Rhodamine was prepared at nanomolar range in 85 % ethanol (replicates for each concentration 1, 2, & 3), and the

fluorescence was measured immediately. Figure 3.28 shows the titration curve generated using integrated emission intensity of each dilution.

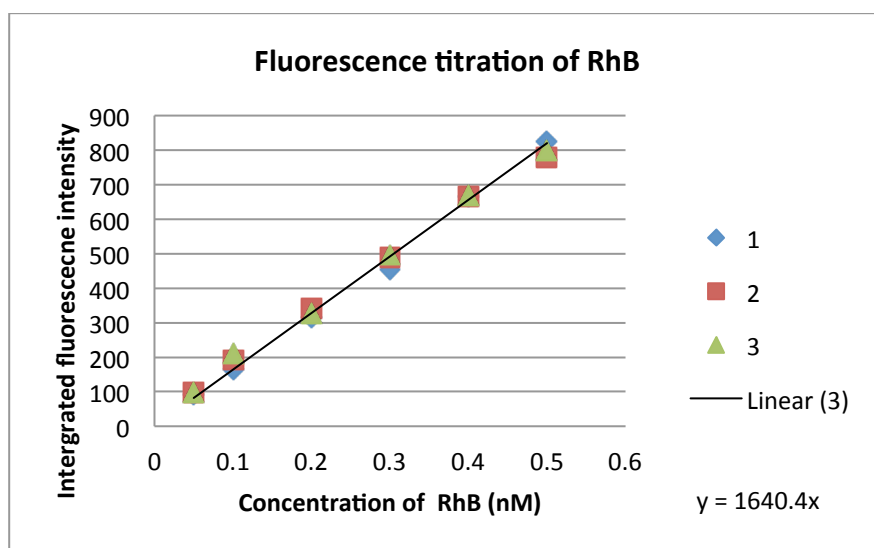


Figure 3.28 Fluorescence emission of Rhodamine B dilution series at monomolar concentrations (replicates 1,2,&3).

The average integrated fluorescence emission of the control sample without AuNPs was 189.8(+/-18). Therefore, the concentration of RhB in the enhanced sample was calculated using the above curve to be 0.11(+/- 0.0007) nM. Using the initial amount of SiNPs used to prepare the stock solution, the concentration of dye doped silica in a sample was calculated to be 7.5×10^{-4} mg/mL. Using the density of silica, and the volume of a 70 nm sphere, the amount of dye molecules per particle was calculated. Table 5 lists the values we have calculated.

Table 5 List of facts about the amounts of dye molecules incorporated in silica.

Concentration of RhB in a 4 mL sample	0.11 nM
Number of RhB molecules in the sample	2.78×10^{11}
Concentration of silica in the sample	7.4×10^{-4} mg/mL
Volume of silica in the sample	1.5×10^{15} nm ³
Number of Dye molecules per nm ³	1.8×10^{-4} / nm ³
Volume of 70 nm sphere	179646 nm ³
Dye molecules per 70 nm particle	32 molecules

By this method we also realized the RhB doped SiNPs are much more photo stable than the free dye in solution. The intensity of free RhB at nanomolar concentrations would decrease over time, whereas, the intensity of the dye doped silica would remain constant even when exposed to light at bench top conditions. The metal-fluorophore aggregates also showed enhanced photo stability. The fluorescence emission of the enhanced aggregates remained unchanged through a period of 3 months.

3.3.6 How Could Rhodamine B show enhancements greater than a 2 fold?

Rhodamine B is considered highly fluorescent dye with a quantum yield of 0.5. According to classical fluorescence, a dye with a 0.5 quantum yield can only be enhanced two-fold. However, our results show that RhB can be easily enhanced greater than two-fold. We have observed enhancements greater than a 100-fold several times, and also a 200-fold enhancement by this method. According to our perspective of MEF, this enhancement could be due to two factors. One is due to the increased excitations and the other is due to the modification in radiative decay rates.^{1a, 2a, 10} Since modification of the ratio of the non-radiative and radiative decay rates can only enhance the dye by a twofold, we believe that a large part of the enhancement is caused by increased excitations or by the lightning rod effect. Increased excitations would increase the enhancement of the fluorophore without affecting the quantum yield by increasing the number of excited molecules per unit time.^{1a} The available literature also predicts that for high quantum yield fluorophores, increased number of excitations would dominate the enhancement. We believe that increased excitations could result due to enhanced electromagnetic fields of the coupled plasmons.²¹ [ENREF 29](#) Furthermore, the enhanced scattering due to formation of larger aggregates over time would also assist in radiating the fluorophores emission to the far-field resulting in faster decay rates and the possibility of faster cycling to produce more emitted photons per unit time.

3.4 Chapter Summary

In this study we have investigated methods to form metal-fluorophore aggregates with enhanced fluorescence using dye doped silica nanoparticles and gold nanoparticles. Our results show that strong binding between metal and the fluorophore led to observed enhancements. We have developed a new solution based approach for metal-fluorophore binding using DTC chemistry. Our results show that Rhodamine B can enhance greater than a 100 fold by this method. Furthermore, the metal-fluorophore aggregates are more photostable or long lived than free dye in solution. Thus, we believe further development of this technique would aid in producing bright fluorescent marker for solution based sensing.

3.5 Experimental Section

3.5.1 Synthesis of Dye Doped Silica Particles (Preparation-1)

Spherical dye doped silica nanoparticles (70 nm diameter) were synthesized using an established procedure. In this synthesis, first the dye was covalently attached to silica, using a silane coupling agent (APTES). For this coupling a mixture of Rhodamine B (0.100 g, 0.2 mmol), 1-(3-dimethylaminopropyl)-3-ethylcarbodiimide hydrochloride (EDC) (0.080 g, 0.40 mmol), n-hydroxysuccinimide (NHS) (0.050 g, 0.40 mmol) 4-dimethylaminopyridine (DMAP) (0.005 g, 0.040 mmol) and dimethylformamide (DMF) (5 mL) was stirred under nitrogen at room temperature for 12 hours. After 12 hours, APTES (94.7 μ L, 0.40 mmol) was added and the mixture was again stirred for another 24 hours. Next a mixture of 95 % ethanol (8.375 mL) and 30% ammonium hydroxide (0.64 mL) was prepared in a capped scintillation vial and the silane coupled RhB in DMF (1.5 mL) was added, and this mixture was stirred at room temperature for 12 hours for hydrolysis of siloxane group of APTES. After 12 hours TEOS (0.355 mL) was added and the mixture was stirred for another 24 hours. Next portions (1.5 mL) of reaction mixture were transferred to micro-centrifuge tubes and were centrifuged at 12,000 rpm for 10 min to yield dark pink pellets of silica. The purple supernatant was removed using a pipette, and the particles were resuspended in 95% ethanol (1.5 mL) by sonication. The washing of particles was repeated 3 times with 95 % ethanol and 3 times with milipore water as described above until the color of the supernatant was almost clear. Next the particles were dried in a vacuum oven at 35 °C overnight to give a pink powdery solid.

3.5.2 Surface Functionalization of SiNPs with Propylamine

Surface functionalization of dye doped SiNPs with propylamine was accomplished using an established procedure. Vacuum dried RhB doped SiNPs (50 mg) was dissolved in milipore water (5 mL) by sonicating for 10 min in a capped scintillation vial. Next glacial acetic acid (100 μ L) and APTES (100 μ L) were added and the mixture was stirred for 3-4 hours. Again the reaction was quenched by centrifugation and the particles were washed with milipore water and 95 % ethanol three times as described previously. The sample was vacuum dried for 30 min at 35 °C and a stock solution was prepared by dissolving SiNPs (30 mg) in milipore water (25 mL) in a volumetric flask so that the final concentration would be 1.2 mg/mL.

3.5.3 Synthesis of Dye Doped Silica Particles (Preparation-2)

In preparation-2, the amide coupling step was carried out in the same manner as in preparation-1. Next a mixture of 95% ethanol (8.375 mL) and 30% ammonium hydroxide (0.640 mL) was prepared in a capped scintillation vial and the silane coupled dye in DMF (1.5 mL) was added to the mixture. This mixture was only stirred for 10 minutes. After 10 min, TEOS (0.355 mL) was added and the mixture was stirred for another 24 hours. Since TEOS was added only after 10 minutes, less dye was loaded to these samples. Thus, these particles looked lighter in color than the ones prepared in preparation-1. The surface functionalization with propylamine was carried out in the same manner as in preparation-1.

3.5.4 Calculation of Concentration of 70 nm SiNPs in Stock Solution

Volume of a 70 nm sphere $(4/3\pi r^3) = 1.8 \times 10^5 \text{ nm}^3$

Density of silica = 2.65 g/cm^3

Weight of a 70 nm particle = $4.67 \times 10^{-13} \text{ mg}$

Weight of SiNPs used to prepare the stock solution = 30 mg

Number of 70 nm SiNPs in stock solution = $30 \text{ mg} / 4.67 \times 10^{-13} \text{ mg}$
 $= 6.4 \times 10^{13} \text{ particles}$

Number of moles of SiNPs = $6.4 \times 10^{13} / 6.023 \times 10^{23} \text{ mol}^{-1}$
 $= 1.07 \times 10^{-1} \text{ nmol}$

Volume of stock solution = 25 mL

Concentration of particles = 4.27 nM.

3.5.5 DTC Coupling of AuNPs with SiNPs

AuNPs with 13 nm diameter were synthesized by standard citrate reduction method, and were capped with $\text{CH}_3\text{O}(\text{CH}_2\text{CH}_2\text{O})_2\text{C}_{10}\text{H}_{20}\text{SH}$ ligand. The modified AuNPs were mono-dispersed in 34% ethanol. RhB doped SiNPs with 70 nm diameter were synthesized by Stöber method and their surface was functionalized with 3-aminopropyltriethoxysilane (APTES). All procedures have been described previously.

For the DTC coupling, a solution of APTES modified RhB doped SiNPs (0.15 mg/mL) was prepared in 95% ethanol by mixing 0.5 mL of the SiNP stock solution (1.2 mg/mL) in 3.5 mL of 95 % ethanol (final volume 4 mL). The pH of this

solution was raised to about 9.8 by addition of concentrated KOH. Mixtures of 1 mM CS₂ was prepared in a 20 mL scintillation vials by mixing 3 mM CS₂ (1 mL,) with 95 % ethanol (2 mL). The pH of this mixture was raised to 8.5-9 by adding concentrate KOH (10 μL at pH 12.12). To each mixture RhB doped SiNPs (20 μL, 0.15 mg/mL) was added and the mixtures were stirred for 30 minutes for the activation of DTC. Ether capped AuNPs were added after 30 min. To vary the AuNP ratio, the volume of ether capped AuNPs in 34 % ethanol was varied (0.25, 0.5, 0.75,1 mL) by keeping the SiNP ratio constant (20 μL). The total volume of each solution was brought to 4 mL by adding 34 % ethanol. Since the final volume of each sample was 4 mL, the concentration of RhB doped SiNPs in each sample was 7.5×10^{-4} mg/mL. To test for DTC coupling, controls were made by adding the same amounts of SiNPs and AuNPs and other reagents, but having 95% ethanol (1 mL) instead of 3 mM CS₂ (1mL). To calculate the enhancement factor, SiNP solutions without AuNPs were made at same conditions. These were prepared by mixing 95% ethanol (2 mL), 3mM CS₂ (1 mL) and 34% ethanol (1 mL) and SiNPs from preparation-2 (20 μL, 0.15 mg/mL) Absorbance and fluorescence of all solutions were measured over time. All capped scintillation vials were sealed with Para film to prevent evaporation of solvent.

3.5.6 Fluorescence and Absorbance Measurements

Absorbance measurements were performed using a Shimadzu Scientific Instruments UV-2101 PC UV-Vis scanning spectrometer using disposable 10×5 mm polystyrene cuvettes.

Steady state fluorescence measurements were performed using a Shimadzu Scientific instruments RF 5301 PC spectrofluorophotometer using disposable 10×5 mm polystyrene cuvettes. The excitation source of the instrument was a 150 W Xenon lamp. Samples were excited at 545 nm at 5 nm slit width.

3.5.7 TEM Imaging

For TEM imaging samples were prepared in 300 mesh formvar copper grids. Before preparing the TEM samples, the AuNP-SiNP mixtures were sonicated for 2 min, next 3 μ L aliquot was deposited on copper grid and solvent was left to evaporate in a desiccator. The samples were imaged by ZEISS 10 transmission emission microscope at an accelerated voltage of 80 keV by Nathan Green. All samples were first scanned at low magnification to get an overall picture of the sample and then zoomed in for better resolution.

3.6 Chapter 3 References

1. (a) Aslan, K.; Gryczynski, I.; Malicka, J.; Matveeva, E.; Lakowicz, J. R.; Geddes, C. D., Metal-enhanced fluorescence: an emerging tool in biotechnology. *Current Opinion in Biotechnology* **2005**, *16* (1), 55-62; (b) Lakowicz, J. R., Plasmonics in biology and plasmon-controlled fluorescence. *Plasmonics* **2006**, *1* (1), 5-33; (c) Anker, J. N.; Hall, W. P.; Lyandres, O.; Shah, N. C.; Zhao, J.; Van Duyne, R. P., Biosensing with plasmonic nanosensors. *Nature materials* **2008**, *7* (6), 442-453.
2. (a) Aslan, K.; Lakowicz, J. R.; Geddes, C. D., Plasmon light scattering in biology and medicine: new sensing approaches, visions and perspectives. *Current opinion in chemical biology* **2005**, *9* (5), 538-544; (b) Aslan, K.; Lakowicz, J. R.; Szmacki, H.; Geddes, C. D., Metal-enhanced fluorescence solution-based sensing platform. *Journal of fluorescence* **2004**, *14* (6), 677-679; (c) Geddes, C. D.; Lakowicz, J. R., Editorial: Metal-enhanced fluorescence. *Journal of fluorescence* **2002**, *12* (2), 121-129.
3. Hao, E.; Schatz, G. C., Electromagnetic fields around silver nanoparticles and dimers. *The Journal of Chemical Physics* **2004**, *120*, 357.
4. (a) Su, K. H.; Wei, Q. H.; Zhang, X.; Mock, J.; Smith, D.; Schultz, S., Interparticle coupling effects on plasmon resonances of nanogold particles. *Nano letters* **2003**, *3* (8), 1087-1090; (b) Fromm, D. P.; Sundaramurthy, A.; Schuck, P. J.; Kino, G.; Moerner, W., Gap-dependent optical coupling of single "bowtie" nanoantennas resonant in the visible. *Nano letters* **2004**, *4* (5), 957-961.
5. Gunnarsson, L.; Rindzevicius, T.; Prikulis, J.; Kasemo, B.; Käll, M.; Zou, S.; Schatz, G. C., Confined plasmons in nanofabricated single silver particle pairs: experimental observations of strong interparticle interactions. *The Journal of Physical Chemistry B* **2005**, *109* (3), 1079-1087.
6. (a) Sweatlock, L.; Maier, S.; Atwater, H.; Penninkhof, J.; Polman, A., Highly confined electromagnetic fields in arrays of strongly coupled Ag nanoparticles. *Physical Review B* **2005**, *71* (23), 235408; (b) Zhang, J.; Fu, Y.; Chowdhury, M. H.; Lakowicz, J. R., Metal-enhanced single-molecule fluorescence on silver particle monomer and dimer: coupling effect between metal particles. *Nano letters* **2007**, *7* (7), 2101-2107; (c) Zou, S.; Schatz, G. C., Silver nanoparticle array structures that produce giant enhancements in electromagnetic fields. *Chemical physics letters* **2005**, *403* (1), 62-67.
7. Quinten, M.; Leitner, A.; Krenn, J.; Aussenegg, F., Electromagnetic energy transport via linear chains of silver nanoparticles. *Optics Letters* **1998**, *23* (17), 1331-1333.

8. Lazarides, A. A.; Schatz, G. C., DNA-linked metal nanosphere materials: structural basis for the optical properties. *The Journal of Physical Chemistry B* **2000**, *104* (3), 460-467.
9. Furtaw, M. D.; Lin, D.; Wu, L.; Anderson, J. P., Near-Infrared Metal-Enhanced Fluorescence Using a Liquid-Liquid Droplet Micromixer in a Disposable Poly (Methyl Methacrylate) Microchip. *Plasmonics* **2009**, *4* (4), 273-280.
10. Lakowicz, J. R., Radiative decay engineering 5: metal-enhanced fluorescence and plasmon emission. *Analytical biochemistry* **2005**, *337* (2), 171-194.
11. Zhang, J.; Lakowicz, J. R., Metal-enhanced fluorescence of an organic fluorophore using gold particles. *Optics express* **2007**, *15* (5), 2598.
12. (a) Santra, S.; Wang, K.; Tapeç, R.; Tan, W., Development of novel dye-doped silica nanoparticles for biomarker application. *Journal of biomedical optics* **2001**, *6*, 160; (b) Ma, D.; Tan, S.; Jakubek, Z. J.; Simard, B. In *On the structural stability of dye-doped silica nanoparticles*, IEEE: 2007; pp 651-655; (c) Montalti, M.; Prodi, L.; Zaccheroni, N.; Battistini, G.; Mancin, F.; Rampazzo, E. In *Fluorescent silica nanoparticles*, 2006; p 60990B.
13. Aslan, K.; Wu, M.; Lakowicz, J. R.; Geddes, C. D., Fluorescent core-shell Ag@SiO₂ nanocomposites for metal-enhanced fluorescence and single nanoparticle sensing platforms. *Journal of the American Chemical Society* **2007**, *129* (6), 1524-1525.
14. Wang, L.; Tan, W., Multicolor FRET silica nanoparticles by single wavelength excitation. *Nano letters* **2006**, *6* (1), 84-88.
15. Ulman, A., Formation and structure of self-assembled monolayers. *Chemical reviews* **1996**, *96* (4), 1533.
16. Cookson, J.; Beer, P. D., Exploiting the dithiocarbamate ligand in metal-directed self-assembly. *Dalton Trans.* **2007**, (15), 1459-1472.
17. (a) Zhao, Y.; Pérez-Segarra, W.; Shi, Q.; Wei, A., Dithiocarbamate assembly on gold. *Journal of the American Chemical Society* **2005**, *127* (20), 7328-7329; (b) Colorado Jr, R.; Villazana, R. J.; Lee, T. R., Self-assembled monolayers on gold generated from aliphatic dithiocarboxylic acids. *Langmuir* **1998**, *14* (22), 6337-6340.
18. Park, M. H.; Ofir, Y.; Samanta, B.; Arumugam, P.; Miranda, O. R.; Rotello, V. M., Nanoparticle Immobilization on Surfaces via Activatable Heterobifunctional Dithiocarbamate Bond Formation. *Advanced materials* **2008**, *20* (21), 4185-4188.
19. Singh, A.; Dahanayaka, D. H.; Biswas, A.; Bumm, L. A.; Halterman, R. L., Molecularly Ordered Decanethiolate Self-Assembled Monolayers on Au(111) from in

Situ Cleaved Decanethioacetate: An NMR and STM Study of the Efficacy of Reagents for Thioacetate Cleavage. *Langmuir* **2010**, *26* (16), 13221-13226.

20. Morf, P.; Raimondi, F.; Nothofer, H. G.; Schnyder, B.; Yasuda, A.; Wessels, J. M.; Jung, T. A., Dithiocarbamates: functional and versatile linkers for the formation of self-assembled monolayers. *Langmuir* **2006**, *22* (2), 658-663.

21. Zhang, J.; Fu, Y.; Chowdhury, M. H.; Lakowicz, J. R., Single-molecule studies on fluorescently labeled silver particles: Effects of particle size. *The Journal of Physical Chemistry C* **2008**, *112* (1), 18-26.

Chapter 4:

4.1 Chapter Overview

In this chapter we present the studies conducted to examine the dependence of fluorescence enhancement on the spectral overlap of fluorophore with the localized surface plasmon resonance (LSPR) of the metal nanoparticles. We have studied the spectral overlap of three different dyes Rhodamine B, Rubpy [tris(bipyridine) ruthenium(II) dichloride] and carboxy-BODIPY shown in Figure 4.1 with the plasmon of 13 nm AuNPs. The silica nanoparticles used for this study was synthesized using a method that produces layered particles. The particles were much smaller (30 nm) and uniform in size. It was predicted that trapping the dye in smaller more uniform particles would result greater enhancements due to better overlap of the plasmons. However, we did not observe large enhancements with this study except for the first attempt, but the results were useful to investigate the wavelength dependence on fluorescence enhancement.

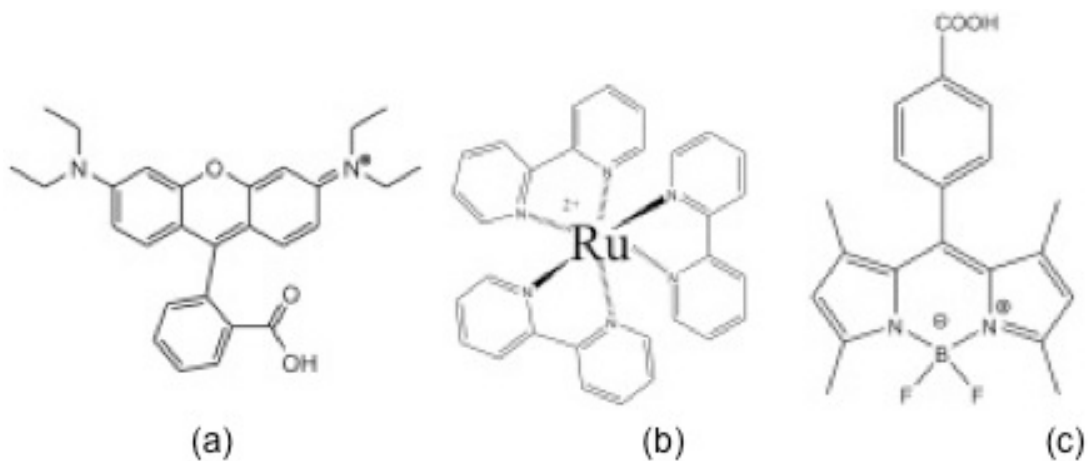


Figure 4.1 Chemical structure of (a) Rhodamine B, (b) Rubpy [tris(bipyridine) ruthenium (II) dichloride] and (c) carboxy-BODIPY.

4.2 Introduction

The discovery of metal enhanced fluorescence (MEF) has opened new paths in fluorescence spectroscopy,¹ changing our perceptions in classical fluorescence. During the past decade, many efforts have been made theoretically and experimentally to better understand the near- field metal-fluorophore interactions that give rise to MEF.^{1b, 2} It is known that metallic colloids can enhance the brightness of the fluorophore by increasing the probability of excitations, modifying the radiative decay rate and by increasing the far field emission by coupling fluorescence emission to the far-field through nanoparticle scattering.^{1d, 2} Previous studies show that these processes are mostly influenced by the distance between the metal and the fluorophore and also the size and geometry of the metal.^{1d, 3} However, the dependence of the spectral overlap of the plasmon with the excitation and emission of the fluorophore also has a significant contribution to MEF. The role of plasmons with respect to the excitation and emission of the fluorophore has been recently investigated by several groups.⁴ In one study, the plasmon was tuned with respect to the emission and excitation of the low quantum yield fluorophore ICG (indocyanine green) by varying the size of the metal particle.^{4b} They report 50 fold enhancements by placing the fluorophore next to an AuNP coated SiNP with a large scattering cross-section which overlaps with the emission frequency of the fluorophore; they have also reported about decreased lifetimes of the fluorophore. Thus, their results support that overlap between the scattering cross-section of the plasmon with emission spectra of the dye would enhance low-quantum yield fluorophores by changing the radiative decay rates. Another study to investigate the wavelength dependence on MEF has been conducted by choosing a fluorophore which varies the

emission wavelength with respect to the solvent polarity.⁵ This study also indicates that the fluorophore couples and radiates through the scattering modes of the plasmon. These results also agree with the Mie theory which also predicts that it is the scattering cross-section of the plasmon that contributes to far-field radiation. However, for high quantum yield fluorophores one would expect the excitation enhancement to dominate since modification of radiative decay rates would not have a greater influence on the enhancement.^{4a} Thus, for the excitation enhancement to dominate it is assumed that the plasmon should overlap with the absorbance spectra of the fluorophore. But overlap of absorption spectra with plasmon can also increase the non-radiative energy transfer to the metal. Another study conducted using high quantum yield fluorophores coupled to silver nano particles with large scattering cross-sections suggest that, for maximum enhancement both excitation and emission should overlap with the plasmon and the plasmon should be slightly blue shifted to the emission of the dye.^{4a}

Most studies conducted to investigate the wavelength dependence have used interactions between a single metal colloid with multiple fluorophores.^{4a, b, 5} Furthermore, most studies have utilized silver nanoparticles which have larger scattering cross-sections than gold. Since AuNPs are more attractive for biological studies,⁶ here, we have investigated the spectral overlap of fluorophore with the AuNP coupled plasmons using metal-fluorophore aggregation. By trapping fluorophores between coupled plasmons, the fluorophore can be exposed to highly enhanced fields and furthermore, the fluorophore should be able to radiate to the far field by coupling to the increased scattering cross-section of aggregated particles.

4.3 Results and Discussion

To investigate the spectral overlap of the fluorophore with the AuNP plasmon, three different dyes having different excitation and emission maxima respect to AuNP plasmon were selected. The dyes selected for the study are shown in Figure 4.1 were Rhodamine B (RhB), carboxy-BODIPY, and Rubpy. Furthermore, the dye doped SiNPs used for this study were not synthesized using the previously used Stöber method. The new silica particles are known as “layered silica nano particles,” since the dye is trapped between two layers of silica; a silica core (16 nm diameter) and a silica shell (7 nm – thickness). The layered SiNPs are more attractive than the ones prepared using the Stöber method, due to their uniform spherical structure and smaller particle size (30 nm). For this study all layered SiNPs were synthesized and APTES surface functionalized by Nathan Green in Dr. Halterman’s lab following the procedure of Hartlen et al.⁷ The AuNPs were capped with $(\text{CH}_3\text{O}(\text{CH}_2\text{CH}_2\text{O})_2\text{C}_{10}\text{H}_{20}\text{SH})$ ligand synthesized by Anuradha Singh. SiNPs were interacted with AuNPs using DTC chemistry.

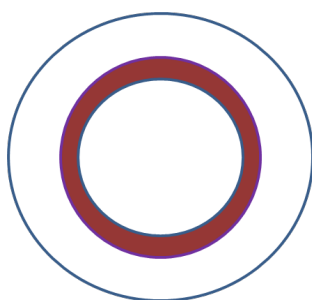


Figure 4.2 Structure of dye doped layered silica nanoparticle.

4.3.1 Study of Spectral Overlap between RhB and the Plasmon of 13 nm AuNPs

Rhodamine B is a highly fluorescent dye with 0.5 quantum yield in 95 % ethanol which absorbs at 550 nm and emits with a maximum at 575 nm. 13 nm AuNPs capped with ether-terminated thiols have a broad absorption spectra with an absorbance maximum at 520 nm. Therefore, both absorption and emission peaks of RhB are red shifted with respect to the plasmon resonance maximum of the AuNPs. However, both excitation and emission spectra of RhB partially overlap with the AuNP plasmon since the latter spreads within a broad range (470-600 nm). Figure 4.3 shows the spectral overlap of RhB with the AuNP plasmon.

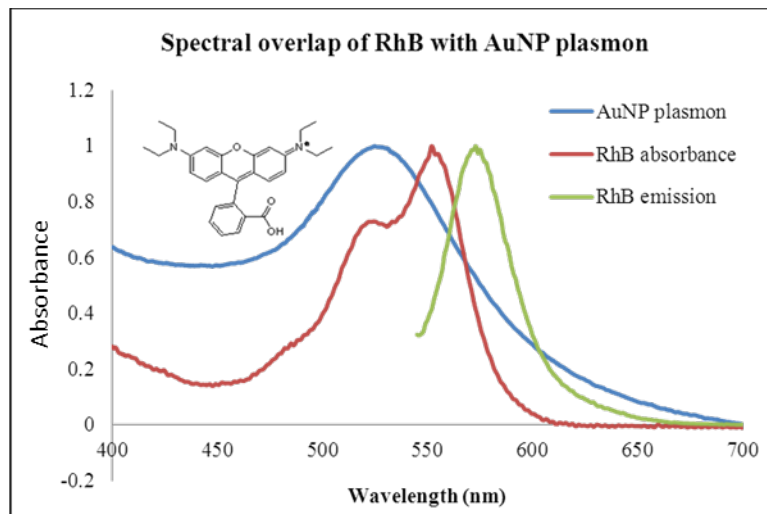


Figure 4.3 Spectral overlap of normalized fluorescence emission and absorbance of RhB with normalized absorbance of 13 nm AuNP plasmon.

The plasmon resonance frequency (SPR) overlaps with the RhB dye absorption. This interaction can result increased excitations. Since the emission is red to the SPR, the non-radiative energy transfer may not dominate.

4.3.1.1 Metal-Fluorophore Aggregation of Layered RhB Doped SiNPs using DTC Chemistry

The DTC activation of layered RhB doped SiNPs was carried out using the procedure developed in chapter 3. However, we were not able to ascertain the AuNP:SiNP ratio since the weight of the particles was unknown. Therefore, a dilution series of free SiNPs was prepared and the dilution giving the same emission intensity as the previous control experiment (chapter 3), was chosen. Thus, 10 μL of the SiNP stock solution was diluted in 85 % ethanol (4 mL). Then 10 μL of the diluted solution was added to 1 mM CS_2 (3 mL) in a glass vial. The pH of the mixture was raised to 8.6 by adding concentrated KOH and the mixture was stirred for 30 min for DTC activation. After 30 minutes ether capped AuNPs (0.5 mL in 34 % ethanol) were added and the mixture was stirred over time. The absorbance and fluorescence were measured over time. Figure 4.4, shows the fluorescence emission of DTC coupled sample and the control after 2 days and after 8 days (Layered-1).

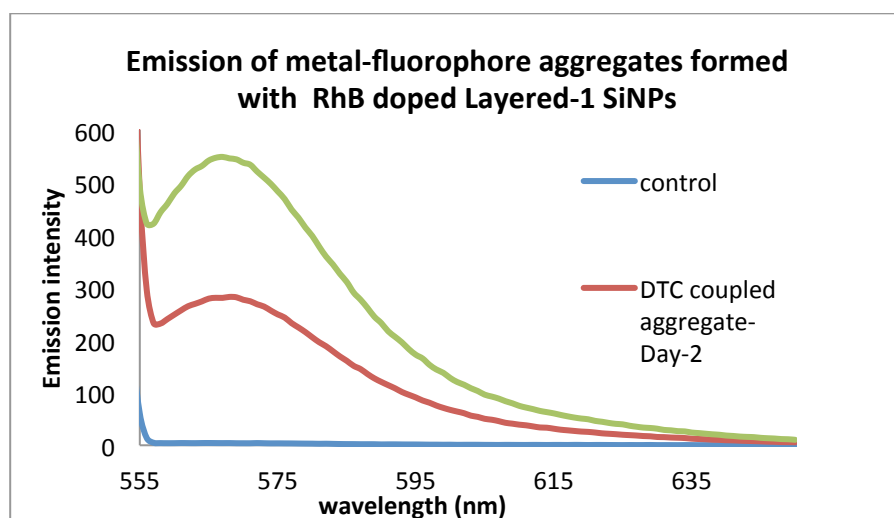


Figure 4.4 Fluorescence emission of metal-fluorophore aggregates of DTC coupled layered RhB doped SiNPs (layered-1) after 2 days and after 8 days, and the fluorescence of the control sample. Samples were excited at 545 nm at 5nm slit width.

Interestingly, the fluorescence emission of the DTC activated sample increased 60 fold after two days and greater than a 100-fold after 8 days. However, after this attempt we were unable to reproduce large enhancements above 100-fold with the layered SiNPs. The maximum enhancement we could reproduce was about 10-fold.

The aggregation with layered SiNPs was repeated by keeping the amount of AuNPs constant (0.5 mL) and varying the SiNPs ratio (10-100 μ L). Figure 4.5 shows the fluorescence emission of varying amounts of the DTC coupled SiNPs (Layered-2) with 0.5 mL AuNPs. The fluorescence emission of control samples without AuNPs is shown in Figure 4.6. In this study (Layered-2) the highest enhancement was observed for the sample with 25 μ L SiNPs. Enhancement factor with varying SiNP additions is shown in Figure 4.7. Figure 4.8 shows the absorbance spectra of the above samples.

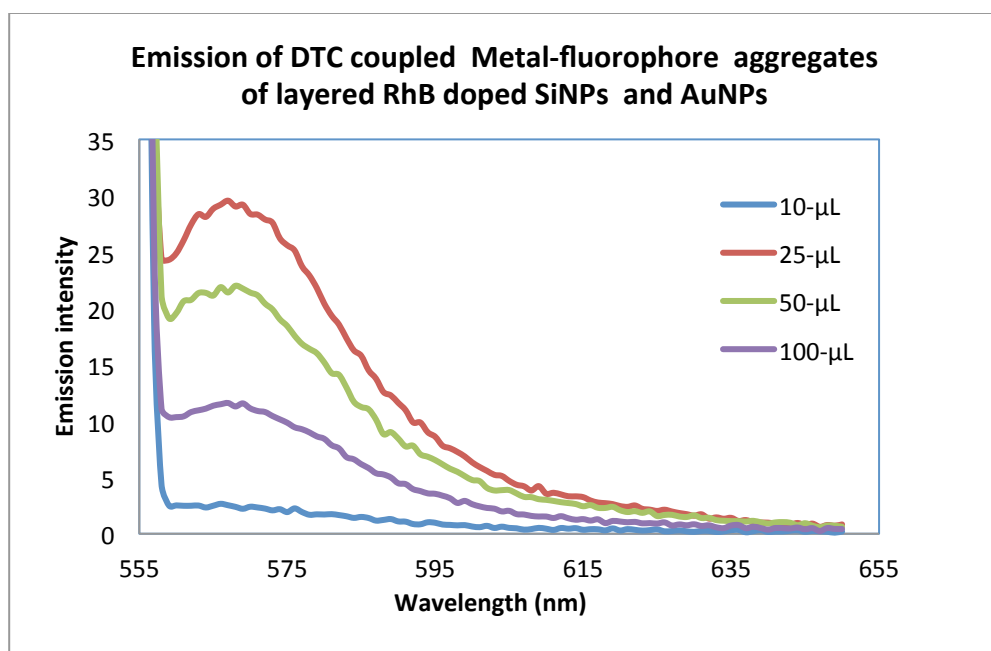


Figure 4.5 Fluorescence emission of varying amounts of layered RhB doped SiNPs, DTC COupled with 0.5 mL of AuNPs (Layered-2, samples excited at 545 nm).

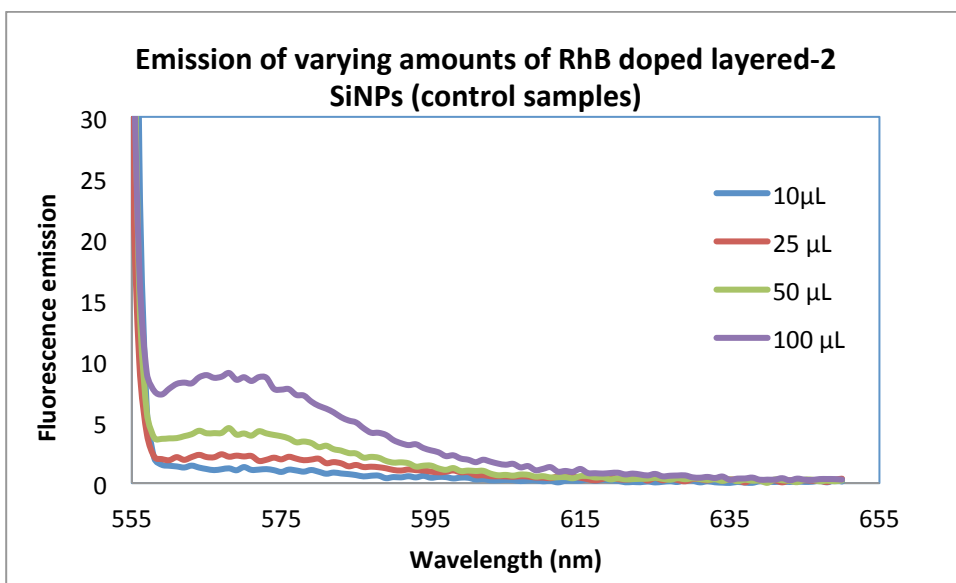


Figure 4.6 Fluorescence emission of varying amounts of layered RhB doped SiNPs . Samples excited at 545 nm at 5nm slit width.

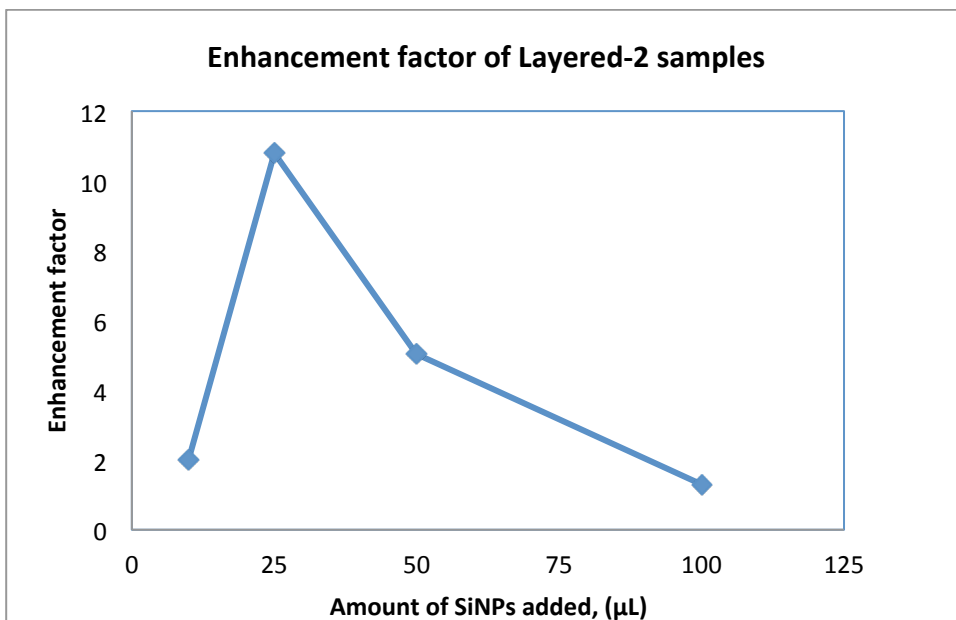


Figure 4.7 Enhancement factor of DTC coupled metal-fluorophore aggregates formed by mixing varying amounts of layered-2 RhB doped SiNPs with 0.5 m< of AuNPs. Enhancement plotted against the amount of SiNPs added.

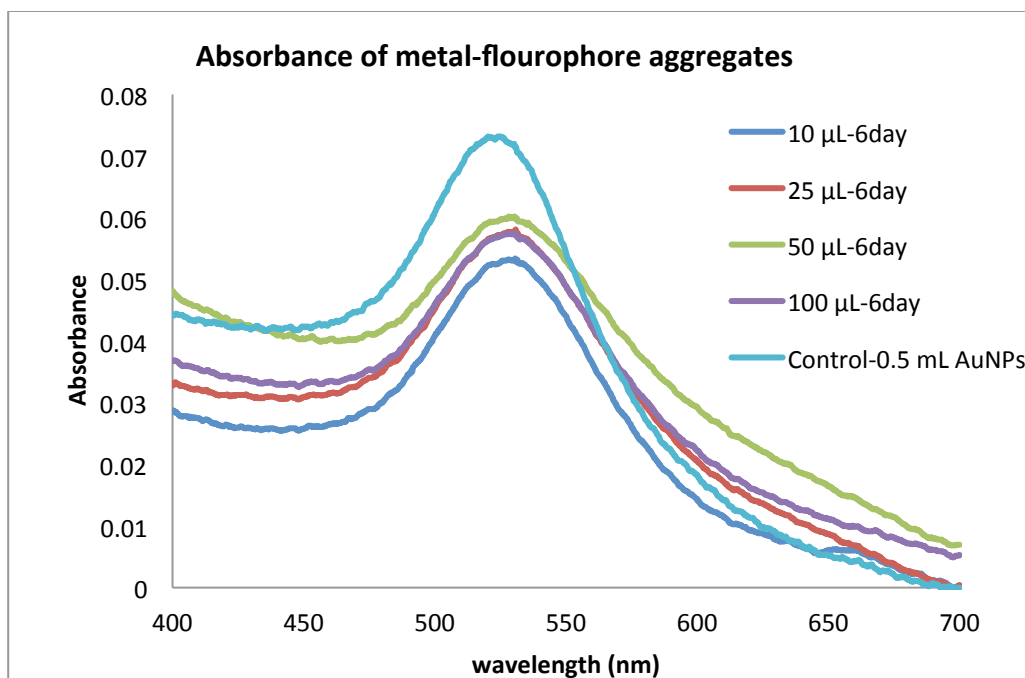


Figure 4.8 Absorbance of metal fluorophore aggregates formed by DTC coupling of varying amounts (10-100 μL) of layered-2 RhB doped SiNPs with 0.5 mL of AuNPs and the absorbance of control sample with 0.5 mL AuNPs without SiNPs.

The red shift in the absorbance spectra indicates aggregation of AuNPs. This may indicate the formation of metal fluorophore aggregates. Although we could not produce large enhancements, the results indicate that each DTC coupled sample has enhanced (Figure 4.7). We speculate that further improvements in the DTC coupling procedure are needed to gain more reproducibility in the aggregation of the nanoparticles.

The experiment was also repeated by keeping SiNP ratio constant (20 μL) and varying the AuNP ratio from 0.25-1 mL (Layered-3). Figure 4.9 shows the fluorescence emission of the DTC coupled samples (left) and the controls (right). The DTC coupled samples and the controls are represented 1, 2, 3 & 4 according to the amount of AuNPs added to each sample. [(1)-0.25 mL-AuNPs, (2)-0.5 mL-AuNPs, (3)-0.75 mL-AuNPs, (4)-1 mL-AuNPs]. The DTC coupled samples show about 0.5 fold enhancement with

increasing additions of AuNPs. The absorbance spectra of the DTC coupled and the control samples are shown in Figure 4.10 The red shift in absorbance spectra indicates the aggregation of AuNPs.

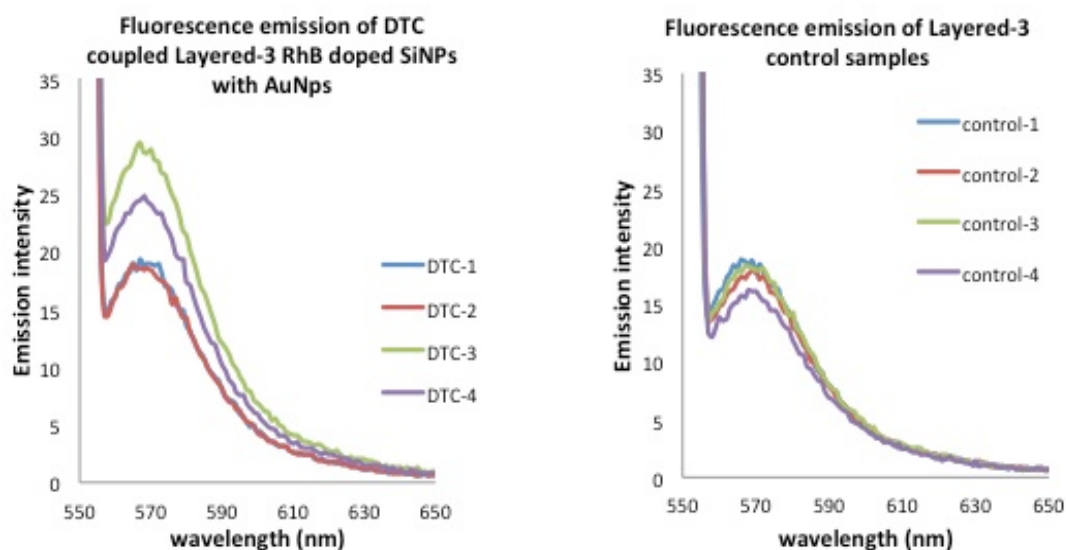


Figure 4.9 Fluorescence emission of metal fluorophore aggregates formed by mixing 20 μL of DTC activated layered-3 RhB doped SiNPs with varying amounts of AuNPs(left). Control samples were prepared by mixing the same ratios of SiNPs and AuNPs without CS2 (right). [(1)-0.25 mL-AuNPs, (2)-0.5 mL- AuNPs, (3) -0.75 mL-AuNPs, (4)-1 mL-AuNPs).

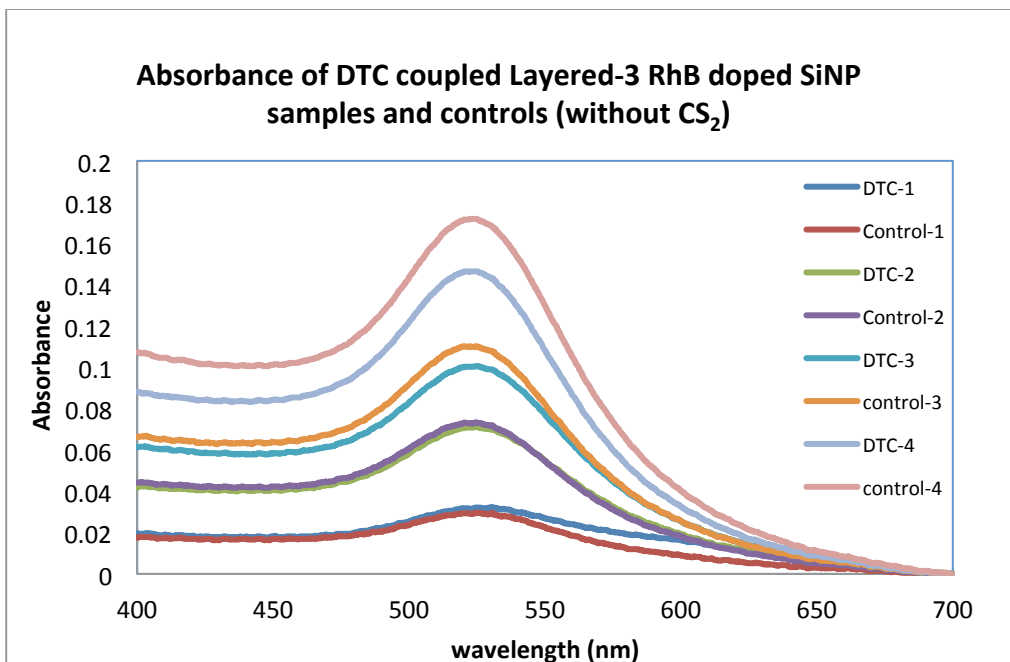


Figure 4.10 Absorbance of metal fluorophore aggregates formed by mixing 20 μ L of DTC activated layered RhB doped SiNPs with varying amounts of AuNPs. Control samples were prepared by mixing the same ratios of SiNPs and AuNPs without CS₂. [(1)-0.25 mL-AuNPs, (2)-0.5 mL-AuNPs, (3)-0.75 mL-AuNPs, (4)-1 mL-AuNPs]

4.3.1 Study of Spectral Overlap of Rubpy Doped Layered SiNPs with 13 nm

AuNPs

Rubpy [tris(bipyridine)ruthenium(II) dichloride] is a dye which absorbs at 450 nm and emits with a maximum at 580 nm. Thus, the absorption of Rubpy is blue relative to the gold SPR and the emission is red to the gold SPR (Figure 4.11). When we consider the spectral overlap, neither absorption nor emission of the dye overlaps the AuNP plasmon directly. If the plasmon is sufficiently red shifted, there is some probability for partial overlap of dye emission with the gold plasmon.

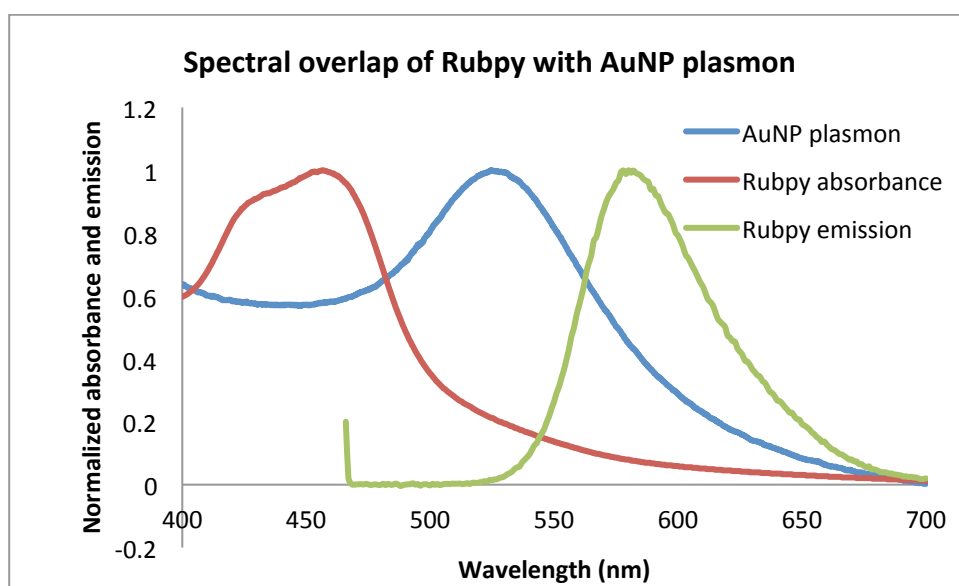


Figure 4.11 Spectral overlap of normalized fluorescence emission and absorbance of Rubpy, with normalized absorbance of 13 nm AuNP plasmon.

For this experiment the DTC coupling of the Rubpy doped layered SiNPs were was carried out in the same manner as described in the previous studies. The experiment was carried out by keeping the amount of silica constant and varying the amount of AuNPs (0.25-1 mL). To each sample 10 μ L of SiNPs were added from the stock solution. Figure 4.12 & 4.13 show emission and absorbance spectra of DTC coupled samples and

the controls. The fluorescence was measured by exciting the sample at 450 nm at 10 nm slit width. The DTC coupled samples and the controls are numbered as 1,2,3 & 4 according to the amount of AuNPs added to each sample. [(1)-0.25 mL-AuNPs, (2)-0.5 mL-AuNPs, (3)-0.75 mL-AuNPs, (4)-1 mL-AuNPs).

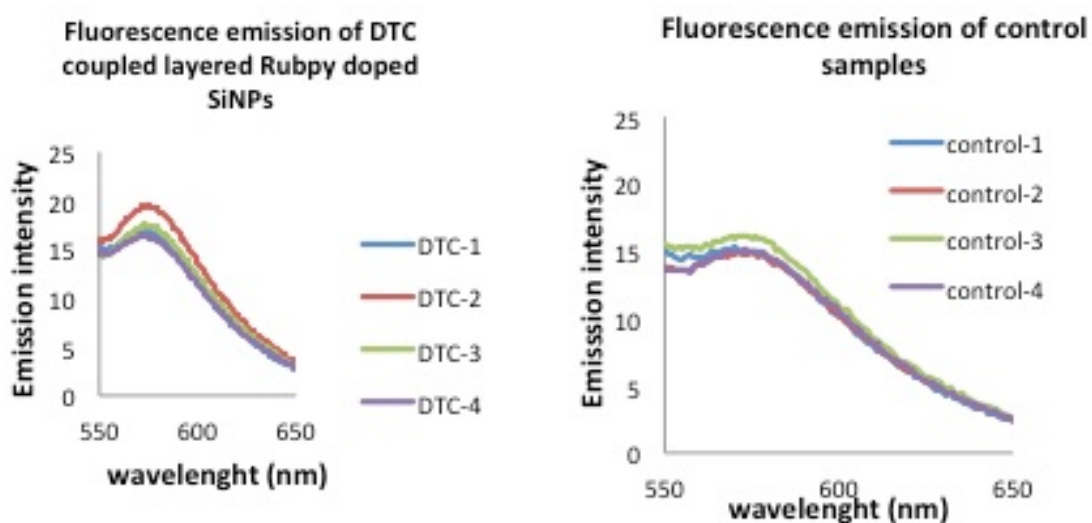


Figure 4.12 Fluorescence emission of metal fluorophore aggregates formed by mixing 10 μ L of DTC activated layered Rubpy doped SiNPs with varying amounts of AuNPs (left). Control samples were prepared by mixing the same ratios of SiNPs and AuNPs without CS₂ (right) [(1)-0.25 mL-AuNPs, (2)-0.5 mL-AuNPs, (3)-0.75 mL-AuNPs, (4)-1 mL-AuNPs). Samples excited at 450 nm at 10 nm slit width.

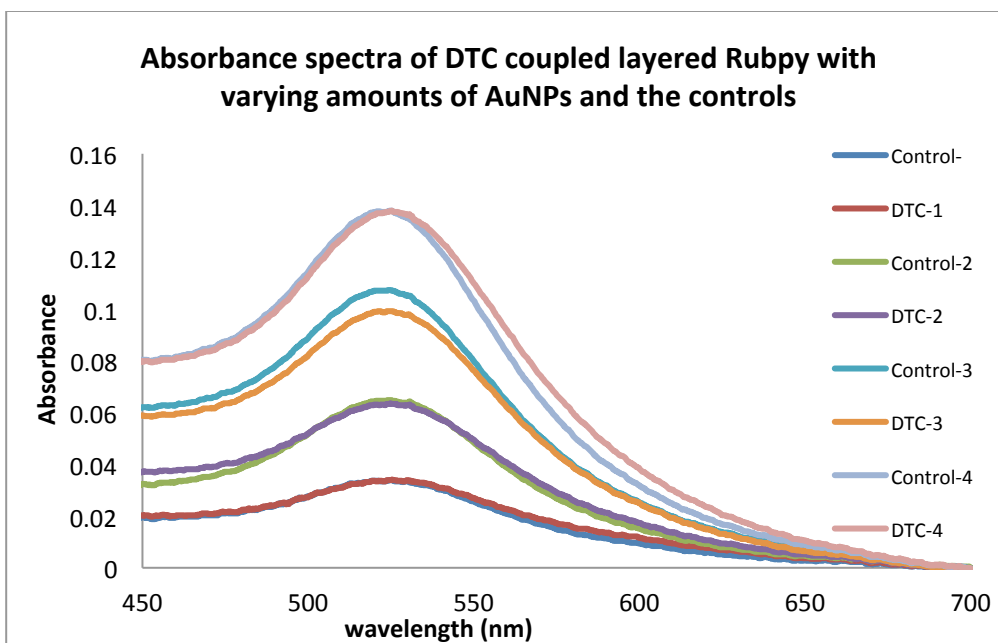


Figure 4.13 Absorbance of metal-fluorophore aggregates formed by mixing 10 μ L of DTC activated layered Rubpy doped SiNPs with varying amounts of AuNPs. Control samples were prepared by mixing the same ratios of SiNPs and AuNPs without CS2. [(1)-0.25 mL-AuNPs, (3)-0.75 mL-AuNPs, (4)-1 mL-AuNPs.]

The absorption spectra of the DTC coupled samples have red shifted, indicating aggregation of the AuNPs (Figure 4.13). The fluorescence emission of DTC coupled samples shows very little enhancement (Figure 4.12-left). The slight enhancement could be due to the partial overlap of emission spectra with the coupled plasmon. Since the absorption of Rubpy (450 nm) does not overlap with the SPR, there is no effect due increased excitations. However, the overlap of emission with the coupled plasmon indicates that there could be energy transfer to the plasmon. The observed enhancement could be due to fluorophore induced plasmons. These results show the desirability of better spectral overlap being more beneficial. Strong conclusions must be tempered by the possibility that these particles are not sufficiently aggregated.

4.3.1 Study of Spectral Overlap of BODIPY Doped Layered SiNPs with 13 nm AuNPs

BODIPY is neutral fluorescent dye which absorbs at 498 nm and emits at 510 nm. Thus, absorption of the dye is clearly blue to the gold plasmon but emission is only slightly blue. Since 13 nm AuNP plasmon resonance maximum is at 520 nm, the emission of this dye overlaps the non-coupled gold plasmon more than any other dye we have chosen; the absorbance also overlaps blue to the plasmon. Although the overlap of the plasmon can cause some increased excitations of the dye, there is a greater potential for resonance energy transfer since the dye emission directly overlaps the acceptor absorbance (SPR). The Figure 4.14 shows the overlap of absorption and emission with the gold plasmon. Carboxy- BODIPY was synthesized by Anuradha Singh.

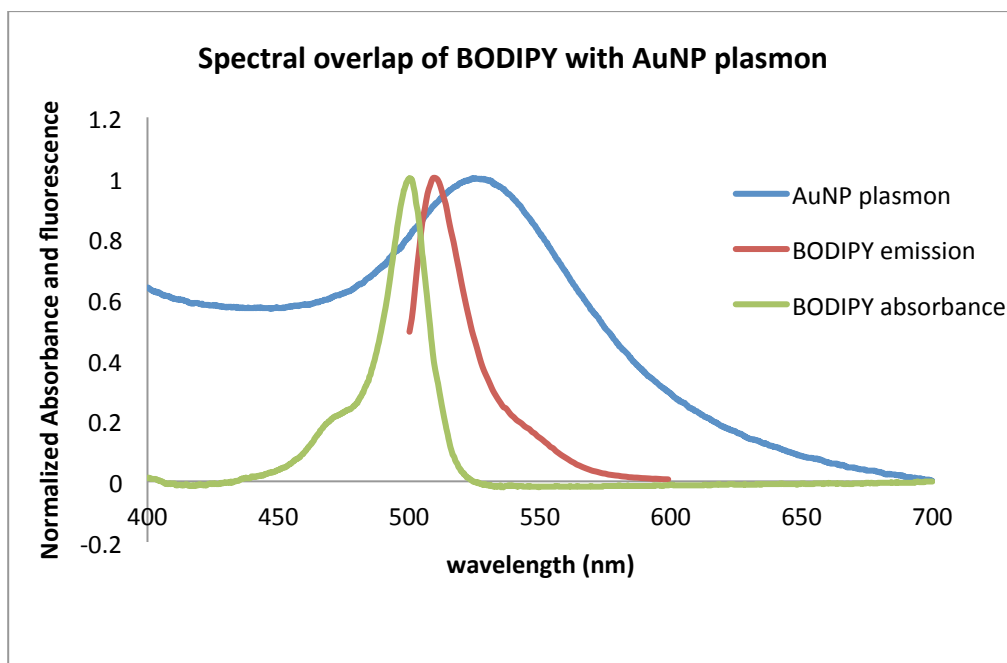


Figure 4.14 Spectral overlap of normalized fluorescence emission and absorbance of BODIPY with normalized absorbance of 13 nm AuNP plasmon.

The DTC coupling of carboxy-BODIPY doped SiNPs and AuNPs were carried out by keeping the amount of silica constant and varying the amount of AuNPs (0.25-1 mL). Figure 4.4 & 4.5 show absorbance and the emission spectra of DTC coupled samples and the controls. The fluorescence was measured by exciting the sample at 490 nm at 5 nm slit width. The DTC coupled samples and the controls are numbered as 1,2,3 & 4 according to the amount of AuNPs added to each sample.[(1)-0.25 mL-AuNPs, (2)-0.5 mL-AuNPs, (3)-0.75 mL-AuNPs, (4)-1 mL-AuNPs].

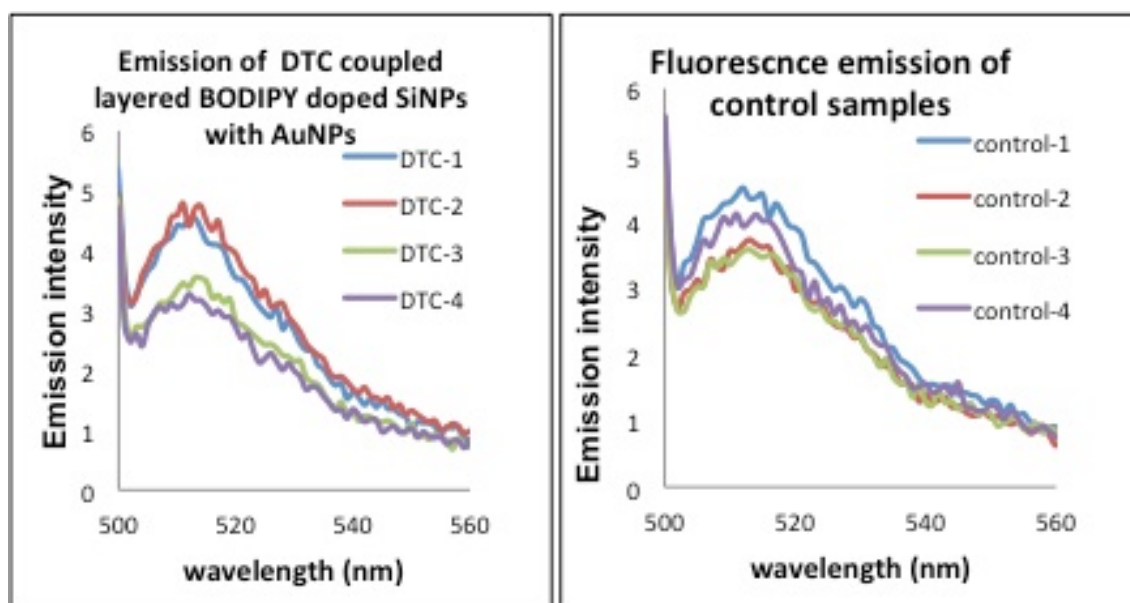


Figure 4.15 Fluorescence emission of metal fluorophore aggregates formed by mixing 10 μL of DTC activated layered BODIPY doped SiNPs with varying amounts of AuNPs (left). Control samples were prepared by mixing the same ratios of SiNPs and AuNPs without CS2 (right). [(1) 0.25 mL- AuNPs, (2) 0.5 mL – AuNPs, (3) 0.75 mL –AuNPs, (4) 1 mL-AuNPs). Samples were excited at 490 nm at 5 nm slit width.

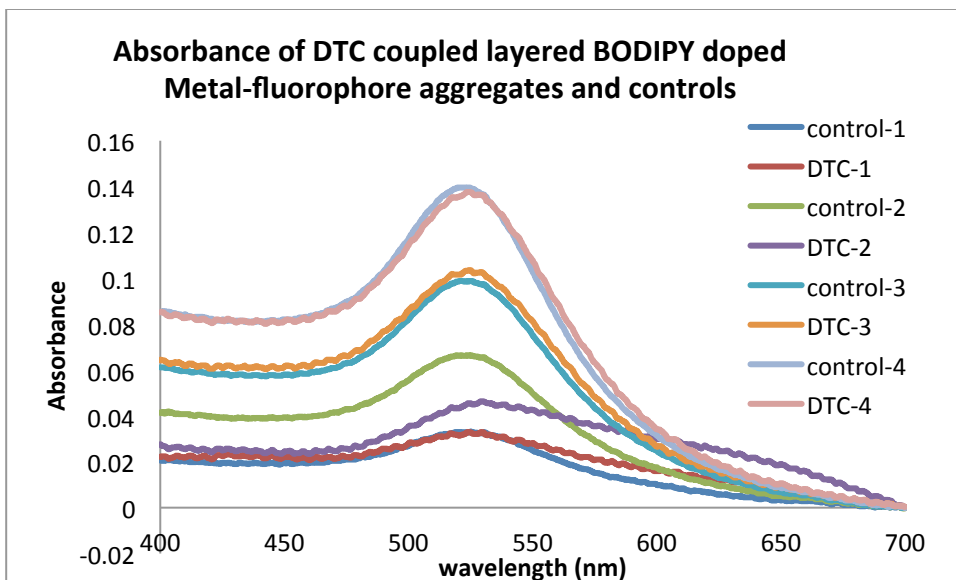


Figure 4.16 Absorbance of metal-fluorophore aggregates formed by mixing 10 μL of DTC activated layered BODIPY doped SiNPs with varying amounts of AuNPs without CS₂. [(1) 0.25 mL - AuNPs, (2) 0.5 mL -AuNPs, (3) 0.75 mL -AuNPs, (4) 1mL- AuNPs)

The examination of fluorescence spectra indicates that fluorescence of DTC coupled samples have decreased than that of the control samples. This could be due to resonance energy transfer to the metal. The red shift in absorption spectra indicates the aggregation of the AuNPs.

4.3.2 Conclusions on Wavelength Dependence on MEF

When we consider the behavior of the three dyes, it is evident that maximum enhancement is given by Rhodamine B. Both BODIPY and Rubpy did not show significant enhancement. With Rubpy, the absorbance is very much blue shifted and the emission is red shifted from the SPR of AuNPs. Thus, the SPR does not significantly interact with the dye excitation, however, the coupled plasmon can interact with the dye emission. For BODIPY both excitation and emission are blue to the plasmon resonance maximum, but the emission strongly overlaps with the plasmon, giving more opportunity for non-radiative energy transfer to the metal.

Our results indicate that the best match for 13 nm AuNP facilitated MEF is Rhodamine B. In RhB, both excitation and emission are red shifted from the gold plasmon resonance maximum; however, both peaks partially overlap the tail of the plasmon. This overlap could result in increased excitations, of the fluorophore, furthermore, since the emission of the dye is red shifted relative to the plasmon, the non-radiative energy transfer (resonance energy transfer) would not be dominant as in BODIPY. However, the emission overlap more red to the plasmon may increase the interactions of the dye with the scattering cross-section of the plasmon. Furthermore, the red shifting of the plasmon due to aggregation would further increase the scattering cross section of the metal. Thus, if the emission couples to the plasmon scattering, plasmon could radiate fluorophores emission to far-field and produce MEF. We believe the observed enhancement of RHB is due contributions from both factors.

4.4 Enhancement of Layered Dye Doped SiNPs

The layered SiNPs were synthesized to achieve better plasmon overlap of metal fluorophore aggregates and to produce more consistent data. Although we were able to observe a large enhancement in our first attempt, after that the maximum enhancements we have observed are 10 fold or less. TEM studies of these metal fluorophore aggregates reveal that AuNPs are binding with SiNPs. However, the binding events observed with the layered SiNPs are much lower than the binding events observed with the particles made using the Stöber method. This could be due to the difference in particle size or some inconsistency in amine functionalization which prevents DTC activation. Particles made with Stöber method were much larger and less uniform than the layered particles. Thus, the AuNPs would easily attach to the SiNP surface. Furthermore, in the Stöber method since the particles were completely doped with the dye, the distance dependency on MEF did not matter; always there was some probability for dye to exist in the enhancement region. However, with the layered particles, if the distance between the dye layer and the metal did not match, even though the particles aggregate with each other, the dye cannot be enhanced. Figure 4.17 shows a TEM image of a metal fluorophore aggregate of layered SiNP trapped between two AuNPs.

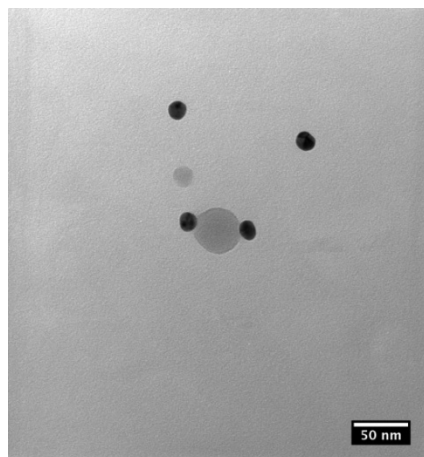


Figure 4.17 TEM image of RhB doped layered SiNP trapped between two AuNPs.

We would expect more of these events to occur to optimize MEF. Thus, future directions to improve MEF using layered SiNPs should focus on getting more interaction between the metal and the fluorophore.

4.5 Chapter Summary

In this chapter we have investigated the wavelength dependence of fluorophore and the plasmon on MEF, by interacting dye doped layered SiNPs with 13 nm AuNPs. Three dyes were doped to layered SiNPs (RhB, Rubpy and BODIPY). Our results indicate that spectral overlap of RhB facilitates MEF the most. Thus, to observe MEF, the SPR should overlap with the dye absorption and emission. But the spectral overlap would be beneficial for fluorescence enhancement if the absorbance and the emission of the fluorophore are red to the SPR. Furthermore, the results indicate that the metal-fluorophore coupling method with the layered SiNPs should be further improved.

4.6 Experimental

4.6.1 Metal-Fluorophore Aggregation of Layered RhB Doped SiNPs using DTC

Chemistry (Layered-1)

Initial steps prior to DTC coupling

APTES coated RhB doped layered SiNPs (sample # 187) was provided by Nathan Green. Citrate capping of 13 nm AuNPs were exchanged with $\text{CH}_3\text{O}(\text{CH}_2\text{CH}_2\text{O})_2\text{C}_{10}\text{SH}$ (“ether”), using a ligand exchange procedure described in 2.5.4. A 34% ethanol/water mixture was prepared by mixing milipore water (9 mL) with 95 % ethanol (5 mL). Since the concentration of the SiNP stock solution was unknown, best concentration range to conduct the experiment had to be determined. For this determination, stock solution of SiNPs (10 μL) was diluted in a mixture of 95% ethanol (3 mL) and 34 % ethanol (1 mL), which is equivalent to the composition of a DTC coupled sample. The fluorescence measurements showed that the samples were too concentrate (when sample was excited at 545 nm at 5 nm slit width, the signal went off scale). Thus, 10 μL from the above diluted SiNP solution (solution-A) was added to another mixture of 95% ethanol (3 mL) and 34% ethanol (1 mL), and the fluorecence was measured. The fluorescence intensity of this solution was similar to the intensity of the previously enhanced SiNP control samples. To test whether the concentration is directly proportional to fluorecence at this range, fluorecence was measured while adding increasing amounts of SiNPs (20 μL additions) to the above mixture. The DTC coupling was carried out after performing these initial measurements.

DTC Coupling of layered-1 SiNPs

To perform the DTC coupling, 3 mM CS₂ (1 mL,) was added to 95 % ethanol (2 mL) in a capped glass vial and the pH was raised to 8.5-9 by adding concentrate KOH (10 μL of pH 12.12 KOH). To this solution RhB doped layered SiNPs (10 μL) from solution-A was added and the mixture was stirred for 30 minutes for the activation of DTC. Next ether capped AUNPs (0.5 mL) and 34 % ethanol (0.5 mL) was added and the mixtures were stirred continuously to form metal-fluorophore aggregates. The fluorescence and the absorbance of the aggregates were measured after 24 h.

4.6.2 Metal-Fluorophore Aggregation of Layered RhB Doped SiNPs using DTC

Chemistry (Layered-2)

APTES coated RhB doped layered SiNPs (sample # 209) was provided by Nathan Green. The initial steps prior to DTC coupling were carried out as described in layered-1 procedure. In this experiment amount of AuNPs was kept constant while varying the SiNP ratio. DTC activation was performed in the same manner as above in 4 different vials containing varying amounts of SiNPs (10, 25, 50, 100 μL). After 30 min ether capped AuNPs (0.5 mL) and 34% ethanol (0.5 mL) were added to each mixture. The fluorescence and the absorbance of the aggregates were measured overtime (24 h, 3 days and 6 days).

4.6.3 Metal-Fluorophore Aggregation of Layered RhB Doped SiNPs using DTC

Chemistry (Layered-3)

APTES coated RhB doped layered SiNPs (sample # 219) was provided by Nathan Green. The initial steps prior to DTC coupling were carried out as described in layered-1 procedure. In this experiment amount of SiNPs was kept constant while varying the AuNP ratio. DTC activation was performed in the same manner as above (layered-1) in 4 different vials containing constant amounts of SiNPs (20 μ L). After 30 min varying amounts of ether capped AuNPs (0.25, 0.5, 0.75, 1 mL) were added to each mixture. The final volume of each solution was brought to 4 mL by adding 34% ethanol to mixtures having less than 1 mL of AuNPs. Control samples were prepared by having same amounts of SiNPs and AuNPs, but adding 95 % Ethanol (1 mL) instead of CS₂ (1 mL). Mixtures were continuously stirred over time, fluorescence and the absorbance of the aggregates were measured. Fluorescence was measured by exciting the samples at 545 nm at 5 nm slit width.

4.6.4 Metal-Fluorophore Aggregation of Layered Rubpy Doped SiNPs using DTC

Chemistry

APTES coated Rubpy doped layered SiNPs was provided by Nathan Green. The Initial steps prior to DTC coupling were carried out as described in layered-1 procedure. In this experiment amount of SiNPs was kept constant while varying the AuNP ratio. Samples were prepared by adding Rubpy stock solution (10 μ L) to each sample. DTC activation was performed in the same manner as above (layered-3) in 4 different vials containing constant amounts of SiNPs (10 μ L). After 30 min varying amounts of ether

capped AuNPs (0.25, 0.5, 0.75, 1 mL) were added to each mixture. The final volume of each solution was brought to 4 mL by adding 34% ethanol to mixtures having less than 1 mL of AuNPs. Control samples were prepared by having same amounts of SiNPs and AuNPs, but adding 95 % Ethanol (1 mL) instead of CS₂ (1 mL).

Mixtures were continuously stirred over time, fluorescence and the absorbance of the aggregates were measured over time. Fluorescence measurements were obtained exciting the sample at 450 nm at 10 nm slit width.

4.6.5 Metal-Fluorophore Aggregation of Layered BODIPY Doped SiNPs using DTC Chemistry

APTES coated BODIPY doped layered SiNPs (225-C) was provided by Nathan Green. The Initial steps prior to DTC coupling were carried out as described in layered-1 procedure. In this experiment amount of SiNPs was kept constant while varying the AuNP ratio. Samples were prepared by adding BODIPY stock solution (10 μL) to each sample. DTC activation was performed in the same manner as above (layered-3) in 4 different vials containing constant amounts of SiNPs (10 μL). After 30 min varying amounts of ether capped AuNPs (0.25, 0.5, 0.75, 1 mL) were added to each mixture. The final volume of each solution was brought to 4 mL by adding 34% ethanol to mixtures having less than 1 mL of AuNPs. Mixtures were continuously stirred over time, fluorescence and the absorbance of the aggregates were measured over time. Control samples were prepared by having same amounts of SiNPs and AuNPs, but adding 95 % Ethanol (1 mL) instead of CS₂ (1 mL).

Fluorescence measurements were obtained by exciting the sample at 490 nm at 5 nm slit width.

3.5.6 Fluorescence and Absorbance Measurements

Absorbance measurements were performed using a Shimadzu Scientific Instruments UV-2101 PC UV-Vis scanning spectrometer using disposable 10×5 mm polystyrene cuvettes.

Steady state fluorescence measurements were performed using a Shimadzu Scientific instruments RF 5301 PC spectrofluorophotometer using disposable 10×5 mm polystyrene cuvettes. The excitation source of the instrument was a 150 W Xenon lamp. Samples were excited at 545 nm at 5 nm slit width.

4.7 Chapter 4 References

1. (a) Aslan, K.; Gryczynski, I.; Malicka, J.; Matveeva, E.; Lakowicz, J. R.; Geddes, C. D., Metal-enhanced fluorescence: an emerging tool in biotechnology. *Current Opinion in Biotechnology* **2005**, *16* (1), 55-62; (b) Aslan, K.; Lakowicz, J. R.; Geddes, C. D., Plasmon light scattering in biology and medicine: new sensing approaches, visions and perspectives. *Current opinion in chemical biology* **2005**, *9* (5), 538-544; (c) Geddes, C. D.; Lakowicz, J. R., Editorial: Metal-enhanced fluorescence. *Journal of fluorescence* **2002**, *12* (2), 121-129; (d) Lakowicz, J. R., Plasmonics in biology and plasmon-controlled fluorescence. *Plasmonics* **2006**, *1* (1), 5-33.
2. (a) Lakowicz, J. R., Radiative decay engineering 5: metal-enhanced fluorescence and plasmon emission. *Analytical biochemistry* **2005**, *337* (2), 171-194; (b) Lakowicz, J. R.; Ray, K.; Chowdhury, M.; Szmackinski, H.; Fu, Y.; Zhang, J.; Nowaczyk, K., Plasmon-controlled fluorescence: a new paradigm in fluorescence spectroscopy. *Analyst* **2008**, *133* (10), 1308-1346.
3. (a) Tovmachenko, O. G.; Graf, C.; van den Heuvel, D. J.; van Blaaderen, A.; Gerritsen, H. C., Fluorescence Enhancement by Metal-Core/Silica-Shell Nanoparticles. *Advanced materials* **2006**, *18* (1), 91-95; (b) Zhang, J.; Fu, Y.; Chowdhury, M. H.; Lakowicz, J. R., Metal-enhanced single-molecule fluorescence on silver particle monomer and dimer: coupling effect between metal particles. *Nano letters* **2007**, *7* (7), 2101-2107.
4. (a) Chen, Y.; Munechika, K.; Ginger, D. S., Dependence of fluorescence intensity on the spectral overlap between fluorophores and plasmon resonant single silver nanoparticles. *Nano letters* **2007**, *7* (3), 690-696; (b) Tam, F.; Goodrich, G. P.; Johnson, B. R.; Halas, N. J., Plasmonic Enhancement of Molecular Fluorescence. *Nano letters* **2007**, *7* (2), 496-501; (c) Kühn, S.; Håkanson, U.; Rogobete, L.; Sandoghdar, V., Enhancement of Single-Molecule Fluorescence Using a Gold Nanoparticle as an Optical Nanoantenna. *Physical Review Letters* **2006**, *97* (1), 017402.
5. Zhang, Y.; Dragan, A.; Geddes, C. D., Wavelength dependence of metal-enhanced fluorescence. *The Journal of Physical Chemistry C* **2009**, *113* (28), 12095-12100.
6. (a) Eustis, S.; El-Sayed, M. A., Why gold nanoparticles are more precious than pretty gold: Noble metal surface plasmon resonance and its enhancement of the radiative and nonradiative properties of nanocrystals of different shapes. *Chemical Society Reviews* **2006**, *35* (3), 209-217; (b) Zhang, J.; Lakowicz, J. R., Metal-enhanced

fluorescence of an organic fluorophore using gold particles. *Optics express* **2007**, *15* (5), 2598.

7. Hartlen, K. D.; Athanasopoulos, A. P. T.; Kitaev, V., Facile preparation of highly monodisperse small silica spheres (15 to > 200 nm) suitable for colloidal templating and formation of ordered arrays. *Langmuir* **2008**, *24* (5), 1714-1720.